DIPLOMARBEIT

Micromagnetic Simulation of Thermally Activated Switching in Fine Particles

ausgeführt am Institut für
Angewandte und Technische Physik
der Technischen Universität Wien

unter der Anleitung von
A.o. Univ.Prof. Dipl.Ing. Dr.techn. Josef Fidler und
Univ.Doz. Dipl.Ing. Dr.techn. Thomas Schrefl

durch

Werner Scholz
Margaretengürtel 62-64/63/3
1050 Wien
Matr.Nr. 9426502

Wien, am 14. September 1999 _____

Abstract

Micromagnetic simulations of permanent magnetic materials reveal the details of the magnetization distribution and dynamic magnetization reversal processes. The knowledge of the dynamic behaviour is of great importance for the design of future magnetic recording media. When the desired magnetization switching frequencies reach an order of magnitude, which is comparable to the intrinsic relaxation time of the media, the switching dynamics have to be investigated in more detail.

Especially effects of thermal activation have to be included in the simulations, which is achieved by adding a random thermal field to the effective magnetic field. As a result, the Landau-Lifshitz equation, which is the equation of motion for the magnetization, is converted into a stochastic differential equation of Langevin type with multiplicative noise. The solution of this stochastic differential equation has to be found by applying the rules of stochastic calculus. The correct interpretation in the context of our physical system is the Stratonovich interpretation of the stochastic Landau-Lifshitz equation, since it leads to the correct thermal equilibrium properties.

The proper generalization of Taylor expansions to stochastic calculus gives suitable time integration schemes. These are tested with a micromagnetic simulation program using the finite difference method. For a single rigid magnetic moment the thermal equilibrium properties are investigated. It is found, that the Heun scheme is a good compromise between numerical stability and computational complexity.

The results of simulations of fine cubic particles whose magnetization reverses coherently show a switching behaviour in agreement with the Arrhenius-Néel law. The implementation of the time integration scheme in a finite element package is verified by comparing its results with those of the finite difference package.

Small spherical magnetic particles exhibit complex magnetization reversal mechanisms for different material parameters and external fields. Depending on the strength of the external field three different magnetization reversal regimes have been identified. For particles with small magnetocrystalline anisotropy coherent reversal modes are found at fields, which are smaller than the anisotropy field. High anisotropy leads to the nucleation of a small volume of reversed magnetization, which expands through the whole particle. For external fields which are comparable to the anisotropy field single droplet nucleation occurs and for higher fields multi-droplet nucleation is the driving reversal process.

The interaction of fine magnetic particles is caused by the magnetic stray field. Depending on distance and alignment the metastable lifetime of a pair of particles changes. Particles aligned along their easy axes stabilize each other, whereas two particles aligned perpendicular to their easy axes exhibit a reduced metastable lifetime.

Kurzfassung

Mikromagnetische Simulationen von Permanentmagneten bringen die Details der Magnetisierungsverteilung und der dynamischen Ummagnetisierungsprozesse zum Vorschein. Die genaue Kenntnis des dynamischen Verhaltens ist besonders für die Entwicklung magnetischer Speichermaterialien wichtig. Wenn die Ummagnetisierungsfrequenzen die Größenordnung der intrinsischen Relaxationszeit erreichen, muß das Ummagnetisierungsverhalten genauer untersucht werden.

Effekte der thermischen Aktivierung müssen in der Simulation berücksichtigt werden. Dies wird dadurch erreicht, daß dem effektiven Magnetfeld ein stochastisches thermisches Feld hinzugefügt wird. Damit wird die Landau-Lifshitz-Gleichung, die Bewegungsgleichung der Magnetisierung, zu einer stochastischen Differentialgleichung vom Typ einer Langevin-Gleichung mit multiplikativem Rauschen. Die geeignete Interpretation der stochastischen Differentialgleichung für unser physikalisches System ist die Stratonovich-Interpretation, da sie zum richtigen Verhalten im thermischen Gleichgewicht führt.

Geeignete Integrationsformeln werden durch die Verallgemeinerung des Begriffs der Taylorreihe für stochastische Prozesse hergeleitet. Mit einem Simulationsprogramm, das die Methode der finiten Differenzen verwendet, werden die Integrationsformeln getestet und verglichen. Das Verhalten im thermischen Gleichgewicht wird am Beispiel eines starren magnetischen Moments untersucht. Das Heun-Schema erweist sich dabei als guter Kompromiß zwischen numerischer Stabilität und Komplexität bei der Berechnung.

Die Ergebnisse der Simulation von kleinen, würfelförmigen Partikeln, deren Magnetisierung homogen rotiert, zeigen ein Ummagnetisierungsverhalten in Übereinstimmung mit dem Arrhenius-Néel-Gesetz. Die Implementierung der Zeitintegrationsalgorithmen in einem Fintite-Elemente-Paket wurde durch Vergleich der Ergebnisse überprüft.

Kleine magnetische Kugeln zeigen ein komplexes Ummagnetisierungsverhalten für verschiedene Materialparameter und externe Felder. Abhängig von der Stärke des äußeren Feldes, wurden drei Bereiche mit unterschiedlichem Ummagnetisierungsverhalten gefunden. Für geringe Kristallanisotropie findet man als Keimbildungsmode homogene Rotation, wenn ein äußeres Feld anliegt, das geringer als das Anisotropiefeld ist. Hohe Anisotropie führt zur Ausbildung eines magnetischen Keims mit umgekehrter Magnetisierung, der sich durch das ganze Teilchen ausbreitet. Ist das äußere Feld vergleichbar mit dem Anisotropiefeld, dann führt ein einzelner Keim zur Ummagnetisierung. Bei höheren Feldern entstehen spontan mehrere Keime, die die Magnetisierung des Teilchens umdrehen.

Die Wechselwirkung kleiner magnetischer Teilchen wird durch das magnetische Streufeld hervorgerufen. Teilchen, deren leichte Achsen auf einer gemeinsamen Geraden ausgerichtet sind, können die Magnetisierung stabilisieren. Bei Teilchen, deren Verbindungsgerade normal auf die leichten Richtungen steht, wird die Zeit, bis sich die Magnetisierung umgedreht hat, verkürzt.

Contents

Chapter 1

Introduction

The physical properties of magnetic materials have been utilized since the ability of loadstone (Fe_2O_3) to attract iron and to align in the earth's magnetic field was discovered. About 1000 years ago compasses were used by Chinese sailors [1]. In the 13th century their use became known in Europe.

Until the 19th century electric and magnetic effects were seen as two independent physical occurrences. In 1820 Oersted proved, that electric currents can influence the needle of a compass. Ampère and Faraday explained that behaviour and laid the foundation for the unified theory of electrodynamics, which was elaborated by James Clerk Maxwell.

Since then, permanent magnets have found many applications in energy transforming and storage devices. In microphones and electric generators they transform the mechanical energy of a membrane or a rotor into electric energy. In loudspeakers and motors the electric energy is transformed back into mechanical energy.

Around 1900 a new application has been found: magnetic recording [2]. Poulsen was the first who recorded acoustic signals on a ferromagnetic wire. In 1927 the magnetic tape, a paper tape coated with dried ferrimagnetic liquid, was invented in the USA and Germany, where a tape containing iron powder was used. The magnetic material was no longer a bulk magnet, but consisted of small magnetic particles. In the 1940's oxide tapes were developed and soon after the appearance of audio recording devices also video signals were stored on magnetic tape.

With the invention of digital computers there was need to store data on reliable and fast, yet easy to handle media. Magnetic tapes and later floppy disks and hard disks proved to be suitable storage devices. Storage capacity and density, access time and data transfer rate have improved constantly due to continuous research and development in magnetic materials. However, there is one parameter which can be hardly influenced: temperature. Products, which are not designed for a few highly specialized applications but for widespread use in a mass market must not require special environment conditions. They should operate at room temperature and normal pressure. As the space required by a piece of information in a magnetic storage device (the bit size) shrinks, the effects of temperature (thermal

activation, thermal perturbations) become increasingly important. These can cause spontaneous switching of the magnetization, which modifies the stored data and results in data loss.

For future magnetic storage devices there are designs of "quantum magnetic disks" and magnetic random access memory devices (MRAMs). These consist of small magnetic elements (with typical dimensions of a few nanometres), where each element stores a single bit. The storage density is given by the size of and distance between the elements. The data writing speed is limited by the magnetization switching time. Projected data storage systems with a frequency greater than 250 MHz [3] will be a challenge for both head and media design, as the desired switching rate leads to writing times, which approach the intrinsic relaxation time of the media. Therefore, a precise understanding of the magnetization process is crucial for the optimal design of magnetic recording media. Micromagnetic simulations can provide information, which is experimentally not accessible. It is possible to study the magnetization switching process [4], optimize the shape [5], and the magnetization reversal time [6, 7] of magnetic nano-elements.

It is the aim of this thesis to investigate the implementation and effects of thermal perturbations in micromagnetic simulations. The micromagnetic formalism is extended by a temperature dependent fluctuation field. The resulting stochastic differential equation is studied by a finite difference simulation program. Simple geometries like a rigid magnetic moment and small magnetic cubes are simulated. Then the algorithms are implemented in a finite element simulation package, which has been developed for deterministic problems and improved over the years [8]. It provides a reliable and flexible tool for micromagnetic simulations and my contribution is the implementation of time integration schemes for the solution of the Langevin type equation of motion for the magnetization.

In chapter 2 the basic theory of micromagnetism is explained and the Landau-Lifshitz equation of motion for the magnetization derived. Its solution by the finite difference and finite element method, and an outline of these methods for numerical computer simulations are described in chapters 3 and 4. Then we extend the theory to take into account thermal perturbations and find a stochastic differential equation in chapter 5. In chapter 6 stochastic calculus is summarized and we find the quantitative properties of the thermal field. For the numerical solution of our Langevin equation we develop suitable numerical integration schemes in chapter 7. The implementation of the finite difference and the finite element model as well as the numerical time integration schemes are explained in chapter 8. Then we study the behaviour of a rigid magnetic moment in chapter 9 before we go on to cubic and spherical particles in chapter 10, which are discretized into smaller computational cells. Furthermore we study the interaction of spherical particles. Finally, a review of experimental results is given.

Chapter 2

Micromagnetics

First quantitative investigations of electric and magnetic phenomena were done by Charles-Augustin de Coulomb (1736-1806). Their unified description is the work of James Clerk Maxwell (1831-1879). Maxwell's equations describe electric and magnetic fields on a macroscopic length scale. However, on an atomic length scale quantum theory has to be used for the proper microscopic description of the physical properties of matter.

The investigation of magnetization processes in *fine* ferromagnetic particles is on a somewhat intermediate level. On the one hand the size of the particles is in the order of nanometres or micrometres. Thus, the effects of magnetic domain formation have to be included in the physical model and Maxwell's equations will not be sufficient for a realistic description.

On the other hand effects which originate from the atomic structure of solids have to be considered. Magnetocrystalline anisotropy for example is caused by the crystal lattice, the periodical positions of atoms which compose the solid. Moreover the exchange interaction between the spin momentum of electrons is a typical quantum mechanical effect.

In purely quantum mechanical models, the size of the particles exceeds the size of systems which can be handled with today's computing power. Therefore, the only way is to 'neglect' quantum mechanics, ignore the atomic nature of matter, and use classical physics in a continuous medium.

Such a classical theory started with a paper by Landau and Lifshitz in 1935 on the structure of the domain wall between two antiparallel magnetic domains. William Fuller Brown contributed several works and gave this theory the name *micromagnetics*. He wanted to emphasize the fact, that this theory should describe the details of the walls which separate magnetic domains as opposed to *domain theory* which considers the domains, but neglects the walls in between. Still, the microscopic details of the atomic structure are ignored and the material is considered from a macroscopic point of view by taking it to be continuous.

2.1 Thermodynamic relations

First, we assume, that the magnetic moment $\mathbf{m}$ and the external field $\mathbf{H}$ together with the temperature T provide a complete characterization of states of our magnetic system. If $\mathbf{H}$ and $\mu_0\mathbf{m}$ are conjugate work variables and F is the Helmholtz free energy, then

$$G(\mathbf{H}, T) = F - \mu_0 \mathbf{m} \cdot \mathbf{H} \tag{2.1}$$

is the corresponding Gibbs free energy [9]. It is known from thermodynamics, that G is the thermodynamic potential controlling spontaneous transformations under fixed $\mathbf{H}$ and T. Any transformation of this kind can only proceed in the sense of producing a decrease of G, and thermodynamic equilibrium is reached when G attains its globally minimum value. In our magnetic system the internal degrees of freedom, which give rise to these spontaneous transformations, can be represented by the magnetic moment $\mathbf{m}$ itself. Here, we assume, that $\mathbf{m}$ varies during the relaxation process and the internal processes leading to a certain value and direction of $\mathbf{m}$ have characteristic relaxation times much shorter than the time scale over which $\mathbf{m}$ varies significantly and the system globally approaches equilibrium. This means, that the system relaxes by passing through a sequence of nonequilibrium states, each characterized by a well-defined value of $\mathbf{m}$. The energy of these intermediate states, for fixed $\mathbf{H}$ and T, is given by

$$G_L(\mathbf{m}; \mathbf{H}, T) = F - \mu_0 \mathbf{m} \cdot \mathbf{H} \quad . \tag{2.2}$$

This is the Landau free energy. The important difference between G and G_L lies in the role of $\mathbf{m}$. G is a function of $\mathbf{H}$ and T only, in which $\mathbf{m}$ must be expressed as a function of $\mathbf{H}$ and T through the equation of state of the system. On the contrary, G_L is the energy of that particular restriction where the state variable $\mathbf{m}$ is forced to take a certain given value, as if it were an external constraint.

The equation of state of the system for the conjugate work variables $\mathbf{H}$ and $\mathbf{m}$ is given by

$$\mathbf{H} = \frac{1}{\mu_0} \left(\frac{\partial F}{\partial \mathbf{m}} \right)_T \tag{2.3}$$

and

$$\mu_0 \mathbf{m} = - \left(\frac{\partial G}{\partial \mathbf{H}} \right)_T \quad . \tag{2.4}$$

So far we did not consider the dependence of the magnetization on space coordinates, but magnetic materials exhibit complicated magnetization patterns. Thus, we subdivide our ferromagnetic body into many elementary volumes, which are small enough with respect to the typical length over which the magnetization varies significantly and at the same time large enough to contain a sufficient number of atoms, so that we can make use of statistical and thermodynamic methods to describe the properties of the volume. We can then calculate the Landau free energy for each elementary volume. At this point the different time scales become obvious again:

The assumption, which led to the definition of G_L means, that the relaxation time over which individual elementary volumes reach thermal equilibrium with respect to the given local value of the magnetization $\mathbf{M}(\mathbf{r})$ is much shorter than the time over which the system as a whole approaches equilibrium through time changes of $\mathbf{M}(\mathbf{r})$.

There are four important contributions to the Landau free energy of a ferromagnetic body: the exchange energy, the magnetocrystalline anisotropy energy, the magnetostatic energy, and the Zeeman energy in an external field [10].

Another contribution, magnetoelastic energy, which arises from magnetostriction, is omitted for two reasons. When a ferromagnet is magnetized it shrinks (or expands) in the direction of the magnetization. As a result, the volume changes and with it the saturation magnetization, which is defined as the magnetic moment in saturation per unit volume. However, in micromagnetics it is a basic assumption, that the saturation magnetization remains constant. Secondly, a large part of the internal magnetostriction in a ferromagnetic crystal can be expressed in the same mathematical form as magnetocrystalline anisotropy. If the anisotropy constants are taken from experiment, the effect of magnetostriction is already included, and therefore we do not have to consider it in an additional energy term.

2.1.1 Exchange energy

The Heisenberg Hamiltonian of the exchange interaction is usually written in the form

$$\mathcal{H}_{\text{exch}} = -\sum_{i,j=1}^{M} J_{ij}\mathbf{S}_i \cdot \mathbf{S}_j \quad ,$$

where J_{ij} is the exchange integral, which can be calculated using quantum mechanics [11, 12]. It decreases rapidly with increasing distance between the atoms, and so the sum has to be taken only for nearest neighbours and we can write J for J_{ij}. $\mathbf{S}_{i,j}$ stands for the spin operators. If we replace them by classical vectors and rewrite the dot product, we obtain for the exchange energy

$$E_{\text{exch}} = -JS^2 \sum_{i,j|i\neq j} \cos\phi_{i,j} \quad .$$

Next, we assume, that the angles $\phi_{i,j}$ are small and develop the cosine into its Taylor series expansion. We also take the sum for each pair of nearest neighbours only once and redefine the zero level of the exchange energy by removing the constant term.

$$E_{\text{exch}} = JS^2 \sum_{NN} \phi_{i,j}^2$$

If we use the continuous variable $\mathbf{m} = \mathbf{M}/M_{\text{s}}$ for the magnetization, we get for small angles

$$|\phi_{i,j}| \approx |\mathbf{m}_i - \mathbf{m}_j| \approx |(\mathbf{r}_i \cdot \nabla)\mathbf{m}| \quad ,$$

where $\mathbf{r}_i$ is the position vector from lattice point i to j. Then, the exchange energy is given by

$$E_{\text{exch}} = JS^2 \sum_i \sum_{\mathbf{r}_i} [(\mathbf{r}_i \cdot \nabla)\mathbf{m}]^2 \quad .$$

Changing the summation over i to an integral over the ferromagnetic body, we get

$$E_{\text{exch}} = \int_V A \left[(\nabla m_x)^2 + (\nabla m_y)^2 + (\nabla m_z)^2 \right] d^3r \quad . \tag{2.5}$$

The exchange constant A is given by

$$A = \frac{JS^2 c}{a} \quad ,$$

where a is the distance between nearest neighbours and $c \in \{1, 2, 4\}$ for a simple cubic, body centred cubic, and face centred cubic crystal structure, respectively.

2.1.2 Magnetocrystalline anisotropy energy

The Heisenberg Hamiltonian is completely isotropic, and its energy levels do not depend on the direction in space in which the crystal is magnetized. If there was no other energy term, the magnetization would always vanish in zero applied field. However, real magnetic materials are not isotropic. So the permanent magnets in microphones and loudspeakers do not lose their permanent magnetization after production. The most common type of anisotropy is the magnetocrystalline anisotropy, which is caused by the spin-orbit interaction of the electrons. The electron orbits are linked to the crystallographic structure, and by their interaction with the spins they make the latter prefer to align along well-defined crystallographic axes. Therefore, there are directions in space, in which a magnetic material is easier to magnetize than in others. The spin-orbit interaction can also be evaluated from basic principles. However, it is easier to use phenomenological expressions (power series expansions that take into account the crystal symmetry) and take the coefficients from experiment.

The magnetocrystalline energy is usually small compared to the exchange energy. But the direction of the magnetization is determined only by the anisotropy, because the exchange interaction just tries to align the magnetic moments parallel, no matter in which direction.

In hexagonal crystals the anisotropy energy is a function of only one parameter, that is the angle between the magnetization and the c-axis. Experiments show, that it is symmetric with respect to the base plane, and so odd powers of $\cos\theta$ can be omitted in a power series expansion for the anisotropy energy density w_{ani}. The first two terms are thus

$$w_{\text{ani}} = -K_1 \cos^2\theta + K_2 \cos^4\theta = -K_1 m_z^2 + K_2 m_z^4 \quad ,$$

where z is parallel to the c-axis. It is known from experiment, that terms of higher order, and in most cases even K_2 are negligible. If $K_1 > 0$, then the c-axis is an easy axis, which means it is a direction of minimal energy. For $K_1 < 0$ it is a hard axis with an easy plane perpendicular to it.

2.1.3 Magnetostatic energy

The origin of domains still cannot be explained by the two energy terms above. Another contribution comes from the magnetostatic self-energy, which originates from the classical interactions between magnetic dipoles. For a continuous material it is described by Maxwell's equations

$$\begin{aligned} \text{div } \mathbf{D} &= \rho && (2.6)\\ \text{div } \mathbf{B} &= 0 && (2.7)\\ \text{curl } \mathbf{E} &= -\frac{\partial \mathbf{B}}{dt} && (2.8)\\ \text{curl } \mathbf{H} &= \frac{\partial \mathbf{D}}{dt} + \mathbf{j} \quad . && (2.9) \end{aligned}$$

In our magnetostatic problem, we do not have any electric fields $\mathbf{E}$ or free currents $\mathbf{j}$. Thus, there are two remaining equations

$$\begin{aligned} \text{div } \mathbf{B} &= 0 && (2.10)\\ \text{curl } \mathbf{H} &= 0 \quad . && (2.11) \end{aligned}$$

The magnetic induction $\mathbf{B}$ is given by $\mathbf{B} = \mu_0(\mathbf{H} + \mathbf{M})$. A general solution of (2.11) is given by

$$\mathbf{H} = -\nabla U \quad , \tag{2.12}$$

where U is the magnetic scalar potential. Inserting the expressions for $\mathbf{B}$ and $\mathbf{H}$ in (2.10) gives

$$\Delta U_{\text{in}} = \text{div } \mathbf{M} \tag{2.13}$$

inside magnetic bodies and

$$\Delta U_{\text{out}} = 0 \tag{2.14}$$

outside in air or vacuum.

These equations have to be solved with the boundary conditions

$$U_{\text{in}} = U_{\text{out}}, \qquad \frac{\partial U_{\text{in}}}{\partial n} - \frac{\partial U_{\text{out}}}{\partial n} = \mathbf{M} \cdot \mathbf{n} \tag{2.15}$$

on the surface of the magnet to obtain U and derive from it $\mathbf{H}$. $\mathbf{n}$ is the unit normal to the magnetic body, taken to be positive in outward direction.

In micromagnetics, the magnetization distribution $\mathbf{M}(\mathbf{r})$ is given. With relation (2.13) the magnetic scalar potential can be calculated from the magnetization distribution. The demagnetizing field $\mathbf{H}_{\text{ms}}$ is then obtained by using (2.12).

Finally the magnetostatic energy is given by

$$E_{\rm ms} = -\frac{1}{2}\mu_0 \int_V \mathbf{M}\cdot\mathbf{H}_{\rm ms}\, d^3r \quad .$$

2.1.4 Zeeman energy

For the energy of a magnetic body in an external field $\mathbf{H}_{\rm ext}$ we obtain

$$E_{\rm ext} = -\mu_0 \int_V \mathbf{M}\cdot\mathbf{H}_{\rm ext}\, d^3r \quad .$$

Due to the linearity of Maxwell's equations, the superposition principle allows a simple adding also of this energy term.

2.2 Energy minimization

If the magnetization is given by

$$\mathbf{M} = M_{\rm s}\mathbf{m} = M_{\rm s}\begin{pmatrix} m_x \\ m_y \\ m_z \end{pmatrix} \quad , \tag{2.16}$$

where the saturation magnetization $M_{\rm s}$ is assumed to be constant, we get for the Landau free energy

$$\begin{aligned} G_L &= E_{\rm exch} + E_{\rm ani} + E_{\rm ms} + E_{\rm ext} = & (2.17)\\ &= \int_V \Big\{ A\left[(\nabla m_x)^2 + (\nabla m_y)^2 + (\nabla m_z)^2\right] \\ &\quad -K_1 m_z^2 + K_2 m_z^4 \\ &\quad -\frac{1}{2}\mu_0 \mathbf{M}\cdot\mathbf{H}_{\rm ms} \\ &\quad -\mu_0 \mathbf{M}\cdot\mathbf{H}_{\rm ext}\Big\}\, d^3r \quad . & (2.18) \end{aligned}$$

From this equation we can calculate the Landau free energy, if the magnetization distribution within the magnetic body is known. However, in micromagnetics the task is to determine the magnetization distribution which minimizes the Landau free energy. So we need a technique to find this energy minimum and Brown [13] proposed a variational method.

He considered a small variation of the direction of the magnetization vector, rather a small variation of the magnetization distribution function by arbitrary functions. At an energy minimum the coefficients of the linear term for any choice of the variation should vanish. Proper application of this variational principle [14] finally leads to Brown's equations (in vector notation)

$$\mathbf{m}\times\left(2A\nabla^2\mathbf{m} + \mu_0 M_{\rm s}\mathbf{H}_{\rm ms} + \mu_0 M_{\rm s}\mathbf{H}_{\rm ext} - \frac{\partial w_{\rm ani}}{\partial \mathbf{m}}\right) = 0 \quad .$$

In other words, in equilibrium the magnetization is parallel to an effective field

$$\mathbf{H}_{\text{eff}} = \frac{2A}{M_{\text{s}}}\nabla^2\mathbf{m} + \mu_0\mathbf{H}_{\text{ms}} + \mu_0\mathbf{H}_{\text{ext}} + \frac{1}{M_{\text{s}}}\frac{\partial w_{\text{ani}}}{\partial \mathbf{m}} \tag{2.19}$$

and the torque on the magnetization vanishes

$$\mathbf{m} \times \mathbf{H}_{\text{eff}} = 0 \quad . \tag{2.20}$$

Since $\mathbf{M} \times \mathbf{M} = 0$ any arbitrary vector proportional to $\mathbf{M}$ may be added to $\mathbf{H}_{\text{eff}}$ without changing the result. It is therefore of no consequence if $\mathbf{H}$ or $\mathbf{B} = \mu_0(\mathbf{H}+\mathbf{M})$ is used for the effective field.

Brown's equations have to be solved together with Maxwell's equations for the magnetostatic field and the proper boundary conditions. And it is necessary to check, if the solution is a minimum or a maximum, for which the variation vanishes, too. Static energy minimization using the finite element method is very efficient in calculating equilibrium magnetization distributions and nucleation fields of polycrystalline permanent magnets [15].

2.3 The dynamic equation

The solution of Brown's equations gives us the magnetization distribution in equilibrium. If we are interested in the dynamic properties and time evolution of the magnetization, we have to consider the precession of the magnetization in a magnetic field [16].

The torque $\mathbf{l}$ is given by the rate of change of angular momentum $\mathbf{g}$ with time

$$\frac{d\mathbf{g}}{dt} = \mathbf{l} \quad , \quad |\mathbf{g}| = \hbar \quad .$$

The torque acting on a magnetic moment $\mathbf{m}$ in a magnetic field $\mathbf{H}$ is given by

$$\mathbf{l} = \mathbf{m} \times \mathbf{H} \quad .$$

The magnetic moment is linked to the angular momentum by the gyromagnetic ratio γ

$$\mathbf{g} = -\frac{\mu_0\mathbf{m}}{\gamma} \quad , \quad \gamma = \frac{\mu_0 g|e|}{2m_{\text{e}}} = 2.210173 \times 10^5 \frac{\text{m}}{\text{As}} \quad .$$

$g \approx 2$ is the Landé factor, $|e|$ the elementary charge, and m_{e} the electron's mass. The magnetic field constant μ_0 has been pulled into γ. By the above definition γ is positive, but the electron's charge is negative. As a result, we obtain

$$\frac{d\mathbf{m}}{dt} = -\gamma\mathbf{m} \times \mathbf{H} \tag{2.21}$$

as the equation of motion for the magnetic moment of the electron.

We can replace the magnetic moment of the electrons by the magnetization. The magnetic field, which drives the precession, can be identified with the effective field (2.19), but we simply write $\mathbf{H}$. Thus, we obtain

$$\frac{d\mathbf{M}}{dt} = -\gamma \mathbf{M} \times \mathbf{H} \quad .$$

This equation describes the undamped precession of the magnetization vector $\mathbf{M}$ about the field direction. It is the well known Larmor precession with the Larmor frequency $\omega = \gamma H$. From experiments it is known, that changes in the magnetization decay in finite time. As this damping cannot be derived rigorously from basic principles, it is just added by a phenomenological term. In reality it is caused by a complex interaction of the electron's magnetic moment with the crystal lattice.

Gilbert [17] proposed a damping term of the form

$$\frac{\alpha}{M_\mathrm{s}} \mathbf{M} \times \frac{d\mathbf{M}}{dt}$$

with the dimensionless damping parameter α.

It is equivalent to a an older form of Landau and Lifshitz [18], which is usually written as

$$-\frac{\lambda\gamma'}{M_\mathrm{s}} \mathbf{M} \times (\mathbf{M} \times \mathbf{H})$$

with the dimensionless damping parameter λ.

The relationship between α and λ can be derived as follows. First, we apply $\mathbf{M}\cdot$ to both sides of the *Gilbert equation*

$$\frac{d\mathbf{M}}{dt} = -\gamma \mathbf{M} \times \mathbf{H} + \frac{\alpha}{M_\mathrm{s}} \mathbf{M} \times \frac{d\mathbf{M}}{dt} \quad . \tag{2.22}$$

Since the right hand side vanishes, we obtain

$$\mathbf{M} \cdot \frac{d\mathbf{M}}{dt} = 0$$

or

$$\frac{dM^2}{dt} = 0 \quad .$$

Thus, it is ensured, that the saturation magnetization $|\mathbf{M}| = M_\mathrm{s}$ remains constant during the motion, as assumed in (2.16).

When we apply $\mathbf{M}\times$ to both sides of Gilbert's equation (2.22), we get

$$\begin{aligned}
\mathbf{M} \times \frac{d\mathbf{M}}{dt} &= -\gamma \mathbf{M} \times (\mathbf{M} \times \mathbf{H}) + \frac{\alpha}{M_\mathrm{s}} \mathbf{M} \times \left(\mathbf{M} \times \frac{d\mathbf{M}}{dt} \right) \\
&= -\gamma \mathbf{M} \times (\mathbf{M} \times \mathbf{H}) + \frac{\alpha}{M_\mathrm{s}} \left(\mathbf{M} \cdot \frac{d\mathbf{M}}{dt} \right) \mathbf{M} \\
&\quad -\alpha \frac{d\mathbf{M}}{dt} \\
&= -\gamma \mathbf{M} \times (\mathbf{M} \times \mathbf{H}) - \alpha \frac{d\mathbf{M}}{dt}
\end{aligned} \tag{2.23}$$

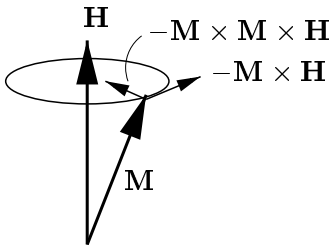

Figure 2.1: Larmor precession with damping

If we substitute this result in (2.22), we arrive at

$$\left(1+\alpha^2\right)\frac{d\mathbf{M}}{dt} = -\gamma\mathbf{M}\times\mathbf{H} - \gamma\frac{\alpha}{M_\mathrm{s}}\mathbf{M}\times(\mathbf{M}\times\mathbf{H}) \quad .$$

With

$$\lambda = \alpha \quad \text{and} \quad \gamma' = \frac{\gamma}{1+\lambda^2} \tag{2.24}$$

we get the *Landau-Lifshitz equation* in Gilbert form

$$\frac{d\mathbf{M}}{dt} = -\gamma'\mathbf{M}\times\mathbf{H} - \frac{\alpha\gamma'}{M_\mathrm{s}}\mathbf{M}\times(\mathbf{M}\times\mathbf{H}) \quad . \tag{2.25}$$

Chapter 3

The finite difference method

In order to solve the Landau-Lifshitz equation (2.25) with the effective field (2.19) numerically, we have to convert it into a form, which can be translated into an algorithm for a digital computer with finite speed and memory.

We have to reduce the problem of finding a continuous solution to one with finite dimensionality [19]. In the finite difference method (as later in the finite element method) we replace the continuous solution domain by a discrete set of lattice points. In each lattice point we replace any differential operators by finite difference operators. The conditions on the boundary of the domain have to be replaced by their discrete counterparts.

For some differential equations, such as the wave equation in one dimension, it is even possible to construct exact algorithms by nonstandard finite difference schemes [20]. However, this is rarely the case, and so the finite difference method gives only an approximate solution.

3.1 Discretization of the exchange energy

For our problem of calculating the effective field and integrating the Landau-Lifshitz equation, we have to discretize time and space into regular lattices. For the space discretization a regular cubic lattice has been chosen, because it allows the simplest implementation and irregular lattices are more efficiently handled with the finite element method (cf. chapter 4). The time integration is also done on a regular lattice and described in detail in chapter 7.

In order to calculate the contribution of the exchange interaction to the effective field, we have to discretize (2.5). The first partial derivative

$$(\nabla m_x)^2 = \left(\frac{\partial m_x}{\partial x}\right)^2 + \left(\frac{\partial m_x}{\partial y}\right)^2 + \left(\frac{\partial m_x}{\partial z}\right)^2$$

is approximated by the finite difference

$$\left(\frac{\Delta_x m_x}{\Delta x}\right)^2 + \left(\frac{\Delta_y m_x}{\Delta y}\right)^2 + \left(\frac{\Delta_z m_x}{\Delta z}\right)^2 \quad , \tag{3.1}$$

where $\Delta x, \Delta y, \Delta z$ denote the lattice spacing in the three dimensions of space, which is identical on a regular cubic lattice and we will simply write Δx. $\Delta_x, \Delta_y, \Delta_z$ indicate the finite difference operators in x, y, and z direction, respectively.

Let us now consider the magnetization vector $\mathbf{m}_i$ at lattice point i and $\mathbf{m}_{i+1}$ on the neighbouring lattice point in $+x$ direction. Then, we can rewrite the first term in (3.1) as

$$\left(\frac{m_{i+1,x} - m_{i,x}}{\Delta x}\right)^2 = \frac{(m_{i+1,x} - m_{i,x})^2}{\Delta x^2} = \frac{m_{i+1,x}^2 - 2m_{i+1,x}m_{i,x} + m_{i,x}^2}{\Delta x^2} \quad .$$

From the second and third term in (2.5) we get the contribution of the y and z component of the magnetization vectors. Since $|\mathbf{m}| = 1$ we can simplify and get for the finite difference

$$\frac{1}{\Delta x^2}(2 - 2\mathbf{m}_i \cdot \mathbf{m}_j) \quad . \tag{3.2}$$

From the second and third term in (3.1), which represent the contributions of the nearest neighbours in y and z direction, we get analogous expressions. The same procedure can be carried out for the opposite neighbours in the negative directions of space. Then we take the arithmetic mean of the two opposite nearest neighbours.

Our final result for the exchange energy density is

$$\omega_{\text{exch}} = \frac{A}{\Delta x^2} \sum_i \sum_{j \in NN} (1 - \mathbf{m}_i \cdot \mathbf{m}_j) \quad , \tag{3.3}$$

where NN stands for the indices of the nearest neighbours.

The approximation of the partial derivatives by finite differences is only valid for small arguments, and in our case for small angles between neighbouring magnetization vectors. Other exchange energy representations have been suggested and compared [21], but none of them has significant advantages over the one derived above.

In a discretized form [22] the effective field is defined by

$$\mathbf{H}_{\text{eff}} = \frac{\partial \omega}{\partial \mathbf{M}} \quad .$$

For the "exchange field" at lattice site i we find

$$\mathbf{H}_{\text{exch},i} = \frac{2A}{M_{\text{s}} \Delta x^2} \sum_{j \in NN} \mathbf{m}_j \quad .$$

3.2 Discretization of the demagnetizing field

Another difficulty arises from the calculation of the demagnetizing field. Within each computational cell, the Wigner-Seitz cell of the lattice point, the magnetization is assumed to be homogeneous. We could now try to discretize Poisson's equation (2.13) and Laplace's equation (2.14). The main difficulty arises from the open boundary conditions, which are discussed in section 4.2. However, for a lattice of homogeneously magnetized cubes, it is possible to calculate the demagnetizing field analytically [23]. The expressions obtained are quite complex and computationally expensive to implement. Since the calculation of the demagnetization field by a magnetic scalar potential is very efficiently implemented in the finite element package, a third possibility has been chosen for the finite difference program. That is the approximation of the demagnetization field of each computational cell by the field of a magnetic dipole in the centre of the cell with the magnetic moment $\mathbf{m}_i = \mathbf{M}_i \Delta x^3$ [24, 25].

$$\mathbf{H}_{\text{dip}} = -\frac{1}{4\pi} \sum_{j \neq i} \frac{\mathbf{M}_j}{R_{ij}^3} - 3 \frac{\mathbf{R}_{ij}(\mathbf{M}_j \mathbf{R}_{ij})}{R_{ij}^5}$$

The inaccuracy is not large and the true long-range nature of the problem is kept [26]. This is due to the fact, that the quadrupole moment of a uniformly magnetized cube is identically zero. Only the next term in a multipole expansion, the octapole term, would give an non-zero contribution [27]

The contributions by the external field and the magnetocrystalline anisotropy to the effective field are straightforward, and they are all summarized in chapter 8.

3.3 Evaluation of the method

Many research groups use the finite difference method for their micromagnetic simulations. The calculation of the demagnetizing field is often done by more advanced methods based on the analytic solution for homogeneously magnetized hexahedra [23] or fast Fourier transformations [28, 29]. However, stiff modes cause deteriorating convergence rates [30].

Another problem arises from complicated geometries (possibly with curved boundaries) and irregular microstructures. As the finite difference method requires the use of a regular lattice, it is difficult to handle curved boundaries, because they are always approximated by small steps. Only recently, the "Embedded Curved Boundary Method" succeeded in generating results similar to those of the finite element method [31, 32].

Chapter 4

The finite element method

The finite element method has become a well established method in many fields of computer aided engineering, such as structural analysis, fluid dynamics, and electromagnetic field computation. However, its flexibility in modeling arbitrary geometries comes at the cost of a more complex mathematical background.

There are tree main steps during the solution of a partial differential equation (PDE) with the finite element method. First, the domain, on which the PDE should be solved, is discretized into finite elements. Depending on the dimension of the problem these can be triangles, squares, or rectangles in two dimensions or tetrahedrons, cubes, or hexahedra for three dimensional problems. The solution of the PDE is approximated by piecewise continuous polynomials and the PDE is hereby discretized and split into a finite number of algebraic equations. Thus, the aim is to determine the unknown coefficients of these polynomials in such a way, that the distance (which is defined by the norm in a suitable vector space) from the exact solution becomes a minimum. Therefore, the finite element method is essentially a minimization technique for variational problems. Since the number of elements is finite, we have reduced the problem of finding a continuous solution for our PDE to calculating the finite number of coefficients of the polynomials.

4.1 Finite element micromagnetics

The solution of Poisson's equation (2.13), which is required to calculate the demagnetizing field $\mathbf{H}_{\mathrm{ms}}$, has to be solved for a given magnetization distribution $\mathbf{M}(\mathbf{r})$. We write Poisson's equation in a more general form

$$\Delta u(\mathbf{r}) = f(\mathbf{r}) \quad . \tag{4.1}$$

In order to apply the finite element method, we have to find a so-called "weak" or variational formulation.

But first we have to define the vector spaces, in which we are searching for a solution [33]. Given a bounded domain Ω, we denote by $L^2(\Omega)$ the space of

quadratically integrable functions defined on Ω. The usual inner product

$$(u, v) := \int_\Omega u(\mathbf{r})v(\mathbf{r})\, d\mathbf{r}$$

induces the norm $\|u\| = \sqrt{(u, u)}$ and $L^2(\Omega)$ becomes a Hilbert space. The space $H^1(\Omega)$ consists of those functions in $L^2(\Omega)$, whose (weak) derivative of order one also lie in $L^2(\Omega)$. The H^1-inner product is defined as

$$(u, v)_1 := \int_\Omega \left(uv + \frac{\partial u}{\partial x}\frac{\partial v}{\partial x} + \frac{\partial u}{\partial y}\frac{\partial v}{\partial y} + \frac{\partial u}{\partial z}\frac{\partial v}{\partial z} \right) d\mathbf{r} = (u, v) + (\nabla u, \nabla v) \quad .$$

The space $H^1(\Omega)$ belongs to a family of function spaces known as Sobolev spaces. They can be physically interpreted as the space of functions of finite energy with respect to the problem under consideration. In this sense, it is the correct space in which to seek solutions of the weak formulation.

Further, we define the trial space S

$$S = \{v \in H^1(\Omega) : v(\mathbf{r}) = g_1(\mathbf{r}) \text{ on } \Gamma\}$$

and the test space or weighting space V

$$V = \{v \in H^1(\Omega) : v(\mathbf{r}) = 0 \text{ on } \Gamma\} \quad .$$

The functions in V are called test functions.

To derive the weak formulation we multiply Poisson's equation (4.1) with a test function $v(\mathbf{r})$ and integrate over the solution domain

$$\int_\Omega \Delta u(\mathbf{r})v(\mathbf{r})\, d\mathbf{r} = \int_\Omega f(\mathbf{r})v(\mathbf{r})\, d\mathbf{r} \quad .$$

Integration by parts gives

$$-\int_\Omega \nabla u(\mathbf{r})\nabla v(\mathbf{r})\, d\mathbf{r} + \int_\Gamma \nabla u(\mathbf{r})v(\mathbf{r})\, d\mathbf{r}_n = \int_\Omega f(\mathbf{r})v(\mathbf{r})\, d\mathbf{r} \quad ,$$

where $\mathbf{r}_n$ denotes the surface normal on the boundary Γ. If appropriate boundary conditions define the values of u (Dirichlet boundary conditions) or of its derivatives $\nabla u =: g$ (Neumann boundary conditions) on the boundary, we can simplify (since v vanishes, where Dirichlet boundary conditions apply)

$$-\int_\Omega \nabla u(\mathbf{r})\nabla v(\mathbf{r})\, d\mathbf{r} + \int_{\Gamma_N} gv(\mathbf{r})\, d\mathbf{r}_n = \int_\Omega f(\mathbf{r})v(\mathbf{r})\, d\mathbf{r} \quad . \tag{4.2}$$

The variational formulation of (4.1) can then be stated in the following general form: Find $u \in S$ such, that

$$a(u, v) = F(v) \quad \forall v \in V \quad , \tag{4.3}$$

where the bilinear form $a(u,v)$ and the linear functional $F(v)$ are given by

$$a(u,v) = -\int_\Omega \nabla u(\mathbf{r})\nabla v(\mathbf{r})\,d\mathbf{r} \quad \text{and} \quad F(v) = -\int_{\Gamma_N} gv(\mathbf{r})\,d\mathbf{r}_n + \int_\Omega f(\mathbf{r})v(\mathbf{r})\,d\mathbf{r}\,. \tag{4.4}$$

We can homogenize the Dirichlet boundary condition by which the trial space, in which the solution u is sought, becomes equivalent to the test space V. Without loss of generality, we can thus assume that we seek the solution in the space V. It is noted, that the weak form is a generalization of the classical formulation. Therefore, the solution of the weak formulation need not be a classical solution at the same time.

Not only Poisson's equation, but a large number of boundary value problems lead to symmetric and positive definite bilinear forms. Also for (4.4) we find

$$a(u,v) = a(v,u) \quad \forall u, v$$

and

$$a(u,u) > 0 \quad \forall u \neq 0 \quad .$$

In this case the weak formulation is equivalent to a minimization problem. u is the sought solution, if it minimizes the functional

$$J(u) = \frac{1}{2}a(u,u) - F(u) \quad .$$

$J(u)$ can often be interpreted as an energy functional. In the context of Poisson's equation for the demagnetizing field (2.13), this functional gives the energy of the magnetization distribution $\mathbf{M}$ in the magnetic field $\mathbf{H}$

$$J(\mathbf{H}) \geq -E(\mathbf{H}) = \mu_0 \int \mathbf{H}\mathbf{M}\,d^3r + \frac{\mu_0}{2}\int \mathbf{H}^2\,d^3r \quad .$$

Minimization of this functional with respect to $\mathbf{H}$ reduces E to the stray field energy E_{ms} and makes $\mathbf{H}$ equal to the self demagnetizing field $\mathbf{H}_{\mathrm{ms}}$ [34].

In general, the trial and test space V is too large and complex to deal with numerically. Thus, the *Galerkin discretization* seeks an approximation of the solution $u_h \in V_h$ by restricting it to a finite dimensional subspace V_h. We rewrite the weak formulation (4.3) as follows: Find $u_h \in V_h$ such, that

$$a(u_h, v) = F(v) \quad \forall v \in V_h \quad . \tag{4.5}$$

The exact solution $u(\mathbf{r})$ shall be approximated by a linear combination of trial functions $\phi_i(\mathbf{r})$ from a finite dimensional subspace V_h of V

$$u_h(\mathbf{r}) = \sum_{i=0}^{n} u_i\phi_i(\mathbf{r}) \quad .$$

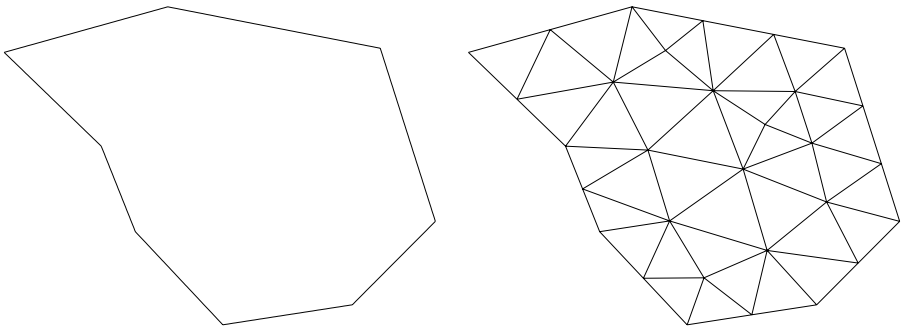

(a) Polygonal domain (b) Triangulation

Figure 4.1: Triangulation of a 2D domain

If we insert this expansion in (4.5), we obtain

$$a(u_h, v) = a\left(\sum_{i=1}^{n} u_i \phi_i, v\right) = \sum_{i=1}^{n} u_i a(\phi_i, v) = F(v_h) \quad \forall v \in V_h \quad . \tag{4.6}$$

Since each basis function ϕ_i lies in V, relation (4.6) holds trivially for $v = \phi_i, i \in \{1, \ldots, N\}$. Conversely, if relation (4.6) holds for each basis function ϕ_i, then it also holds for all $v \in V_h$. Hence it is sufficient to determine the coefficients u_i of u_h such, that

$$\sum_{i=1}^{n} u_i a(\phi_i, \phi_j) = F(\phi_j), \quad j = 1, \ldots, N \quad . \tag{4.7}$$

Therefore we arrive at a linear system of algebraic equations, which can be solved with any standard method, such as the Gauß method, by Cholesky decomposition or iterative schemes like the conjugate gradient method.

The finite element method is a particular Galerkin method [35], which uses piecewise polynomial functions to construct the finite dimensional subspace V_h. The solution domain is divided into many small subdomains, referred to as elements. In two space dimensions these elements are usually triangles (fig. 4.1) or convex quadrilaterals, while in three dimensions tetrahedra, prisms and hexahedra are commonly employed. This subdivision process is usually called triangulation. The collection of all elements is referred to as the finite element mesh or grid.

In the finite element method the basis functions $\phi_i \in V_h$ (fig. 4.2) are chosen in such a way, that

1. The support $\mathrm{supp}(\phi_i) := \overline{\{\mathbf{r} \in \Omega : \phi_i(\mathbf{r}) \neq 0\}}$ of each basis function, i.e. the closure of the set, where ϕ_i is nonzero, is small in the sense, that it consists of only a few (connected) elements. (fig. 4.3)

2. Globally, each function $v \in V_h$ has a simple description in terms of N so called *degrees of freedom* which uniquely characterize v. Each basis function is characterized by possessing exactly one nonvanishing degree of freedom.

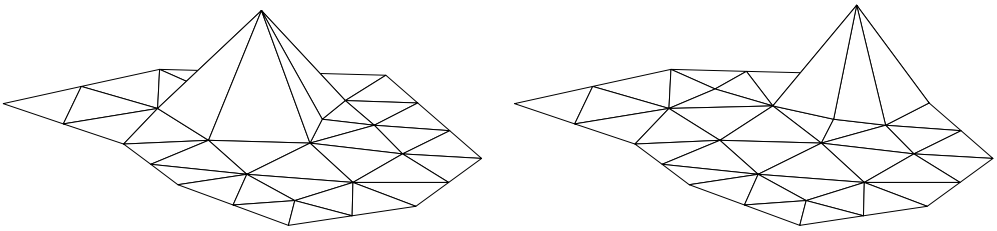

(a) Nodal basis function ϕ_i (b) Nodal basis function ϕ_j

Figure 4.2: Nodal basis functions

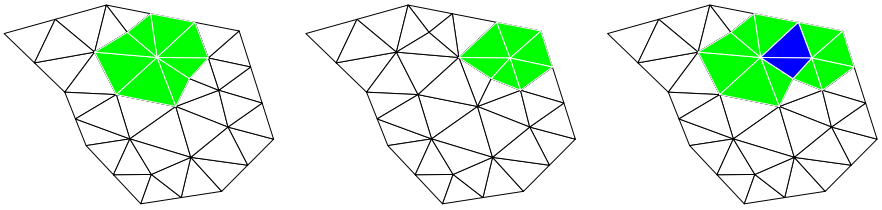

(a) Support of basis function ϕ_i (b) Support of basis function ϕ_j (c) Common support of ϕ_i and ϕ_j

Figure 4.3: Common support of two basis functions

As the support is restricted to a very small local area, the integrals occurring in (4.7) need only be computed over the small support of each basis function. In fact, most of the integrals are zero, and so the matrix of the linear system of algebraic equations is very sparse.

4.2 The open boundary problem

For the solution of partial differential equations like Poisson's equation (4.1), we need boundary conditions to find the physically relevant solution. There are three types of boundary conditions:

Dirichlet boundary conditions

The value of the solution is explicitly defined on the boundary of the solution domain (or part of it). The magnetic scalar potential is usually set to zero along a boundary, which should not be crossed by magnetic flux.

Neumann boundary conditions

The normal derivative of the solution is defined on the boundary. If we set the normal derivative of the magnetic scalar potential to zero, the boundary can be interpreted as an interface with a highly permeable metal. Then, the magnetic flux passes the interface at an angle of 90° to the plane of the interface. In order to find a unique solution, a Dirichlet boundary condition must be defined somewhere on the boundary of the domain.

Robin boundary conditions

This is a combination of the first two. The solution and its derivative are connected by a given function.

Asymptotic boundary conditions

For many problems neither of the three boundary conditions above is suitable: Natural boundary conditions usually set the solution to a distinct value at infinity. However, finite element methods, can only handle finite domains to solve the problem in a computer at finite speed with finite memory.

One workaround is the truncation of outer boundaries. At an arbitrary distance "far enough away" from the area of interest Dirichlet or Neumann boundary conditions are applied. This is very simple, but not very accurate. In addition, it is quite inefficient, because a volume of air, which is much larger than the area of interest, has to be modeled. A fine mesh in the area of interest and a coarse mesh in the exterior can reduce the computational effort again.

Asymptotic boundary conditions transform natural boundary conditions into Robin boundary conditions on the surface of a finite domain. This is achieved by developing the solution into a series expansion of spherical harmonics. Only the leading harmonic is considered, since higher order harmonics decay very quickly.

Hybrid FE/Boundary element method

For the calculation of the magnetic scalar potential the problem of natural boundary conditions applies. Asymptotic boundary conditions require about ten times as many elements for the exterior as for the interior of the magnetic body to obtain a sufficient accuracy [36]. A hybrid finite element/boundary element method combines the advantages of the finite element method (sparse matrices) with those of the boundary element method (no triangulation of the exterior required).

We only know the condition for the potential at the interface between the magnetic body and its surroundings (2.15). The idea of Fredkin and Koehler [37] was to split the magnetic scalar potential U into two parts $U = U_1 + U_2$. The potential U_1 must satisfy Poisson's equation

$$\Delta U_{1,\mathrm{in}} = \nabla \cdot \mathbf{M} \tag{4.8}$$

inside the magnetic body and it is set to zero outside.

$$U_{1,\text{out}} = 0 \quad .$$

The boundary condition on the surface of the magnet (with surface normal $\mathbf{n}$) is

$$\frac{\partial U_{1,\text{in}}}{\partial \mathbf{n}} = -\mathbf{M} \cdot \mathbf{n} \quad . \tag{4.9}$$

U_2 must satisfy Laplace's equation

$$\Delta U_{2,\text{in}} = 0, \quad \Delta U_{2,\text{out}} = 0 \tag{4.10}$$

both, inside and outside the magnetic body. For U_2 we find the boundary condition

$$\frac{\partial U_{2,\text{in}}}{\partial \mathbf{n}} = \frac{\partial U_{2,\text{out}}}{\partial \mathbf{n}}$$

and

$$U_{2,\text{out}} - U_{2,\text{in}} = U_{1,\text{in}} \quad ,$$

which is required by the continuity of the potential U. If we apply the superposition principle, we find, that $U = U_1 + U_2$ satisfies (2.13) and (2.14) and also the boundary condition (2.15) is fulfilled.

Since (4.9) is a simple Neumann boundary condition, we can calculate U_1 from the Poisson equation (4.8) with the standard finite element method. The potential U_2 is equivalent to the potential of a plane of dipoles with moment U_1, in. Hence, the boundary values of U_1 deliver U_2 directly by the boundary integral

$$U_2(\mathbf{r}) = \frac{1}{4\pi} \int \frac{U_1(\mathbf{r}')(\mathbf{r} - \mathbf{r}')}{(\mathbf{r} - \mathbf{r}')^3} \, d\mathbf{n} \quad .$$

In order to save memory, U_2 is evaluated only on the surface of the magnet. These values are used as Dirichlet boundary conditions for the solution of the Laplace equation (4.10).

Chapter 5

Thermal activation

5.1 Stochastic processes

The fundamental equations of classical physics are ordinary or partial differential equations for the observables which describe the state of a system. Newton's equations of classical mechanics, Maxwell's equations of classical electrodynamics, and Einstein's equations of the theory of general relativity describe and predict the state of a system, if the initial and boundary conditions are known. The precision and reliability of these theories were the reason for great scepticism, when the theory of quantum mechanics was developed. Suddenly, it was not possible to calculate the state of a system with arbitrary accuracy. The result of quantum mechanical calculations are probabilities for the happening or non-happening of an event. But also in classical physics there are situations, where it is more adequate to talk about the probability for a certain event or the mean value of an observable, than to calculate the exact trajectories. This is the case when large systems with many degrees of freedom are investigated. Statistical physics uses this paradigm to treat large, complex systems. The well established theory of statistical physics of equilibrium states gives probability distributions for the micro states (characterized by the position and momentum of particles for example), if a certain macro state (defined by energy density, temperature, pressure etc.) is defined.

However, "real life systems" are hardly ever in equilibrium. Usually the observed phenomena are time dependent, or, even if they are stationary, the systems are open due to the exchange of energy or another physical quantity.

In order to describe nonequilibrium systems it is necessary to identify those modes which dominate the time evolution of the system. In complex systems there are usually many different subsystems, which can be characterized by their own dynamics. There are fast, slow and almost steady subsystems. If the time scales are far enough apart, the fast subsystem can be treated as a noise. The almost steady subsystem can be treated as static. So, there is only the slow system left, which has to be considered in greater detail.

For the micromagnetic systems which are considered in this thesis, the influence

of thermal activation is identified with the fast subsystem and can therefore be treated as noise. The almost steady influence can arise from external magnetic fields. The typical time scale for the dynamics of the magnetization is given by the Larmor precession frequency which is in the order of 10^{12} Hz. However, if the switching frequency of external magnetic fields reaches a comparable order of magnitude, it has to be studied in more detail.

This problem is of immediate scientific interest for magnetic recording applications. The increasing data transfer rates and writing speeds require higher frequencies of the applied fields. As the typical frequencies of the recording head currents approach the precession frequency, the process of magnetization switching can be expected to be influenced. The basic theory, algorithms, and programs, which are studied in this thesis, will provide a framework for advanced research and investigations of these phenomena.

5.2 The stochastic Landau-Lifshitz equation

Thermal activation is introduced in the Landau-Lifshitz equation (2.25) by a stochastic thermal field $\mathbf{H}_{\mathrm{th}}$, which is added to the effective field (2.19). It accounts for the effects of the interaction of the magnetization with the microscopic degrees of freedom (eg. phonons, conducting electrons, nuclear spins, etc.), which cause fluctuations of the magnetization distribution. This interaction is also responsible for the damping, since fluctuations and dissipation are related manifestations of one and the same interaction of the magnetization with its environment.

Since a large number of microscopic degrees of freedom contribute to this mechanism, the thermal field is assumed to be a Gaussian random process with the following statistical properties:

$$\langle H_{\mathrm{th},i}(t)\rangle = 0 \tag{5.1}$$

This means, that the average of the thermal field taken over different realizations vanishes in each direction $i \in \{x, y, z\}$ of space. The second moment, or variance, is given by

$$\langle H_{\mathrm{th},i}(t) H_{\mathrm{th},j}(t')\rangle = 2D\delta_{ij}\delta(t - t') \tag{5.2}$$

This equation is a manifestation of the fluctuation-dissipation theorem. It relates the strength of the thermal fluctuations (the thermal field) to the dissipation due to the damping of our system [38]. The Kronecker δ expresses the assumption, that the different components of the thermal field are uncorrelated, whereas the Dirac δ expresses, that the autocorrelation time of the thermal field is much shorter than the response time of the system ("white noise", cf. section 6.1).

After adding the thermal field we get the *stochastic Landau-Lifshitz equation*

$$\frac{d\mathbf{M}}{dt} = -\gamma'\mathbf{M} \times (\mathbf{H}_{\mathrm{eff}} + \mathbf{H}_{\mathrm{th}}) - \frac{\alpha\gamma'}{M_{\mathrm{s}}}\mathbf{M} \times (\mathbf{M} \times (\mathbf{H}_{\mathrm{eff}} + \mathbf{H}_{\mathrm{th}})) \quad . \tag{5.3}$$

Rearrangement to separate deterministic from stochastic contributions gives

$$\begin{aligned}\frac{d\mathbf{M}}{dt} &= -\gamma'\mathbf{M}\times\mathbf{H}_{\text{eff}} - \frac{\alpha\gamma'}{M_{\text{s}}}\mathbf{M}\times(\mathbf{M}\times\mathbf{H}_{\text{eff}}) \\ &\quad -\gamma'\mathbf{M}\times\mathbf{H}_{\text{th}} - \frac{\alpha\gamma'}{M_{\text{s}}}\mathbf{M}\times(\mathbf{M}\times\mathbf{H}_{\text{th}}) \quad , \end{aligned} \tag{5.4}$$

which reveals, that it is a Langevin type stochastic differential equation with multiplicative noise.

To keep the notation simple, we rewrite (5.4) by substituting

$$A_i(\mathbf{M},t) = \left[-\gamma'\mathbf{M}\times\mathbf{H}_{\text{eff}} - \frac{\alpha\gamma'}{M_{\text{s}}}\mathbf{M}\times(\mathbf{M}\times\mathbf{H}_{\text{eff}})\right]_i \tag{5.5}$$

and

$$\begin{aligned}B_{ik}(\mathbf{M},t) &= -\gamma'\varepsilon_{ijk}M_j - \frac{\alpha\gamma'}{M_{\text{s}}}\varepsilon_{ijn}M_j\varepsilon_{nmk}M_m \\ &= -\gamma'\varepsilon_{ijk}M_j - \frac{\alpha\gamma'}{M_{\text{s}}}(\delta_{im}\delta_{jk}-\delta_{ik}\delta_{jm})M_jM_m \\ &= -\gamma'\varepsilon_{ijk}M_j - \frac{\alpha\gamma'}{M_{\text{s}}}(M_iM_k-\delta_{ik}M^2) \quad , \end{aligned} \tag{5.6}$$

where we have written M^2 for $M_{jj} = M_{\text{s}}$. We have used the Einstein summation convention and we will do so in the following. The outer products have been rewritten with the totally antisymmetric unit tensor ε (Levi-Civita symbol).

Hence, we can simplify the stochastic Landau-Lifshitz equation (5.3) and get

$$\frac{dM_i}{dt} = A_i(\mathbf{M},t) + B_{ik}(\mathbf{M},t)H_{\text{th},k}(t) \quad . \tag{5.7}$$

This is the general form of a system of Langevin equations with multiplicative noise, because the multiplicative factor $B_{ik}(\mathbf{M},t)$ for the stochastic process $H_{\text{th},k}(t)$ is a function of $\mathbf{M}$.

Chapter 6

Stochastic calculus

As we have seen in chapter 5, the effect of thermal activation can be introduced in the formalism of micromagnetics by adding a random fluctuation field to the effective magnetic field. A trajectory of the magnetization can be obtained by integrating the equation of motion. However, in addition to the well known deterministic terms we also have a stochastic contribution.

6.1 Gaussian white noise

It is assumed that the thermal activation is caused by perturbations of very high frequency. "Very high" means in this case that the frequency is well above the typical precession frequency of the magnetization vector. Thus, the fluctuating field, which is used to simulate the effect of thermal activation, is represented by a stochastic process. It is assumed to be Gaussian white noise, because the fluctuations emerge from the interaction of the magnetization with a large number of independent microscopic degrees of freedom with equivalent stochastic properties (eg. phonons, conducting electrons, nuclear spins, etc.) [39]. As a result of the central limit theorem, the fluctuation field is Gaussian distributed.

A stochastic process $\eta(t)$ is called Gaussian white noise [40], if its time average is zero

$$\langle \eta(t) \rangle = 0$$

and the two time covariance function is given by

$$\langle \eta(t)\eta(t+\tau) \rangle = \sigma^2 \delta(\tau) \quad . \tag{6.1}$$

For the Fourier transform of the stationary two time covariance function we obtain

$$\begin{aligned} F(\omega) &= \int d\tau \, \langle \eta(t)\eta(t+\tau) \rangle e^{i\omega\tau} = & (6.2) \\ &= \sigma^2 \int d\tau \, \delta(\tau) e^{i\omega\tau} = & (6.3) \\ &= \sigma^2 \quad . & (6.4) \end{aligned}$$

In other words it does not depend on ω, because there is no correlation in time. This is why it is called "white" noise.

6.2 Stochastic differential equations

For simplicity let us assume a one dimensional stochastic differential equation with additive noise [41]

$$\frac{dX(t)}{dt} = a(X(t),t) + \eta(t) \quad .$$

$a(X(t),t)$ in this *Langevin equation* can be interpreted as a deterministic or averaged drift term perturbed by a noisy diffusive term $\eta(t)$ which is a Gaussian random variable.

For the increase dX during a time step dt we get (to first order)

$$dX(t) = a(X(t),t)\,dt + dW(t) \tag{6.5}$$

with

$$dW(t) = \int_t^{t+dt} \eta(t')\,dt' \quad .$$

If we interpret the above integral as a limit of a sum, then dW is a Gaussian random variable, because it is the sum of Gaussian random variables. Thus,

$$\langle dW(t) \rangle = 0$$

and (cf. eqn. (6.1))

$$\begin{aligned} \langle (\,dW(t)\,)^2 \rangle &= \int_t^{t+dt} dt_1 \int_t^{t+dt} dt_2\, \langle \eta(t_1)\eta(t_2) \rangle & (6.6)\\ &= \int_t^{t+dt} dt_1 \int_t^{t+dt} dt_2\, \sigma^2 \delta(t_1 - t_2) & (6.7)\\ &= \sigma^2\,dt \quad . & (6.8) \end{aligned}$$

As long as the intervals $[t, t+dt\,]$ and $[t', t'+dt\,]$ do not overlap, which is true for successive time steps, we get

$$\langle\, dW(t)\; dW(t')\,\rangle = 0 \quad .$$

It should be emphasized, that only the second moment of $dW(t)$ is linear in dt. $dW(t)$ is only of the order of $\sqrt{dt}$. This important aspect is made clear by writing

$$dW(t) = \sigma\eta(t)\sqrt{dt}$$

where $\eta(t)$ denotes a Gaussian random variable.

6.3 Interpretation of stochastic integrals

Let us assume a one dimensional stochastic differential equation with *multiplicative* noise [41]

$$\frac{dX(t)}{dt} = a(X(t),t) + b(X(t),t)\,\eta(t) \quad . \tag{6.9}$$

The increment dX during a short time interval dt is given by

$$dX(t) \;= \int_t^{t+\,dt} a(X(t'),t')\,dt' + \int_t^{t+\,dt} b(X(t'),t')\eta(t')\,dt' \quad .$$

The second term, which is a stochastic integral, has to be investigated in more detail. We can evaluate the integrand at the beginning of the interval $[t, t+\,dt\,]$, multiply it by the length of the interval and use the result as the increment for small dt. Thus, we obtain

$$dX(t) \;= a\Big(X(t),t\Big)\,dt \;+ b\Big(X(t),t\Big)\eta(t)\sqrt{dt} \quad ,$$

where $\eta(t)$ is a standard Gaussian random variable at each discrete time step with

$$\langle \eta(t)\eta(t')\rangle = \delta(t,t') \quad .$$

For $b(X(t),t) = \sigma = \text{const.}$, that is the case for additive noise, it is equivalent to equation (6.5).

However, we could also evaluate the integrand b at any other time t' in the interval $[t, t+\,dt\,]$ and at

$$\begin{aligned} \bar{X}(t) &= (1-\alpha)X(t) + \alpha X(t+\,dt\,) = \\ &= (1-\alpha)X(t) + \alpha\Big(X(t) + \,dX(t)\Big) = \\ &= X(t) + \alpha\,dX(t) \end{aligned} \tag{6.10}$$

In this general case we get for the increment $dX(t)$ an implicit expression

$$dX(t) \;= a\Big(\bar{X}(t),t'\Big)\,dt \;+ b\Big(X(t) + \alpha\,dX(t)\,,t'\Big)\eta(t)\sqrt{dt} \quad .$$

With the abbreviation $b' = \partial b(X,t)/\partial X$ we get

$$\begin{aligned} b\Big(X(t) + \alpha\,dX(t)\,,t'\Big)\eta(t)\sqrt{dt} &= b\Big(X(t),t\Big)\eta(t)\sqrt{dt} + \\ &\quad \alpha b'\Big(X(t),t'\Big)\,dX(t)\,\eta(t)\sqrt{dt} + \cdots \\ &= b\Big(X(t),t\Big)\eta(t)\sqrt{dt} + \\ &\quad \alpha b'\Big(X(t),t'\Big)b\Big(X(t),t'\Big)\eta^2(t)\sqrt{dt} + \\ &\quad O(\,dt^{3/2}\,) \end{aligned} \tag{6.11}$$

(6.12)

Finally, we get for the increment $dX(t)$

$$\begin{aligned} dX(t) &= \Big[a\Big(X(t),t\Big) + \alpha b'\Big(X(t),t\Big)b\Big(X(t),t\Big)\eta^2(t)\Big]\, dt \,+ \\ &\quad b\Big(X(t),t\Big)\eta(t)\sqrt{dt}\,. \end{aligned} \tag{6.13}$$

In this equation we find an additional drift term, which contains α and $\eta^2(t)$. The latter can be replaced by 1 for terms up to the order of dt . Depending on the choice of α and the interpretation of the integral, we get different drift terms.

If we set $\alpha = 0$, we get

$$dX(t) = a(X(t),t)\,dt + b(X(t),t)\eta(t)\sqrt{dt} \tag{6.14}$$

and we call it the *Itô interpretation* of the stochastic differential equation

$$\dot{X}(t) = a(X(t),t) + b(X(t),t)\eta(t) \quad . \tag{6.15}$$

For $\alpha = 1/2$, we get

$$\begin{aligned} dX(t) &= \left[a(X(t),t) + \frac{1}{2}b'(X(t),t)b(X(t),t)\right]\, dt \,+ \\ &\quad b(X(t),t)\eta(t)\sqrt{dt} \end{aligned} \tag{6.16}$$

and we call it the *Stratonovich interpretation*, which is indicated by writing

$$\dot{X}(t) = a(X(t),t) + b(X(t),t) \circ \eta(t) \quad . \tag{6.17}$$

Thus, we have to distinguish between the interpretation of a stochastic differential equation and the version, in which it is written. The stochastic differential equation (6.17) can be written in an Itô version using (6.16) as

$$\dot{X}(t) = a(X(t),t) + \frac{1}{2}b(X(t),t)b'(X(t),t) + b(X(t),t)\eta(t) \tag{6.18}$$

where we find the noise induced drift term

$$\frac{1}{2}b(X(t),t)b'(X(t),t) \quad . \tag{6.19}$$

Reversely, (6.15) can be written in a Stratonovich version as

$$\begin{aligned} \dot{X}(t) &= a(X(t),t) - \frac{1}{2}b(X(t),t)b'(X(t),t) + b(X(t),t) \circ \eta(t) \\ &= \bar{a}(X(t),t) + b(X(t),t) \circ \eta(t) \quad . \end{aligned} \tag{6.20}$$

Due to the different drift terms, the two interpretations yield different dynamical properties [41]. Itô calculus is commonly chosen on certain mathematical grounds, since rather general results of probability theory can then be employed. On the

other hand, white noise is usually an idealization of physical (coloured) noise with short autocorrelation time, in which case the two time covariance function is given by

$$\langle \eta(t)\eta(t+\tau)\rangle = \frac{\sigma^2}{2m}\mathrm{e}^{-m|\tau|}$$

with a short time constant m^{-1}.

The Wong-Zakai-Theorem [42] then says, that in the formal zero-correlation-time limit

$$\sigma \to \sigma m \quad , \quad m \to \infty$$

the coloured noise becomes white noise and we obtain the Stratonovich-Interpretation for the stochastic differential equation. The results coincide with those obtained in the limit of fluctuations with finite autocorrelation time. Therefore, Stratonovich calculus is usually preferred in physical applications.

6.4 Taylor expansions

In the two time covariance function (6.1) there appears a Dirac-delta function. This is a consequence of the fact, that a stochastic process is a distribution rather than a simple function. Therefore, a random variable is not differentiable and we cannot use the standard Taylor expansions. Instead we must use integration expansions, which are given below for the Itô and Stratonovich interpretation.

6.4.1 Itô-Taylor expansion

The Itô-Taylor expansion of an Itô process of the form (6.9) is given by [40]

$$\begin{aligned}
X(t) &= X(t_0) + aI_{(0)} + bI_{(1)} + \left(aa' + \frac{1}{2}b^2a''\right) I_{(0,0)} \\
&\quad + \left(ab' + \frac{1}{2}b^2b''\right) I_{(0,1)} + ba'I_{(1,0)} + bb'I_{(1,1)} \\
&\quad + \Bigg[a\left(aa'' + a'^2 + bb'a'' + \frac{1}{2}b^2a'''\right) \\
&\qquad + \frac{1}{2}b^2(aa''' + 3a'a'' + (b'^2 + bb'')a'' + 2bb'a''') + \frac{1}{4}b^4a^{(4)}\Bigg] I_{(0,0,0)} \\
&\quad + \Bigg[a\left(a'b' + ab'' + bb'b'' + \frac{1}{2}b^2b'''\right) \\
&\qquad + \frac{1}{2}b^2(a''b' + 2a'b'' + ab''' + (b'^2 + bb'')b'' + 2bb'b''') + \frac{1}{2}b^2b^{(4)}\Bigg] I_{(0,0,1)} \\
&\quad + \left[a\left(b'a' + ba''\right) + \frac{1}{2}b^2(b''a' + 2b'a'' + ba''')\right] I_{(0,1,0)} \\
&\quad + \left[a\left(b'^2 + bb''\right) + \frac{1}{2}b^2(b''b' + 2bb'' + bb''')\right] I_{(0,1,1)}
\end{aligned}$$

$$
\begin{aligned}
&+b\left(aa'' + a'^2 + bb'a'' + \frac{1}{2}b^2a'''\right) I_{(1,0,0)} \\
&+b\left(ab'' + a'b' + bb'b'' + \frac{1}{2}b^2b'''\right) I_{(1,0,1)} \\
&+b(a'b' + a''b)I_{(1,1,0)} + b(b'^2 + bb'')I_{(1,1,1)} + R \quad .
\end{aligned} \tag{6.21}
$$

The Itô integrals $I_{(j_1,j_2,\ldots)}$ are defined as

$$
\begin{aligned}
I_{(0)} &= \int_{t_0}^{t} dt' \\
I_{(1)} &= \int_{t_0}^{t} dW(t') \\
I_{(0,0)} &= \int_{t_0}^{t}\int_{t_0}^{s} dt'\ ds \\
I_{(0,1)} &= \int_{t_0}^{t}\int_{t_0}^{s} dt'\ dW(s) \\
I_{(1,1)} &= \int_{t_0}^{t}\int_{t_0}^{s} dW(t')\ dW(s) \\
&\vdots
\end{aligned}
$$

6.4.2 Stratonovich-Taylor expansion

The Stratonovich-Taylor expansion of a Stratonovich process of the form (6.20) is given by [40]

$$
\begin{aligned}
X(t) = \; & X(t_0) + \bar{a}J_{(0)} + bJ_{(1)} + +\bar{a}\bar{a}'J_{(0,0)} + \bar{a}b'J_{(0,1)} + b\bar{a}'J_{(1,0)} \\
&+bb'J_{(1,1)} + \bar{a}(\bar{a}\bar{a}'' + \bar{a}'^2)J_{(0,0,0)} + \bar{a}(\bar{a}b'' + \bar{a}'b')J_{(0,0,1)} \\
&+\bar{a}(\bar{a}''b + \bar{a}'b')J_{(0,1,0)} + b(\bar{a}\bar{a}'' + \bar{a}'^2)J_{(1,0,0)} \\
&+\bar{a}(bb'' + b'^2)J_{(0,1,1)} + b(\bar{a}b'' + \bar{a}'b')J_{(1,0,1)} \\
&+b(\bar{a}''b + \bar{a}'b')J_{(1,1,0)} + b(bb'' + b'^2)J_{(1,1,1)} + R
\end{aligned} \tag{6.22}
$$

The Stratonovich integrals $J_{(j_1,j_2,\ldots)}$ are defined as

$$
\begin{aligned}
J_{(0)} &= I_{(0)} \\
J_{(1)} &= I_{(1)} \\
J_{(0,0)} &= I_{(0,0)} \\
J_{(0,1)} &= I_{(0,1)} \\
J_{(1,1)} &= I_{(1,1)} + \frac{1}{2}I_{(1,1)}I_{(0)} \\
J_{(j_1,j_2,j_3)} &= I_{(j_1,j_2,\ldots)} + \frac{1}{2}(I_{\{j_1=j_2\neq 0\}}I_{(0,j_3)} + I_{\{j_2=j_3\neq 0\}}I_{(j_1,0)}) \\
&\vdots
\end{aligned}
$$

6.5 The Fokker-Planck equation

The Fokker-Planck equation, which describes the time evolution of the nonequilibrium probability distribution $P(\mathbf{M},t)$ of a set of Langevin equations like (5.7), in the Stratonovich interpretation is given by [39]

$$\frac{\partial P}{\partial t} = -\frac{\partial}{\partial M_i}\left[\left(A_i + DB_{jk}\frac{\partial B_{ik}}{\partial M_j}\right)P\right] + \frac{\partial^2}{\partial M_i \partial M_j}\left[(DB_{ik}B_{jk})\,P\right] \quad , \tag{6.23}$$

where Stratonovich calculus has been used to treat the multiplicative fluctuating terms in (5.7). We can transform it to a continuity equation for the probability distribution by taking the M_j derivatives of the second term on the right-hand side

$$\frac{\partial P}{\partial t} = -\frac{\partial}{\partial M_i}\left[\left(A_i - DB_{ik}\frac{\partial B_{jk}}{\partial M_j} - DB_{ik}B_{jk}\frac{\partial}{\partial M_j}\right)P\right] \quad . \tag{6.24}$$

On using expression (5.6) we find

$$\frac{\partial B_{ik}}{\partial M_j} = -\gamma'\varepsilon_{ijk} - \frac{\alpha\gamma'}{M_{\rm s}}(\delta_{ij}M_k + \delta_{jk}M_i - 2\delta ik M_j) \quad . \tag{6.25}$$

Thus,

$$\begin{aligned}\frac{\partial B_{jk}}{\partial M_j} &= -\gamma'\varepsilon_{jjk} - \frac{\alpha\gamma'}{M_{\rm s}}(\delta_{jj}M_k + \delta_{jk}M_j - 2M_k) \\ &= -\frac{\alpha\gamma'}{M_{\rm s}}2M_k \end{aligned} \tag{6.26}$$

and

$$\begin{aligned}B_{ik}\frac{\partial B_{jk}}{\partial M_j} &= \left[-\gamma'\varepsilon_{ijk}M_j + \frac{\alpha\gamma'}{M_{\rm s}}(M_iM_k - \delta_{ik}M^2)\right]\left(-2\frac{\alpha\gamma'}{M_{\rm s}}M_k\right) \\ &= \frac{\alpha\gamma'}{M_{\rm s}}(M_iM_kM_k - \delta_{ik}M^2M_k)\left(-2\frac{\alpha\gamma'}{M_{\rm s}}\right) \\ &= 0 \quad . \end{aligned} \tag{6.27}$$

We find, that the second term on the right hand side of (6.24) vanishes identically. For the third term we find

$$\begin{aligned}B_{ik}B_{jk}\frac{\partial P}{\partial M_j} &= \gamma'^2\left[-\varepsilon_{ilk}M_l - \frac{\alpha}{M_{\rm s}}(M_iM_k - \delta_{ik}M^2)\right]\cdot \\ &\qquad \left[-\varepsilon_{jpk}M_p - \frac{\alpha}{M_{\rm s}}(M_jM_k - \delta_{jk}M^2)\right]\frac{\partial P}{\partial M_j} \\ &= \gamma'^2\Big[(\delta_{ij}\delta_{lp} - \delta_{ip}\delta_{jl})M_lM_p \end{aligned}$$

$$
\begin{aligned}
&+\frac{\alpha}{M_{\rm s}}\left(-M^2\varepsilon_{jpi}M_p+\varepsilon_{jpk}M_iM_pM_k-M^2\varepsilon_{ilj}M_l+\varepsilon_{ilk}M_lM_jM_k\right)\\
&+\frac{\alpha^2}{M_{\rm s}^2}\left(M^4\delta_{ik}\delta_{jk}-M^2(\delta_{jk}M_iM_k+\delta_{ik}M_jM_k)+M_iM_jM^2\right)\Bigg]\frac{\partial P}{\partial M_j}\\
= \;& \gamma'^2\Bigg[\delta_{ij}M^2-M_iM_j+\frac{\alpha}{M_{\rm s}}\left(-M^2\varepsilon_{jpi}M_p-M^2\varepsilon_{ilj}M_l\right)\\
&\quad+\frac{\alpha^2}{M_{\rm s}^2}\left(M^4\delta_{ij}-M^2M_iM_j\right)\Bigg]\frac{\partial P}{\partial M_j}\\
= \;& \gamma'^2\left[(\alpha^2+1)(M^2\delta_{ij}-M_iM_j)\frac{\partial P}{\partial M_j}\right]\\
= \;& -\gamma'^2(\alpha^2+1)\left[\mathbf{M}\times\left(\mathbf{M}\times\frac{\partial P}{\partial M_j}\right)\right]_i \quad . \qquad (6.28)
\end{aligned}
$$

Our result for the Fokker-Planck equation is

$$
\begin{aligned}
\frac{\partial P}{\partial t} \;=\; & -\frac{\partial}{\partial\mathbf{M}}\cdot\Bigg\{\Bigg[-\gamma'\mathbf{M}\times\mathbf{H}_{\rm eff}-\frac{\alpha\gamma'}{M_{\rm s}}\mathbf{M}\times(\mathbf{M}\times\mathbf{H}_{\rm eff})\\
&+\frac{1}{2\tau_N}\mathbf{M}\times\left(\mathbf{M}\times\frac{\partial}{\partial\mathbf{M}}\right)\Bigg]P\Bigg\} \quad , \qquad (6.29)
\end{aligned}
$$

where $P(\mathbf{M},t)$ is the nonequilibrium probability distribution for $\mathbf{M}$ at time t, and $\frac{\partial}{\partial\mathbf{M}}\cdot$ stands for the divergence operator

$$\frac{\partial}{\partial\mathbf{M}}\cdot\mathbf{A}=\frac{\partial A_i}{\partial M_i}$$

and

$$\frac{1}{\tau_N}=2D\gamma'^2(1+\alpha^2) \qquad (6.30)$$

is the Néel (free-diffusion) time.

Finally, we have to ensure, that the stationary properties of the stochastic Landau-Lifshitz equation (5.3), supplemented by the statistical properties of the thermal field (5.1) and (5.2), coincide with the appropriate thermal-equilibrium properties. Therefore, the stationary solution of the Fokker-Planck equation P_0, for which

$$\partial P_0/\partial t=0$$

is forced to be the Boltzmann distribution

$$P_0(\mathbf{M})\propto\exp(-\beta\mathcal{H}(\mathbf{M})) \quad . \qquad (6.31)$$

Since

$$\mu_0 v\mathbf{H}_{\rm eff}=-\frac{\partial\mathcal{H}}{\partial\mathbf{M}} \quad ,$$

where v denotes the discretization volume (the volume of a computational cell) we find

$$\frac{\partial P_0}{\partial \mathbf{M}} = \beta \mu_0 v \mathbf{H}_{\text{eff}} P_0 \quad .$$

Hence,

$$\begin{aligned} \left[\frac{\partial}{\partial \mathbf{M}} \cdot \left(\mathbf{M} \times \frac{\partial P_0}{\partial \mathbf{M}}\right)\right]_i &= \\ \partial_{M_i}(\varepsilon_{ijk} M_j \partial_{M_k} P_0) &= \varepsilon_{ijk}(\delta_{ij}\partial_{M_k} P_0 + M_j \partial_{M_i}\partial_{M_k} P_0) = \\ &= \varepsilon_{iik}\partial_{M_k} P_0 + M_j \varepsilon_{ijk}\partial_{M_i}\partial_{M_k} P_0 \\ &= 0 \end{aligned} \tag{6.32}$$

and the first term on the right hand side of the Fokker-Planck equation (6.29) vanishes.

Thus, the Fokker-Planck equation with the stationary solution P_0 reads

$$0 = \left[-\frac{\alpha\gamma'}{M_{\text{s}}}\mathbf{M} \times (\mathbf{M} \times \mathbf{H}_{\text{eff}})P_0 + \frac{1}{2\tau_N}\mathbf{M} \times (\mathbf{M} \times \beta\mu_0 v \mathbf{H}_{\text{eff}} P_0)\right]$$

from which we find

$$\tau_N = \frac{1}{\alpha}\frac{\mu_0 v M}{2\gamma' k_B T} \quad .$$

By comparison with (6.30) we arrive at

$$D = \frac{\alpha}{1+\alpha^2}\frac{k_B T}{\mu_0 v \gamma' M} \quad , \tag{6.33}$$

which was defined in (5.2) and determines the variance of the thermal field.

Chapter 7

Numerical time integration methods

7.1 Deterministic integration schemes

7.1.1 Fixpoint iteration

This method is suitable for static energy minimization. If one is only interested in finding a minimum of the Landau free energy (2.18), but does not want to consider domain wall motion for example, the modified fixpoint iteration provides a simple algorithm.

Brown's equations (2.20) can be written in an algebraic form as

$$\{H\}\mathbf{m} = 0 \quad ,$$

where $\{H\}$ stands for a matrix. However, this matrix is not constant, because the effective field depends on the magnetization. Therefore, we cannot apply a standard method, like the Jacobi or Gauß-Seidel method. A modified iterative technique has been proposed by LaBonte [43], which is used in a simplified form.

First, the effective field (2.19) in each subdivision of the magnetic body is calculated. Then the magnetization vector in each subdivision is rotated to the direction of the effective field at that position. After all subdivisions have been updated, the maximum angle of this rotation in any one of them is compared with a preset tolerance. Unless the maximum angle is smaller than the tolerance, the effective field is recalculated, the magnetization updated again, and so on.

This "LaBonte-like" method can be extended by an under- or overrelaxation factor. In the former case, the magnetization vectors are not fully rotated into the direction of the effective field (fig. 7.1(a)), whereas in the latter, the magnetization vector "overtakes" the vector of the effective field (fig. 7.1(b)). For this method, the damping term of the dynamic Landau-Lifshitz equation (2.25) can be used. It has been applied for the simulation of the μmag standard problem #3, which is described in section 8.1.1.

(a) Underrelaxation (b) Overrelaxation

Figure 7.1: In the fixpoint iteration method the magnetization vectors are rotated towards the effective field.

7.2 Stochastic integration schemes

The mere translation of a numerical scheme valid for deterministic differential equations does not necessarily yield a proper scheme in the stochastic case. Depending on the selected deterministic scheme its unconditional translation might converge to an Itô solution, to a Stratonovich solution, or to none of them. Even if the scheme converges in the context of stochastic calculus, the order of convergence is usually lower than that of the deterministic scheme. This has to be considered, when deciding for the discretization time step.

7.2.1 Euler scheme

We shall consider an Itô process $X = \{X(t), t_0 \leq t \leq T\}$ satisfying the scalar stochastic differential equation with multiplicative noise

$$dX(t) = a(X(t), t)\, dt \; + b(X(t), t)\, dW(t)$$

on $t_0 \leq t \leq T$ with the initial value

$$X(t_0) = X_0 \quad .$$

For a given discretization $t_0 = \tau_0 < \tau_1 < \cdots < \tau_n < \cdots < \tau_N = T$ of the time interval $[t_0, T]$, an *Euler approximation* [40] is a continuous time stochastic process $Y = \{Y(t), t_0 \leq t \leq T\}$ satisfying the iterative scheme

$$Y_{n+1} = Y_n + a(\tau_n, Y_n)\Delta_n + b(\tau_n, Y_n)\Delta W_n \quad , \tag{7.1}$$

for $n = 0, 1, 2, \ldots, N-1$ with initial value

$$Y_0 = X_0 \quad ,$$

where $Y_n = Y(\tau_n)$, $\Delta_n = \tau_{n+1} - \tau_n$ denotes the time discretization interval, and $\Delta W_n = W_{\tau_{n+1}} - W_{\tau_n}$ is the increment of the stochastic process.

In other words it does not depend on ω, because there is no correlation in time. This is why it is called "white" noise.

6.2 Stochastic differential equations

For simplicity let us assume a one dimensional stochastic differential equation with additive noise [41]

$$\frac{dX(t)}{dt} = a(X(t),t) + \eta(t) \quad .$$

$a(X(t),t)$ in this *Langevin equation* can be interpreted as a deterministic or averaged drift term perturbed by a noisy diffusive term $\eta(t)$ which is a Gaussian random variable.

For the increase dX during a time step dt we get (to first order)

$$dX(t) = a(X(t),t)\,dt + dW(t) \tag{6.5}$$

with

$$dW(t) = \int_t^{t+dt} \eta(t')\,dt' \quad .$$

If we interpret the above integral as a limit of a sum, then dW is a Gaussian random variable, because it is the sum of Gaussian random variables. Thus,

$$\langle dW(t) \rangle = 0$$

and (cf. eqn. (6.1))

$$\begin{aligned} \langle (\,dW(t)\,)^2 \rangle &= \int_t^{t+dt} dt_1 \int_t^{t+dt} dt_2\, \langle \eta(t_1)\eta(t_2) \rangle & (6.6)\\ &= \int_t^{t+dt} dt_1 \int_t^{t+dt} dt_2\, \sigma^2 \delta(t_1 - t_2) & (6.7)\\ &= \sigma^2\,dt \quad . & (6.8) \end{aligned}$$

As long as the intervals $[t, t+dt\,]$ and $[t', t'+dt\,]$ do not overlap, which is true for successive time steps, we get

$$\langle\, dW(t)\; dW(t')\,\rangle = 0 \quad .$$

It should be emphasized, that only the second moment of $dW(t)$ is linear in dt. $dW(t)$ is only of the order of $\sqrt{dt}$. This important aspect is made clear by writing

$$dW(t) = \sigma\eta(t)\sqrt{dt}$$

where $\eta(t)$ denotes a Gaussian random variable.

6.3 Interpretation of stochastic integrals

Let us assume a one dimensional stochastic differential equation with *multiplicative* noise [41]

$$\frac{dX(t)}{dt} = a(X(t),t) + b(X(t),t)\,\eta(t) \quad . \tag{6.9}$$

The increment dX during a short time interval dt is given by

$$dX(t) \;= \int_t^{t+\,dt} a(X(t'),t')\,dt' + \int_t^{t+\,dt} b(X(t'),t')\eta(t')\,dt' \quad .$$

The second term, which is a stochastic integral, has to be investigated in more detail. We can evaluate the integrand at the beginning of the interval $[t, t+\,dt\,]$, multiply it by the length of the interval and use the result as the increment for small dt. Thus, we obtain

$$dX(t) \;= a\Big(X(t),t\Big)\,dt \;+ b\Big(X(t),t\Big)\eta(t)\sqrt{dt} \quad ,$$

where $\eta(t)$ is a standard Gaussian random variable at each discrete time step with

$$\langle \eta(t)\eta(t')\rangle = \delta(t,t') \quad .$$

For $b(X(t),t) = \sigma = \text{const.}$, that is the case for additive noise, it is equivalent to equation (6.5).

However, we could also evaluate the integrand b at any other time t' in the interval $[t, t+\,dt\,]$ and at

$$\begin{aligned} \bar{X}(t) &= (1-\alpha)X(t) + \alpha X(t+\,dt\,) = \\ &= (1-\alpha)X(t) + \alpha\Big(X(t) + \,dX(t)\Big) = \\ &= X(t) + \alpha\,dX(t) \end{aligned} \tag{6.10}$$

In this general case we get for the increment $dX(t)$ an implicit expression

$$dX(t) \;= a\Big(\bar{X}(t),t'\Big)\,dt \;+ b\Big(X(t) + \alpha\,dX(t)\,,t'\Big)\eta(t)\sqrt{dt} \quad .$$

With the abbreviation $b' = \partial b(X,t)/\partial X$ we get

$$\begin{aligned} b\Big(X(t) + \alpha\,dX(t)\,,t'\Big)\eta(t)\sqrt{dt} &= b\Big(X(t),t\Big)\eta(t)\sqrt{dt} + \\ &\quad \alpha b'\Big(X(t),t'\Big)\,dX(t)\,\eta(t)\sqrt{dt} + \cdots \\ &= b\Big(X(t),t\Big)\eta(t)\sqrt{dt} + \\ &\quad \alpha b'\Big(X(t),t'\Big)b\Big(X(t),t'\Big)\eta^2(t)\sqrt{dt} + \\ &\quad O(\,dt^{3/2}\,) \end{aligned} \tag{6.11}$$

(6.12)

Finally, we get for the increment $dX(t)$

$$\begin{aligned} dX(t) &= \Big[a\Big(X(t),t\Big) + \alpha b'\Big(X(t),t\Big)b\Big(X(t),t\Big)\eta^2(t)\Big]\, dt \,+ \\ &\quad b\Big(X(t),t\Big)\eta(t)\sqrt{dt}\,. \end{aligned} \tag{6.13}$$

In this equation we find an additional drift term, which contains α and $\eta^2(t)$. The latter can be replaced by 1 for terms up to the order of dt . Depending on the choice of α and the interpretation of the integral, we get different drift terms.

If we set $\alpha = 0$, we get

$$dX(t) = a(X(t),t)\,dt + b(X(t),t)\eta(t)\sqrt{dt} \tag{6.14}$$

and we call it the *Itô interpretation* of the stochastic differential equation

$$\dot{X}(t) = a(X(t),t) + b(X(t),t)\eta(t) \quad . \tag{6.15}$$

For $\alpha = 1/2$, we get

$$\begin{aligned} dX(t) &= \left[a(X(t),t) + \frac{1}{2}b'(X(t),t)b(X(t),t)\right]\, dt \,+ \\ &\quad b(X(t),t)\eta(t)\sqrt{dt} \end{aligned} \tag{6.16}$$

and we call it the *Stratonovich interpretation*, which is indicated by writing

$$\dot{X}(t) = a(X(t),t) + b(X(t),t) \circ \eta(t) \quad . \tag{6.17}$$

Thus, we have to distinguish between the interpretation of a stochastic differential equation and the version, in which it is written. The stochastic differential equation (6.17) can be written in an Itô version using (6.16) as

$$\dot{X}(t) = a(X(t),t) + \frac{1}{2}b(X(t),t)b'(X(t),t) + b(X(t),t)\eta(t) \tag{6.18}$$

where we find the noise induced drift term

$$\frac{1}{2}b(X(t),t)b'(X(t),t) \quad . \tag{6.19}$$

Reversely, (6.15) can be written in a Stratonovich version as

$$\begin{aligned} \dot{X}(t) &= a(X(t),t) - \frac{1}{2}b(X(t),t)b'(X(t),t) + b(X(t),t) \circ \eta(t) \\ &= \bar{a}(X(t),t) + b(X(t),t) \circ \eta(t) \quad . \end{aligned} \tag{6.20}$$

Due to the different drift terms, the two interpretations yield different dynamical properties [41]. Itô calculus is commonly chosen on certain mathematical grounds, since rather general results of probability theory can then be employed. On the

other hand, white noise is usually an idealization of physical (coloured) noise with short autocorrelation time, in which case the two time covariance function is given by

$$\langle \eta(t)\eta(t+\tau)\rangle = \frac{\sigma^2}{2m}\mathrm{e}^{-m|\tau|}$$

with a short time constant m^{-1}.

The Wong-Zakai-Theorem [42] then says, that in the formal zero-correlation-time limit

$$\sigma \to \sigma m \quad , \quad m \to \infty$$

the coloured noise becomes white noise and we obtain the Stratonovich-Interpretation for the stochastic differential equation. The results coincide with those obtained in the limit of fluctuations with finite autocorrelation time. Therefore, Stratonovich calculus is usually preferred in physical applications.

6.4 Taylor expansions

In the two time covariance function (6.1) there appears a Dirac-delta function. This is a consequence of the fact, that a stochastic process is a distribution rather than a simple function. Therefore, a random variable is not differentiable and we cannot use the standard Taylor expansions. Instead we must use integration expansions, which are given below for the Itô and Stratonovich interpretation.

6.4.1 Itô-Taylor expansion

The Itô-Taylor expansion of an Itô process of the form (6.9) is given by [40]

$$\begin{aligned}
X(t) &= X(t_0) + aI_{(0)} + bI_{(1)} + \left(aa' + \frac{1}{2}b^2a''\right) I_{(0,0)} \\
&\quad + \left(ab' + \frac{1}{2}b^2b''\right) I_{(0,1)} + ba'I_{(1,0)} + bb'I_{(1,1)} \\
&\quad + \Bigg[a\left(aa'' + a'^2 + bb'a'' + \frac{1}{2}b^2a'''\right) \\
&\qquad + \frac{1}{2}b^2(aa''' + 3a'a'' + (b'^2 + bb'')a'' + 2bb'a''') + \frac{1}{4}b^4a^{(4)}\Bigg] I_{(0,0,0)} \\
&\quad + \Bigg[a\left(a'b' + ab'' + bb'b'' + \frac{1}{2}b^2b'''\right) \\
&\qquad + \frac{1}{2}b^2(a''b' + 2a'b'' + ab''' + (b'^2 + bb'')b'' + 2bb'b''') + \frac{1}{2}b^2b^{(4)}\Bigg] I_{(0,0,1)} \\
&\quad + \left[a\left(b'a' + ba''\right) + \frac{1}{2}b^2(b''a' + 2b'a'' + ba''')\right] I_{(0,1,0)} \\
&\quad + \left[a\left(b'^2 + bb''\right) + \frac{1}{2}b^2(b''b' + 2bb'' + bb''')\right] I_{(0,1,1)}
\end{aligned}$$

$$
\begin{aligned}
&+b\left(aa'' + a'^2 + bb'a'' + \frac{1}{2}b^2a'''\right) I_{(1,0,0)} \\
&+b\left(ab'' + a'b' + bb'b'' + \frac{1}{2}b^2b'''\right) I_{(1,0,1)} \\
&+b(a'b' + a''b)I_{(1,1,0)} + b(b'^2 + bb'')I_{(1,1,1)} + R \quad .
\end{aligned} \tag{6.21}
$$

The Itô integrals $I_{(j_1,j_2,\ldots)}$ are defined as

$$
\begin{aligned}
I_{(0)} &= \int_{t_0}^{t} dt' \\
I_{(1)} &= \int_{t_0}^{t} dW(t') \\
I_{(0,0)} &= \int_{t_0}^{t}\int_{t_0}^{s} dt'\ ds \\
I_{(0,1)} &= \int_{t_0}^{t}\int_{t_0}^{s} dt'\ dW(s) \\
I_{(1,1)} &= \int_{t_0}^{t}\int_{t_0}^{s} dW(t')\ dW(s) \\
&\vdots
\end{aligned}
$$

6.4.2 Stratonovich-Taylor expansion

The Stratonovich-Taylor expansion of a Stratonovich process of the form (6.20) is given by [40]

$$
\begin{aligned}
X(t) = \; & X(t_0) + \bar{a}J_{(0)} + bJ_{(1)} + +\bar{a}\bar{a}'J_{(0,0)} + \bar{a}b'J_{(0,1)} + b\bar{a}'J_{(1,0)} \\
&+bb'J_{(1,1)} + \bar{a}(\bar{a}\bar{a}'' + \bar{a}'^2)J_{(0,0,0)} + \bar{a}(\bar{a}b'' + \bar{a}'b')J_{(0,0,1)} \\
&+\bar{a}(\bar{a}''b + \bar{a}'b')J_{(0,1,0)} + b(\bar{a}\bar{a}'' + \bar{a}'^2)J_{(1,0,0)} \\
&+\bar{a}(bb'' + b'^2)J_{(0,1,1)} + b(\bar{a}b'' + \bar{a}'b')J_{(1,0,1)} \\
&+b(\bar{a}''b + \bar{a}'b')J_{(1,1,0)} + b(bb'' + b'^2)J_{(1,1,1)} + R
\end{aligned} \tag{6.22}
$$

The Stratonovich integrals $J_{(j_1,j_2,\ldots)}$ are defined as

$$
\begin{aligned}
J_{(0)} &= I_{(0)} \\
J_{(1)} &= I_{(1)} \\
J_{(0,0)} &= I_{(0,0)} \\
J_{(0,1)} &= I_{(0,1)} \\
J_{(1,1)} &= I_{(1,1)} + \frac{1}{2}I_{(1,1)}I_{(0)} \\
J_{(j_1,j_2,j_3)} &= I_{(j_1,j_2,\ldots)} + \frac{1}{2}(I_{\{j_1=j_2\neq 0\}}I_{(0,j_3)} + I_{\{j_2=j_3\neq 0\}}I_{(j_1,0)}) \\
&\vdots
\end{aligned}
$$

6.5 The Fokker-Planck equation

The Fokker-Planck equation, which describes the time evolution of the nonequilibrium probability distribution $P(\mathbf{M},t)$ of a set of Langevin equations like (5.7), in the Stratonovich interpretation is given by [39]

$$\frac{\partial P}{\partial t} = -\frac{\partial}{\partial M_i}\left[\left(A_i + DB_{jk}\frac{\partial B_{ik}}{\partial M_j}\right)P\right] + \frac{\partial^2}{\partial M_i \partial M_j}\left[(DB_{ik}B_{jk})\,P\right] \quad , \tag{6.23}$$

where Stratonovich calculus has been used to treat the multiplicative fluctuating terms in (5.7). We can transform it to a continuity equation for the probability distribution by taking the M_j derivatives of the second term on the right-hand side

$$\frac{\partial P}{\partial t} = -\frac{\partial}{\partial M_i}\left[\left(A_i - DB_{ik}\frac{\partial B_{jk}}{\partial M_j} - DB_{ik}B_{jk}\frac{\partial}{\partial M_j}\right)P\right] \quad . \tag{6.24}$$

On using expression (5.6) we find

$$\frac{\partial B_{ik}}{\partial M_j} = -\gamma'\varepsilon_{ijk} - \frac{\alpha\gamma'}{M_{\rm s}}(\delta_{ij}M_k + \delta_{jk}M_i - 2\delta ik M_j) \quad . \tag{6.25}$$

Thus,

$$\begin{aligned}\frac{\partial B_{jk}}{\partial M_j} &= -\gamma'\varepsilon_{jjk} - \frac{\alpha\gamma'}{M_{\rm s}}(\delta_{jj}M_k + \delta_{jk}M_j - 2M_k) \\ &= -\frac{\alpha\gamma'}{M_{\rm s}}2M_k \end{aligned} \tag{6.26}$$

and

$$\begin{aligned}B_{ik}\frac{\partial B_{jk}}{\partial M_j} &= \left[-\gamma'\varepsilon_{ijk}M_j + \frac{\alpha\gamma'}{M_{\rm s}}(M_iM_k - \delta_{ik}M^2)\right]\left(-2\frac{\alpha\gamma'}{M_{\rm s}}M_k\right) \\ &= \frac{\alpha\gamma'}{M_{\rm s}}(M_iM_kM_k - \delta_{ik}M^2M_k)\left(-2\frac{\alpha\gamma'}{M_{\rm s}}\right) \\ &= 0 \quad . \end{aligned} \tag{6.27}$$

We find, that the second term on the right hand side of (6.24) vanishes identically. For the third term we find

$$\begin{aligned}B_{ik}B_{jk}\frac{\partial P}{\partial M_j} &= \gamma'^2\left[-\varepsilon_{ilk}M_l - \frac{\alpha}{M_{\rm s}}(M_iM_k - \delta_{ik}M^2)\right]\cdot \\ &\qquad \left[-\varepsilon_{jpk}M_p - \frac{\alpha}{M_{\rm s}}(M_jM_k - \delta_{jk}M^2)\right]\frac{\partial P}{\partial M_j} \\ &= \gamma'^2\Big[(\delta_{ij}\delta_{lp} - \delta_{ip}\delta_{jl})M_lM_p \end{aligned}$$

$$
\begin{aligned}
&+\frac{\alpha}{M_{\rm s}}\left(-M^2\varepsilon_{jpi}M_p+\varepsilon_{jpk}M_iM_pM_k-M^2\varepsilon_{ilj}M_l+\varepsilon_{ilk}M_lM_jM_k\right)\\
&+\frac{\alpha^2}{M_{\rm s}^2}\left(M^4\delta_{ik}\delta_{jk}-M^2(\delta_{jk}M_iM_k+\delta_{ik}M_jM_k)+M_iM_jM^2\right)\Bigg]\frac{\partial P}{\partial M_j}\\
= \;& \gamma'^2\Bigg[\delta_{ij}M^2-M_iM_j+\frac{\alpha}{M_{\rm s}}\left(-M^2\varepsilon_{jpi}M_p-M^2\varepsilon_{ilj}M_l\right)\\
&\quad+\frac{\alpha^2}{M_{\rm s}^2}\left(M^4\delta_{ij}-M^2M_iM_j\right)\Bigg]\frac{\partial P}{\partial M_j}\\
= \;& \gamma'^2\left[(\alpha^2+1)(M^2\delta_{ij}-M_iM_j)\frac{\partial P}{\partial M_j}\right]\\
= \;& -\gamma'^2(\alpha^2+1)\left[\mathbf{M}\times\left(\mathbf{M}\times\frac{\partial P}{\partial M_j}\right)\right]_i \quad . \qquad (6.28)
\end{aligned}
$$

Our result for the Fokker-Planck equation is

$$
\begin{aligned}
\frac{\partial P}{\partial t} \;=\; & -\frac{\partial}{\partial\mathbf{M}}\cdot\Bigg\{\Bigg[-\gamma'\mathbf{M}\times\mathbf{H}_{\rm eff}-\frac{\alpha\gamma'}{M_{\rm s}}\mathbf{M}\times(\mathbf{M}\times\mathbf{H}_{\rm eff})\\
&+\frac{1}{2\tau_N}\mathbf{M}\times\left(\mathbf{M}\times\frac{\partial}{\partial\mathbf{M}}\right)\Bigg]P\Bigg\} \quad , \qquad (6.29)
\end{aligned}
$$

where $P(\mathbf{M},t)$ is the nonequilibrium probability distribution for $\mathbf{M}$ at time t, and $\frac{\partial}{\partial\mathbf{M}}\cdot$ stands for the divergence operator

$$\frac{\partial}{\partial\mathbf{M}}\cdot\mathbf{A}=\frac{\partial A_i}{\partial M_i}$$

and

$$\frac{1}{\tau_N}=2D\gamma'^2(1+\alpha^2) \qquad (6.30)$$

is the Néel (free-diffusion) time.

Finally, we have to ensure, that the stationary properties of the stochastic Landau-Lifshitz equation (5.3), supplemented by the statistical properties of the thermal field (5.1) and (5.2), coincide with the appropriate thermal-equilibrium properties. Therefore, the stationary solution of the Fokker-Planck equation P_0, for which

$$\partial P_0/\partial t=0$$

is forced to be the Boltzmann distribution

$$P_0(\mathbf{M})\propto\exp(-\beta\mathcal{H}(\mathbf{M})) \quad . \qquad (6.31)$$

Since

$$\mu_0 v\mathbf{H}_{\rm eff}=-\frac{\partial\mathcal{H}}{\partial\mathbf{M}} \quad ,$$

where v denotes the discretization volume (the volume of a computational cell) we find

$$\frac{\partial P_0}{\partial \mathbf{M}} = \beta \mu_0 v \mathbf{H}_{\text{eff}} P_0 \quad .$$

Hence,

$$\begin{aligned} \left[\frac{\partial}{\partial \mathbf{M}} \cdot \left(\mathbf{M} \times \frac{\partial P_0}{\partial \mathbf{M}}\right)\right]_i &= \\ \partial_{M_i}(\varepsilon_{ijk} M_j \partial_{M_k} P_0) &= \varepsilon_{ijk}(\delta_{ij}\partial_{M_k} P_0 + M_j \partial_{M_i}\partial_{M_k} P_0) = \\ &= \varepsilon_{iik}\partial_{M_k} P_0 + M_j \varepsilon_{ijk}\partial_{M_i}\partial_{M_k} P_0 \\ &= 0 \end{aligned} \tag{6.32}$$

and the first term on the right hand side of the Fokker-Planck equation (6.29) vanishes.

Thus, the Fokker-Planck equation with the stationary solution P_0 reads

$$0 = \left[-\frac{\alpha\gamma'}{M_{\text{s}}}\mathbf{M} \times (\mathbf{M} \times \mathbf{H}_{\text{eff}})P_0 + \frac{1}{2\tau_N}\mathbf{M} \times (\mathbf{M} \times \beta\mu_0 v \mathbf{H}_{\text{eff}} P_0)\right]$$

from which we find

$$\tau_N = \frac{1}{\alpha}\frac{\mu_0 v M}{2\gamma' k_B T} \quad .$$

By comparison with (6.30) we arrive at

$$D = \frac{\alpha}{1+\alpha^2}\frac{k_B T}{\mu_0 v \gamma' M} \quad , \tag{6.33}$$

which was defined in (5.2) and determines the variance of the thermal field.

Chapter 7

Numerical time integration methods

7.1 Deterministic integration schemes

7.1.1 Fixpoint iteration

This method is suitable for static energy minimization. If one is only interested in finding a minimum of the Landau free energy (2.18), but does not want to consider domain wall motion for example, the modified fixpoint iteration provides a simple algorithm.

Brown's equations (2.20) can be written in an algebraic form as

$$\{H\}\mathbf{m} = 0 \quad ,$$

where $\{H\}$ stands for a matrix. However, this matrix is not constant, because the effective field depends on the magnetization. Therefore, we cannot apply a standard method, like the Jacobi or Gauß-Seidel method. A modified iterative technique has been proposed by LaBonte [43], which is used in a simplified form.

First, the effective field (2.19) in each subdivision of the magnetic body is calculated. Then the magnetization vector in each subdivision is rotated to the direction of the effective field at that position. After all subdivisions have been updated, the maximum angle of this rotation in any one of them is compared with a preset tolerance. Unless the maximum angle is smaller than the tolerance, the effective field is recalculated, the magnetization updated again, and so on.

This "LaBonte-like" method can be extended by an under- or overrelaxation factor. In the former case, the magnetization vectors are not fully rotated into the direction of the effective field (fig. 7.1(a)), whereas in the latter, the magnetization vector "overtakes" the vector of the effective field (fig. 7.1(b)). For this method, the damping term of the dynamic Landau-Lifshitz equation (2.25) can be used. It has been applied for the simulation of the μmag standard problem #3, which is described in section 8.1.1.

(a) Underrelaxation (b) Overrelaxation

Figure 7.1: In the fixpoint iteration method the magnetization vectors are rotated towards the effective field.

7.2 Stochastic integration schemes

The mere translation of a numerical scheme valid for deterministic differential equations does not necessarily yield a proper scheme in the stochastic case. Depending on the selected deterministic scheme its unconditional translation might converge to an Itô solution, to a Stratonovich solution, or to none of them. Even if the scheme converges in the context of stochastic calculus, the order of convergence is usually lower than that of the deterministic scheme. This has to be considered, when deciding for the discretization time step.

7.2.1 Euler scheme

We shall consider an Itô process $X = \{X(t), t_0 \leq t \leq T\}$ satisfying the scalar stochastic differential equation with multiplicative noise

$$dX(t) = a(X(t), t)\, dt \; + b(X(t), t)\, dW(t)$$

on $t_0 \leq t \leq T$ with the initial value

$$X(t_0) = X_0 \quad .$$

For a given discretization $t_0 = \tau_0 < \tau_1 < \cdots < \tau_n < \cdots < \tau_N = T$ of the time interval $[t_0, T]$, an *Euler approximation* [40] is a continuous time stochastic process $Y = \{Y(t), t_0 \leq t \leq T\}$ satisfying the iterative scheme

$$Y_{n+1} = Y_n + a(\tau_n, Y_n)\Delta_n + b(\tau_n, Y_n)\Delta W_n \quad , \tag{7.1}$$

for $n = 0, 1, 2, \ldots, N-1$ with initial value

$$Y_0 = X_0 \quad ,$$

where $Y_n = Y(\tau_n)$, $\Delta_n = \tau_{n+1} - \tau_n$ denotes the time discretization interval, and $\Delta W_n = W_{\tau_{n+1}} - W_{\tau_n}$ is the increment of the stochastic process.

If $b \equiv 0$, that is if the diffusion coefficient is identically zero, the stochastic iterative scheme (7.1) reduces to the deterministic Euler scheme for the ordinary differential equation

$$\frac{dx}{dt} = a(x,t) \quad .$$

The random increments ΔW_n are independent Gaussian random variables with mean

$$\langle \Delta W_n \rangle = 0$$

and variance

$$\langle (\Delta W_n)^2 \rangle = \tau_{n+1} - \tau_n \quad . \tag{7.2}$$

For the integration of the Langevin equation (5.7) with constant step size Δt the Euler scheme results in

$$M_i = M_i(t) + A_i(\mathbf{M},t)\Delta t + B_{ik}(\mathbf{M},t)\Delta W_k \tag{7.3}$$

with

$$\langle \Delta W_k \rangle = 0\,, \quad \langle \Delta W_k \Delta W_l \rangle = 2D\delta_{kl}\Delta t \quad .$$

In the context of Stratonovich stochastic calculus the deterministic drift has to be augmented by a noise induced drift term (6.19) which gives

$$M_i(t+\Delta t) = M_i(t) + \left[A_i(\mathbf{M},t) + 2D\frac{1}{2}B_{jk}\frac{\partial B_{ik}}{\partial M_j} \right] \Delta t + B_{ik}(\mathbf{M},t)\Delta W_k \quad . \tag{7.4}$$

However, in the presence of the stochastic term the order of convergence of the stochastic Euler scheme is lower than that of the deterministic scheme.

A time discrete approximation Y^δ with maximum step size δ *converges strongly* to X at time T if

$$\lim_{\delta \downarrow 0} \langle |X(T) - Y^\delta(T)| \rangle = 0 \quad .$$

If there exists a positive constant C, which does not depend on δ, and a $\delta_0 > 0$ such that

$$\langle |X(T) - Y^\delta(T)| \rangle \leq C\delta^\gamma \tag{7.5}$$

for each $\delta \in (0, \delta_0)$, the time discrete approximation Y^δ is said to *converge strongly with order* $\gamma > 0$ at time T.

If the drift and diffusion coefficients are almost constant, the Euler scheme gives good numerical results. In practice this is rarely the case and then the results can become very poor, because it converges with an order of 0.5 only [40]. (Notice, that the corresponding deterministic scheme has an order of 1.) Therefore, it is recommended to use higher order schemes.

7.2.2 Milshtein scheme

The Milshtein scheme [44] is obtained by adding the term

$$bb' I_{(1,1)} = \frac{1}{2} bb' \left[(\Delta W)^2 - \Delta t \right]$$

from the Itô-Taylor expansion (6.21) to the Euler scheme (7.1).

$$Y_{n+1} = Y_n + a\Delta t + b\Delta W + \frac{1}{2} bb' \left[(\Delta W)^2 - \Delta t \right] \quad . \tag{7.6}$$

The *same* scheme is found for the Stratonovich interpretation from the Stratonovich-Taylor expansion (6.22) with (6.20)

$$Y_{n+1} = Y_n + \bar{a}\Delta t + b\Delta W + \frac{1}{2} bb' (\Delta W)^2 \quad , \tag{7.7}$$

where

$$\bar{a} = a - \frac{1}{2} bb' \quad .$$

The addition of this term increases the order of strong convergence from 0.5 for the Euler scheme to 1 for the Milshtein scheme. It corresponds to that of the deterministic Euler scheme without any noise, that is with $b \equiv 0$. Thus, the Milshtein scheme can be interpreted as the proper generalization of the deterministic Euler scheme for the strong order convergence criterion (7.5).

The generalization for our multidimensional Langevin equation (5.7) gives

$$M_i(t+\Delta t) = M_i(t) + A_i(\mathbf{M}, t)\Delta t + B_{ik}(\mathbf{M}, t)\Delta W_k + \frac{1}{2} B_{jk} \frac{\partial B_{ik}}{\partial M_j} (\Delta W_k)^2 \quad . \tag{7.8}$$

For the noise induced drift term we get

$$\begin{aligned}
B_{jk}\frac{\partial B_{ik}}{\partial M_j} &= \left(-\gamma' \varepsilon_{jlk} M_l - \frac{\alpha\gamma'}{M_\mathrm{s}} (M_j M_k - \delta_{jk} M_\mathrm{s}^2) \right) \\
&\quad \left(-\gamma' \varepsilon_{ijk} - \frac{\alpha\gamma'}{M_\mathrm{s}} (\delta_{ij} M_k + \delta_{jk} M_i - 2\delta_{ik} M_j) \right) \\
&= \gamma'^2 \varepsilon_{jlk}\varepsilon_{ijk} M_l + \\
&\quad \frac{\alpha\gamma'^2}{M_\mathrm{s}} (\varepsilon_{jlk}\delta_{ij} M_k M_l + \varepsilon_{jlk}\delta_{jk} M_i M_l - 2\delta_{ik}\varepsilon_{jlk} M_l M_j \\
&\qquad + \varepsilon_{ijk} M_j M_k - \varepsilon_{ijk}\delta_{jk} M_\mathrm{s}^2) + \\
&\quad \frac{\alpha^2\gamma'^2}{M_\mathrm{s}^2} (\delta_{ij} M_j M_k M_k + \delta_{jk} M_i M_j M_k - 2\delta_{ik} M_k M^2 \\
&\quad - \delta_{jk}\delta_{ij} M_k M_\mathrm{s}^2 - \delta_{jk}\delta_{jk} M_i M_\mathrm{s}^2 + 2\delta_{ik}\delta_{jk} M_j M^2) \\
&= -\gamma'^2 2\delta_{il} M_l + \alpha^2\gamma'^2 (-2\delta_{ij} M_i) \\
&= -\gamma'^2 2(1+\alpha^2) M_i
\end{aligned} \tag{7.9}$$

The additional stochastic term of the Milshtein scheme (7.8) corresponds to the drift term of the Euler scheme in Stratonovich interpretation (7.4) [45]. In the Euler scheme this term is

$$2D\frac{1}{2}B_{jk}\frac{\partial B_{ik}}{\partial M_j}\Delta t$$

whereas in the Milshtein scheme it reads as

$$\frac{1}{2}B_{jk}\frac{\partial B_{ik}}{\partial M_j}(\Delta W_k)^2 \quad .$$

So, the term $(\Delta W_k)^2$ is replaced by its mean value $\langle(\Delta W_k)^2\rangle$, which is $2D\Delta t$ according to (7.2). This small modification accounts for the difference in the order of convergence. However, if one is interested only in computing the moments $\langle M_i^k\rangle$, for example, it can be shown, that the Euler and Milshtein algorithm are of equal accuracy. However, since both algorithms have approximately the same computational complexity, it does not seem to be justified to use the poorer Euler algorithm instead of the Milshtein algorithm.

7.2.3 Heun scheme

The improved Euler or Heun method [39] is an example of a predictor-corrector method. The predictor is given by a simple Euler type integration. If we consider the Langevin equation (5.7), the predictor is

$$\bar{M}_i = M_i(t) + A_i(\mathbf{M},t)\Delta t + B_{ik}(\mathbf{M},t)\Delta W_k \quad . \tag{7.10}$$

Δt is the discretization time step and

$$\Delta W_k = \int_t^{t+\Delta t} H_{\mathrm{th},k}(t')\,dt'$$

are Gaussian random numbers, whose first two moments are given by

$$\langle \Delta W_k\rangle = 0\,, \quad \langle \Delta W_k \Delta W_l\rangle = 2D\delta_{kl}\Delta t$$

$2D$ is the variance of the stochastic thermal field (5.2), which is given by (6.33).

The Heun scheme is then given by

$$\begin{aligned} M_i(t+\Delta t) &= M_i(t) + \frac{1}{2}\left[A_i(\bar{\mathbf{M}},t+\Delta t) + A_i(\mathbf{M},t)\right]\Delta t + \\ &\quad \frac{1}{2}\left[B_{ik}(\bar{\mathbf{M}},t+\Delta t) + B_{ik}(\mathbf{M},t)\right]\Delta W_k \quad . \end{aligned} \tag{7.11}$$

The stochastic Heun scheme converges in quadratic mean to the solution of the general system of Langevin equations (5.7) when interpreted in the sense of Stratonovich.

To conclude, there are two main reasons for the choice of the Heun scheme for the numerical integration of the stochastic Landau-Lifshitz equation: First, the Heun scheme yields Stratonovich solutions of the stochastic differential equations without alterations to the deterministic drift term. Secondly, the deterministic part of the differential equations is integrated with a second order accuracy in Δt, which renders the Heun scheme numerically more stable than Euler type schemes.

7.2.4 Higher order integration schemes

We can obtain more accurate Taylor schemes by including further multiple stochastic integrals from the stochastic Taylor expansions (6.21) and (6.22) [40]. However, their development and implementation is very tedious and in general the improvement in accuracy is not needed. This is so, because one has to solve numerically the Langevin equations and average the results for different realizations of the noise. This generates a source of statistical errors which are in many occasions greater than the systematic errors due to the order of convergence of the numerical method. So it is usually better to spend the computer time in reducing the statistical errors by increasing the number of samples in the average rather than using a more complicated higher order algorithm [45].

7.3 Pseudo-random number generators

The numerical simulation of stochastic processes requires the generation of a large number of random variables. These can be taken from real random variables, which are generated by tossing a die (for small scale simulations) or measuring the noisy voltage drop over a resistor. The advent of digital computers lead to the development of simple, fast, and reproducible deterministic algorithms to generate sequences of random variables. As it is a deterministic procedure in a (hopefully) deterministic machine the numbers are not truly random. However, a good algorithm will produce sequences which resemble random numbers in most properties, in which case they are called *pseudo-random numbers*.

7.3.1 Uniform distribution

Many computer systems are supplied with random number generators in their standard libraries. These are usually *linear congruential pseudo-random number generators* [41], which generate a sequence of integers $I_1, I_2, I_3, \ldots$, each between 0 and $m-1$ by the recurrence relation

$$I_{j+1} = aI_j + c \pmod{m} \quad .$$

The multiplier a and the increment c are positive integers and the modulus m is a large number. If these three parameters are properly chosen, the sequence will be of

maximal length, that is of length m. In that case, all integers between 0 and $m-1$ appear, before the sequence is repeated. Thus, any initial seed I_0 is as good as any other. In order to have a uniform distribution in the interval $[0,1[$, generally I_{j+1}/m is returned. It is clear from the recursive form, that $I_{j+1} = m$ cannot occur and therefore I_{j+1}/m is strictly less than 1.

The quality of this random number generator depends only on the parameters in the recurrence relation, and it is satisfactory for many applications, but far from perfect. For example, successive numbers differ by a multiple, which is orders of magnitude smaller than the modulus. These low-order correlations are removed by shuffling the output. A random deviate derived from the jth value in the sequence, I_j, is output not on the jth call, but rather on a randomized later call.

If even longer random sequences are needed, two different sequences can be combined to obtain a new sequence, whose period is the least common multiple of the two periods. When implementing a random number generator, special care must be taken of the machine's maximum value for an integer number and the size of the mantissa in the floating-point representation.

Thus, the quality of a random number generator should only be limited by its period.

7.3.2 Gaussian distribution

If the random numbers are required to obey a certain distribution function, the transformation method [46] can be applied. By transforming uniformly distributed random numbers, random variables with any probability distribution, given that the indefinite integral is known and invertible, can be generated.

Suppose, we generate uniform deviates $x_1,\ x_2,\ \ldots$ and take some functions $y_1(x_1,\ x_2,\ \ldots),\ y_2(x_1,\ x_2, \ldots),\ \ldots$ of it. The joint probability distribution of the y's is given by the fundamental law of probability

$$|p(y_1,\ y_2, \ldots)\, dy_1\ dy_2\ \ldots| = |p(x_1,\ x_2, \ldots)\, dx_1\ dx_2\ \ldots|$$

or equivalently

$$p(y_1,\ y_2, \ldots)\, dy_1\ dy_2\ \ldots = p(x_1,\ x_2, \ldots) \left|\frac{\partial(x_1,\ x_2, \ldots)}{\partial(y_1,\ y_2, \ldots)}\right| dy_1\ dy_2\ \ldots$$

The Box-Müller method uses this technique to generate random deviates with normal (Gaussian) distribution,

$$p(y)\, dy\ = \frac{1}{2\pi} \mathrm{e}^{-y^2/2}\, dy \quad .$$

The transformation between two uniform random deviates x_1 and x_2 on $(0,1)$ and two quantities y_1 and y_2 is given by

$$y_1 \ = \ \sqrt{-2\ln x_1}\cos(2\pi x_2) \tag{7.12}$$

$$y_2 \ = \ \sqrt{-2\ln x_1}\sin(2\pi x_2) \tag{7.13}$$

or

$$x_1 = \mathrm{e}^{-\frac{1}{2}(y_1^2+y_2^2)} \tag{7.14}$$

$$x_2 = \frac{1}{2\pi}\arctan\left(\frac{y_2}{y_1}\right) \tag{7.15}$$

For the Jacobian determinant we get

$$\left|\frac{\partial(x_2,\, x_2)}{\partial(y_2,\, y_2)}\right| = \frac{1}{\sqrt{2\pi}}\mathrm{e}^{-\frac{1}{2}y_1^2}\frac{1}{\sqrt{2\pi}}\mathrm{e}^{-\frac{1}{2}y_2^2} \quad .$$

Since this is a product of a function of y_1 alone and a function of y_2 alone, each y is an independent Gaussian random variable.

The implementation of these algorithms in the Numerical Recipes [46] and the NAG library [47] have been used for the implementation of the stochastic thermal field.

Chapter 8

Implementation

8.1 Finite difference model

In order to test the time integration techniques a finite difference model has been implemented.

Hexahedral magnetic particles are discretized into cubic computational cells. Each computational cell has a magnetic moment which is the product of its volume and the saturation magnetization of the material. The time evolution of the magnetization is obtained by integrating the Landau-Lifshitz-Gilbert equation (2.25) for each computational cell.

The local magnetic field is calculated after each time step for each computational cell and includes the

External field

$$\mathbf{H}_{\text{ext}}$$

$\mathbf{H}$	(A/m)	

Anisotropy field

$$\mathbf{H}_{\text{ani}} = \frac{2K_1}{\mu_0 M_{\text{s}}^2}\mathbf{a}(\mathbf{M}\cdot\mathbf{a})$$

K_1	(J/m^3)	first anisotropy constant,
μ_0	$= 4\pi 10^{-7}$ Vs/(Am)	magnetic field constant,
M_{s}	(A/m)	saturation magnetization,
$\mathbf{a}$		unit vector in direction of the easy axis,
$\mathbf{M}$	(A/m)	magnetization vector of the computational cell

Exchange field

$$\mathbf{H}_{\text{exch}} = \sum_{j}^{NN} \frac{2A}{\Delta x^2} \mathbf{M}_j$$

NN		sum is taken over all nearest neighbours,
j		index of the nearest neighbour,
A	(J/m)	exchange constant,
Δx	(m)	nearest neighbour distance,
$\mathbf{M}_j$	(A/m)	magnetization vector of the nearest neighbour j

Dipole field

$$\mathbf{H}_{\text{dip}} = -\frac{\Delta x^3}{4\pi} \sum_{j}{}' \left(\frac{\mathbf{M}_j}{R_j^3} - 3\frac{\mathbf{R}_j(\mathbf{M}_j\mathbf{R}_j)}{R_j^5} \right)$$

Δx	(m)	edge length of a cubic computational cell,
Σ'		sum over all other computational cells,
j		index of computational cell j,
$\mathbf{M}_j$	(A/m)	magnetization vector of computational cell j,
$\mathbf{R}_j$	(m)	vector from the current computational cell (for which the local field is calculated) to the computational cell j

Thermal field

$$\mathbf{H}_{\text{th}} = \eta \sqrt{2\frac{\alpha}{1+\alpha^2}\frac{k_B T}{\mu_0 \gamma' \Delta x^3 M_{\text{s}} \Delta t}}$$

η	1	standard Gaussian process with mean zero and variance 1
α		damping constant,
k_B	(J/K)	Boltzmann's constant,
T	(K)	Temperature,
γ'	(1/Ts)	gyromagnetic ratio (2.24),
Δx^3	(m^3)	discretization volume
Δt	(s)	step size of time integration

Then, the equation of motion (2.25) is integrated for each computational cell for a certain discrete time step. Since the magnetization distribution has changed, the effective field is calculated again, before the next time integration step is performed.

8.1.1 μmag standard problem #3

This problem has been chosen to verify the equilibrium states obtained by the finite difference program. A lattice of $11 \times 11 \times 11$ magnetic moments and the fixpoint iteration method (section 7.1.1) have been used to calculate the equilibrium states.

The μmag standard problem #3 [48] consists in calculating the single domain limit of a cubic magnetic particle. This is the size of equal energy for the so-called flower state (fig. 8.1(a)) on the one hand, and the vortex or curling state (fig. 8.1(b)) on the other hand. The easy axis of magnetocrystalline anisotropy is parallel to a principal axis of the cube. The uniaxial anisotropy constant is given by $K_\mathrm{u} = 0.1\,K_\mathrm{m}$, where $K_\mathrm{m} = \frac{1}{2}\mu_0 M_\mathrm{s}^2$ is a magnetostatic energy density.

The results are given in the column marked "FD" in tables 8.1, 8.2, and 8.3 and compared with those published by Rave et al. [49], Ribeiro et al. and Hertel et al. on the web page of NIST [48]. The partial energies are given in units of K_m, the magnetization in units of M_s, and the single domain limit L in units of $l_\mathrm{ex} = \sqrt{A/K_\mathrm{m}}$, where A is the exchange constant.

	Rave	Martins	Hertel	FD
E_demag	0.2794	0.2792	0.2839	0.2807
E_exch	0.0177	0.0177	0.0158	0.0175
E_ani	0.0056	0.0056	0.0052	0.0054
$\langle M_x \rangle$	0.000			
$\langle M_y \rangle$	0.000			
$\langle M_z \rangle$	0.971	0.9710	0.973	0.972

Table 8.1: Flower state, partial energy densities and average magnetization

	Rave	Martins	Hertel	FD
E_demag	0.0783	0.0780	0.0830	0.0756
E_exch	0.1723	0.1724	0.1696	0.1761
E_ani	0.0521	0.0521	0.0522	0.0519
$\langle M_x \rangle$	0.000			
$\langle M_y \rangle$	0.352	0.3516	0.351	0.348
$\langle M_z \rangle$	0.000			

Table 8.2: Vortex state, partial energy densities and average magnetization

	Rave	Martins	Hertel	FD
L	8.47	8.4687	8.52	8.32

Table 8.3: Single domain limit

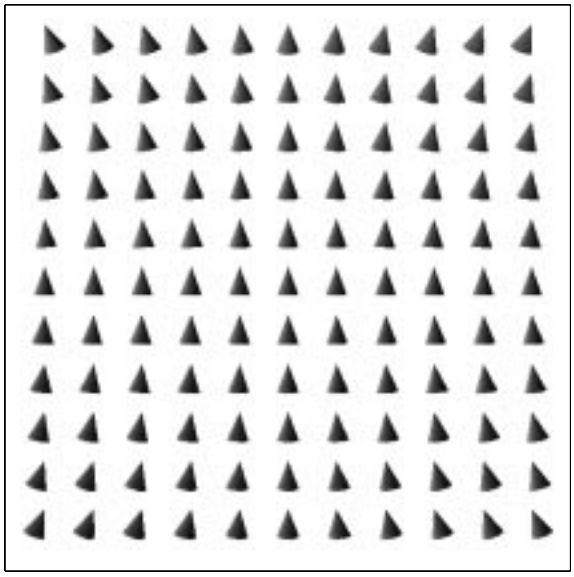

(a) flower state

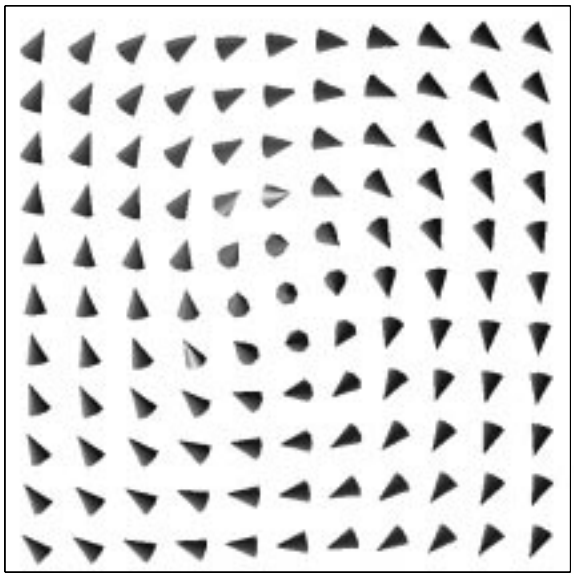

(b) vortex state

Figure 8.1: Magnetization configurations in the μmag standard problem #3

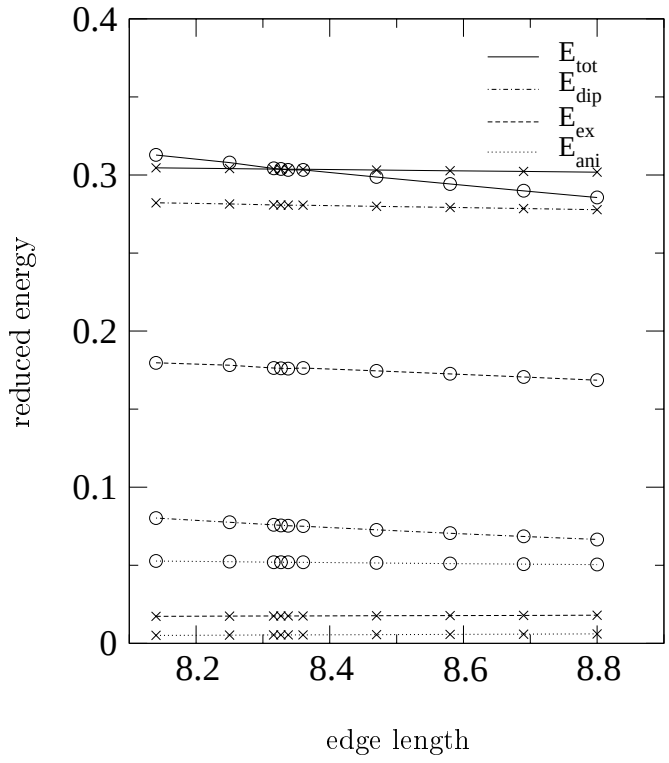

Figure 8.2: Energy of flower (×) and vortex (○) state

8.2 Finite element model

The program package implementing the micromagnetic finite element model has already been developed and used for deterministic simulations [8]. The time integration was performed by an implicit backward difference or alternatively by a Runge-Kutta time integration scheme. Thus, it was only necessary to replace the deterministic time integration algorithm by the stochastic Heun scheme (7.11).

The main advantages of the finite element model are, that it calculates the magnetostatic field using a magnetic scalar potential and reduces the computational effort of treating the open boundary problem by a hybrid finite element/boundary element method [37]. Furthermore, it is easy to simulate arbitrary geometries with curved surfaces, which cause many problems in finite difference simulations.

8.3 Numerical integration

As we are interested in physically relevant solutions, we interpret the Langevin equation (5.7) in Stratonovich sense (cf. section 6.3). The Milshtein (7.7) and Heun scheme (7.11) provide appropriate integration methods, which converge to Stratonovich solutions.

8.3.1 Milshtein scheme

The Milshtein scheme (7.8) for the stochastic Landau-Lifshitz equation (5.4) is implemented as

$$\begin{aligned} M_i(t+\Delta t) &= M_i(t) + \\ &\quad \Big[-\gamma'(\mathbf{M} \times (\mathbf{H}_{\text{eff}} + \mathbf{H}_{\text{th}})) \\ &\quad -\frac{\alpha\gamma'}{M_{\text{s}}} \mathbf{M} \times (\mathbf{M} \times (\mathbf{H}_{\text{eff}} + \mathbf{H}_{\text{th}})) \Big]_i \Delta t + \\ &\quad \gamma'^2 (1+\alpha^2) M_i (H_{\text{th},i} \Delta t)^2 \quad , \end{aligned} \tag{8.1}$$

where the thermal field (5.1, 5.2, 6.33) is a Gaussian process

$$H_{\text{th},i} = \eta \sqrt{2 \frac{\alpha}{1+\alpha^2} \frac{k_B T}{\mu_0 \gamma' v M_{\text{s}} \Delta t}} \tag{8.2}$$

with a Gaussian random variable η. v is the discretization volume of the computational cells. In the finite difference model it is the volume of a cubic computational cell and in the finite element model it is the volume of the finite element.

8.3.2 Heun scheme

The Heun scheme (7.11) requires the calculation of the predictor

$$\begin{aligned} \bar{M}_i(t+\Delta t) &= M_i(t) + \\ &\quad \Big[-\gamma'(\mathbf{M} \times (\mathbf{H}_{\text{eff}} + \mathbf{H}_{\text{eff}})) \\ &\quad -\frac{\alpha\gamma'}{M_{\text{s}}} \mathbf{M} \times (\mathbf{M} \times (\mathbf{H}_{\text{eff}} + \mathbf{H}_{\text{eff}})) \Big]_i \Delta t \quad . \end{aligned} \tag{8.3}$$

Then the magnetization is updated as

$$\begin{aligned} M_i(t+\Delta t) &= M_i(t) + \\ &\quad \frac{1}{2} \Big[-\gamma' \left((\mathbf{M} + \bar{\mathbf{M}}) \times (\mathbf{H}_{\text{eff}} + \mathbf{H}_{\text{th}}) \right) \\ &\quad -\frac{\alpha\gamma'}{M_{\text{s}}} (\mathbf{M} + \bar{\mathbf{M}}) \times \left((\mathbf{M} + \bar{\mathbf{M}}) \times (\mathbf{H}_{\text{eff}} + \mathbf{H}_{\text{th}}) \right) \Big]_i \Delta t. \end{aligned} \tag{8.4}$$

Chapter 9

Rigid magnetic moment

9.1 Deterministic behaviour – The Stoner-Wohlfarth model

A rigid magnetic moment is an approximation for a very small magnetic particle with strong exchange interaction. If it is small enough, the exchange interaction will keep the magnetization uniform which leads to coherent rotation. In this reversal mode the constituent spins rotate in unison. The exchange interaction gives a constant contribution to the Landau free energy in this approximation and therefore does not influence the motion of the magnetization vector. These are the common assumptions in the *Stoner–Wohlfarth model*.

The undamped equation of motion (2.21) describes the continuous precession of the magnetization vector around the direction of the effective magnetic field. However, changes of the magnetization are known from experiment to decay in finite time. Thus, damping is introduced by a phenomenological term. The commonly used Landau-Lifshitz equation of motion (2.25) results in a spiraling movement of the magnetization vector towards its equilibrium direction. The analytical solution [50]

$$\mathbf{M} = M_\mathrm{s} \begin{pmatrix} \operatorname{sech}(\alpha\gamma H t)\cos(\alpha\gamma H t) \\ \operatorname{sech}(\alpha\gamma H t)\sin(\alpha\gamma H t) \\ \tanh(\alpha\gamma H t) \end{pmatrix}$$

is given as a projection into the $x - y$ plane in figure 9.1 for two different values of the damping parameter. If the damping parameter is rather low (fig. 9.1(a)) the magnetization vector precesses many times before it reaches its equilibrium direction. If $\alpha = 1$ the precession is critically damped, and the magnetization turns "directly" into the direction of the effective field.

Figure 9.2 shows, how the switching time depends on the value of the damping parameter. Initially, the magnetization vector points in a direction opposite to the effective field. A small deflection starts the reversal process. We can measure the switching time, which is the time, until the component of the magnetization parallel

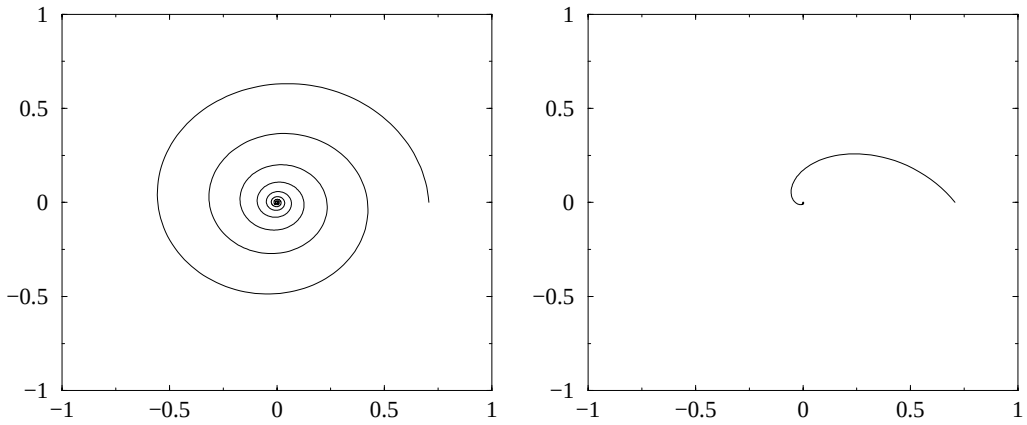

(a) $\alpha = 0.1$ (b) $\alpha = 1$

Figure 9.1: Trajectory of the magnetization vector

material	α
CrO_2	0.051
γ-Fe_2O_3	0.066
Co-γ-Fe_2O_3	0.13
MP (metal particle)	0.92

Table 9.1: Damping parameters of particulate magnetic recording materials

to the effective field has reached a certain value (e.g. $M_z = -0.9$). For $\alpha < 1$ the motion of the magnetization vector is undercritically damped. It makes many precessions around the direction of the effective field. On the contrary, for $\alpha > 1$ the motion is overcritically damped. The minimum of the switching time is found for $\alpha = 1$, which is the case of critical damping [51]. Table 9.1 shows the damping parameters for magnetic materials [50, 52], which are commonly used in magnetic recording tapes. These values are obtained by ferromagnetic resonance experiments: A very strong external DC field keeps the magnetization of the sample homogeneous and parallel to its direction. A small AC field perpendicular to the DC field excites a periodic motion of the magnetization with a small amplitude. As the frequency of the AC field is varied, the absorbed energy varies and at the resonance frequency it reaches a maximum. From the width of the absorption spectrum, the damping constant can be derived.

The equilibrium direction of the magnetic moment is determined by the magnetocrystalline anisotropy axis and the direction of the external field. It can be readily obtained by considering the Landau free energy G_L of the magnetic moment, which is in the case of uniaxial anisotropy given by

$$G_L = -K_1 V \cos^2(\theta - \phi) - M_s V H \cos\phi \quad .$$

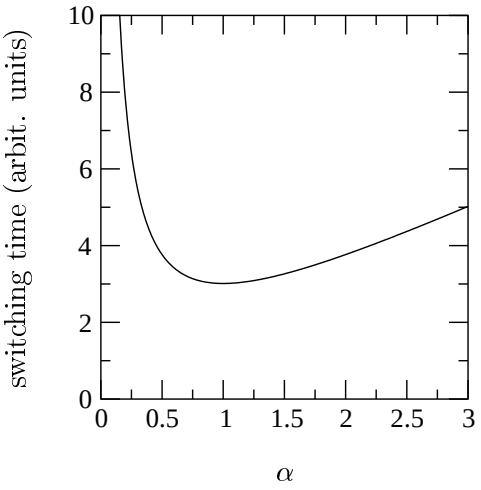

Figure 9.2: Dependence of switching time on damping constant

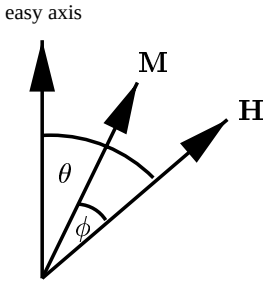

Figure 9.3: Definition of angles in the Stoner-Wohlfarth model

K_1 is the first magnetocrystalline anisotropy constant, V the volume of the magnetic particle, M_s its saturation magnetization, and H the external field. If an external field is applied at an angle θ to the easy axis of the uniaxial anisotropy of the particle, the magnetization vector will reach its equilibrium position at an angle ϕ from the field direction, where the Landau free energy has a local minimum. Since there is not only one minimum the equilibrium direction is also influenced by the history of the magnetization vector. This effect is called *hysteresis*.

Another important aspect can be explained using this simple model: The difference between reversible and irreversible magnetization processes. *Reversible* processes are those, in which the magnetization returns to its initial position after the perturbation has been removed again. For example, when a weak external bias field is applied, the magnetization will change slightly, but upon removal of the bias field, it returns to its initial position. However, if the bias field is strong enough, the magnetization can switch *irreversibly* and remain in a different energy minimum after the bias field has been switched off. Of course, this effect is used to switch the magnetization between different directions and store information thereby.

The "energy landscape" for a cobalt sphere with $K_1 = 4.5 \times 10^5$ J/m^3, $M_\mathrm{s} =$

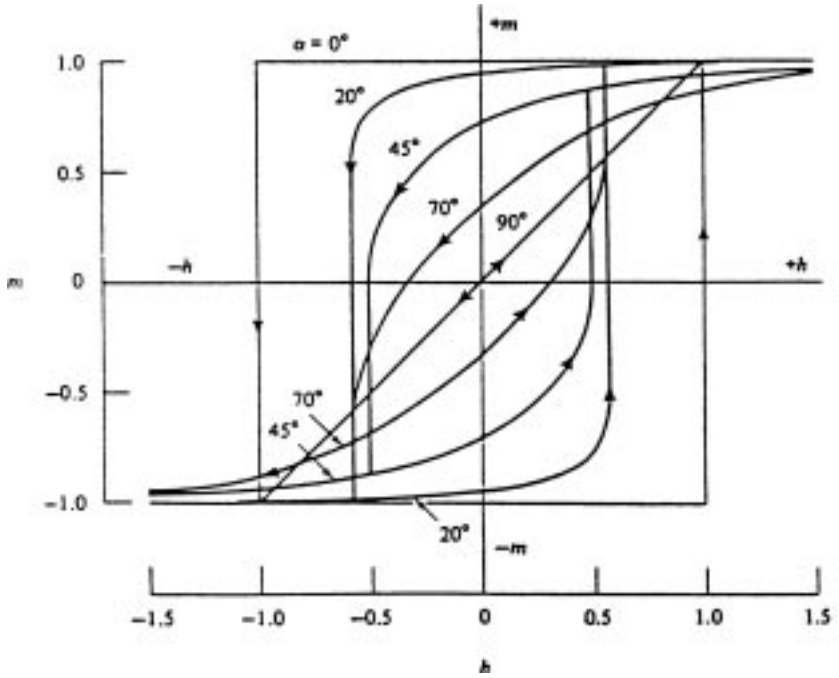

Figure 9.4: Hysteresis curves of a spherical single domain particle for different angles between anisotropy axis and external field [53]

1.4×10^6 A/m and a volume of 1000 nm^3 is given in figure 9.5. An external field of 100 kA/m is applied at an angle of 35° to the easy axis. One energy minimum is found for $\phi = 29.407°$ and a second for $\phi = 226.277°$.

9.2 Stochastic perturbation

The interaction between the electron's magnetic moment and the crystal lattice has already been considered, when we introduced the damping term in the Landau-Lifshitz equation (section 2.3). But this is not a one-way interaction, which transfers energy only from the spins to the lattice and causes the relaxation of the magnetization towards its equilibrium position. Energy can also be transferred from the lattice to the electrons. Thermal energy causes perturbations of the crystal lattice, which induces fluctuations of the magnetization distribution. We incorporate this thermal activation by a stochastic field, as described in section 5.2.

Thus, the magnetization wil not remain in its equilibrium direction but precess in a random walk around it (figure 9.6). The mean distance from the equilibrium direction is determined by the temperature and the height of the potential barrier surrounding the energy minimum.

If we consider a Stoner-Wohlfarth particle without an external field, its energy is given by

$$E(\theta) = -K_1 V \cos^2 \theta \quad ,$$

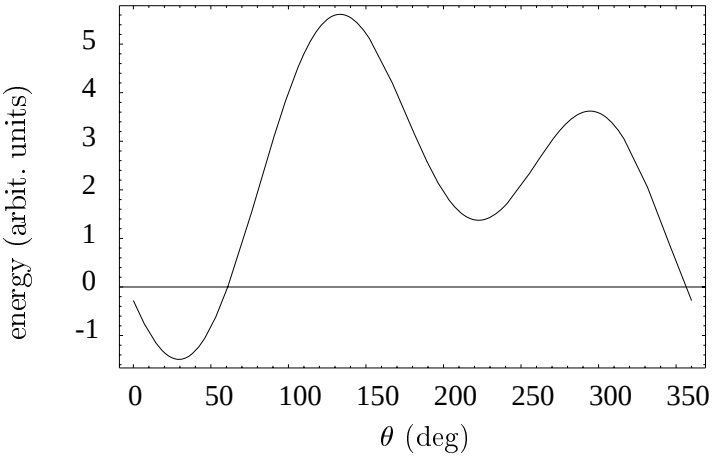

Figure 9.5: Energy landscape

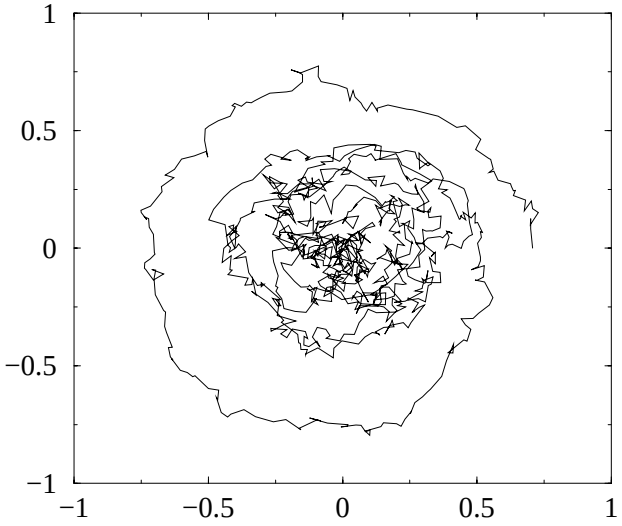

Figure 9.6: Thermally perturbed precession

where θ denotes the angle between the magnetization vector and the easy axis. In thermal equilibrium we expect the probability density for the angle θ to give a Boltzmann distribution (6.31).

$$\begin{aligned} P(\theta) &\propto \exp\left(-\frac{E(\theta)}{k_B T}\right) = \\ &= \exp\left(\frac{K_1 V \cos^2\theta}{k_B T}\right) \end{aligned} \tag{9.1}$$

Then, the probability, that the magnetization points in a direction in the interval $[\theta, \theta + d\theta\,]$ to the easy axis is given by

$$W(\theta)\sin\theta\, d\theta \propto 2\pi \exp\left(\frac{K_1 V \cos^2\theta}{k_B T}\right)\sin\theta\, d\theta \quad .$$

For the average magnetization we get

$$\langle M_z \rangle = \frac{\int_0^{2\pi} \exp(\frac{K_1 V}{k_B T}\cos^2\theta)\sin\theta\cos\theta\, d\theta}{\int_0^{2\pi} \exp(\frac{K_1 V}{k_B T}\cos^2\theta)\sin\theta\, d\theta}$$

If we substitute

$$\chi := \frac{K_1 V}{k_B T}$$

and

$$z := \cos\theta \quad , \quad dz = -\sin\theta\, d\theta$$

we integrate easily

$$\begin{aligned} \langle M_z \rangle &= \frac{\int_0^1 \exp(\chi z^2) z\, dz}{\int_0^1 \exp(\chi z^2)\, dz} = \\ &= \frac{\frac{1}{2\chi}\left[\exp(\chi) - 1\right]}{\frac{\sqrt{\pi}}{2}\mathrm{erf}(1)} \quad , \end{aligned} \tag{9.2}$$

where $\mathrm{erf}(x)$ denotes the error function

$$\mathrm{erf}(x) = \frac{2}{\sqrt{\pi}} \int_0^x \exp(-t^2)\, dt \quad .$$

The distributions obtained by computer experiments are shown in figure 9.7. The experimentally obtained distribution of θ (the histogram bars in figure 9.7(a)) is in excellent agreement with the analytically expected distribution. The time average for M_z (fig. 9.8) is also in good agreement with the analytically expected values, which is obtained from (9.2). The time step size is 1/30th and 1/100th of the typical precession time of the magnetization vector in the effective field (cf. section 9.3).

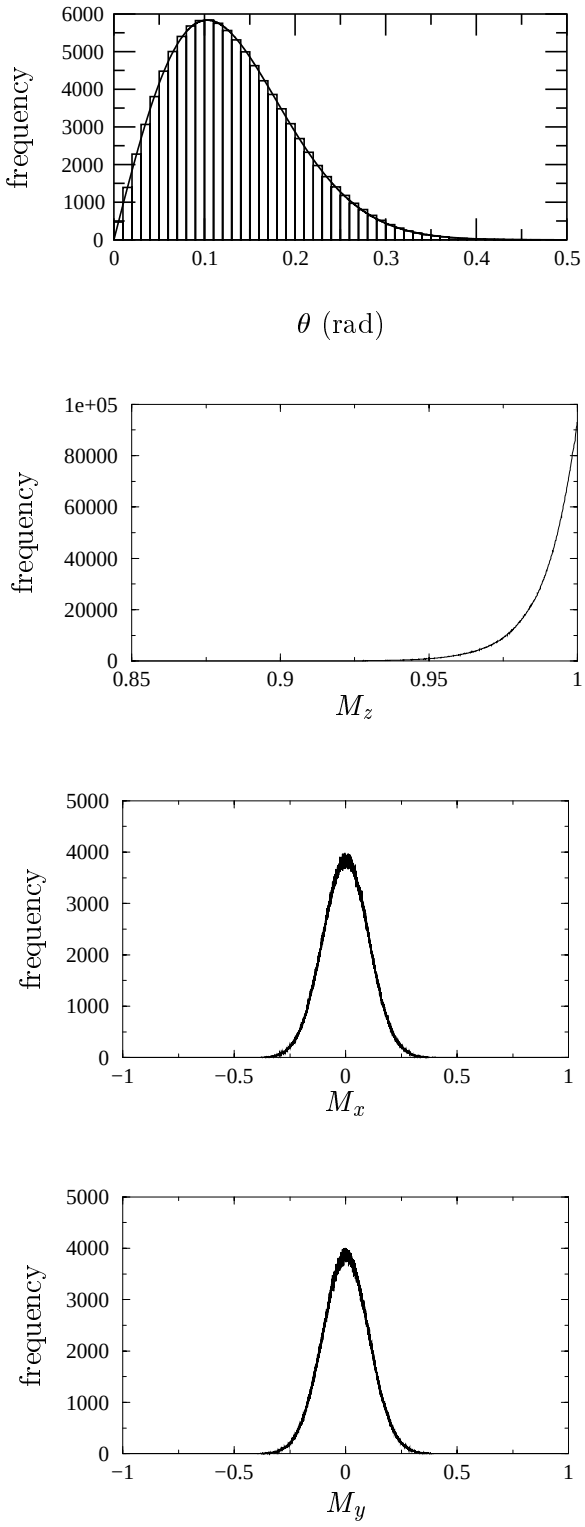

Figure 9.7: Distributions in thermal equilibrium

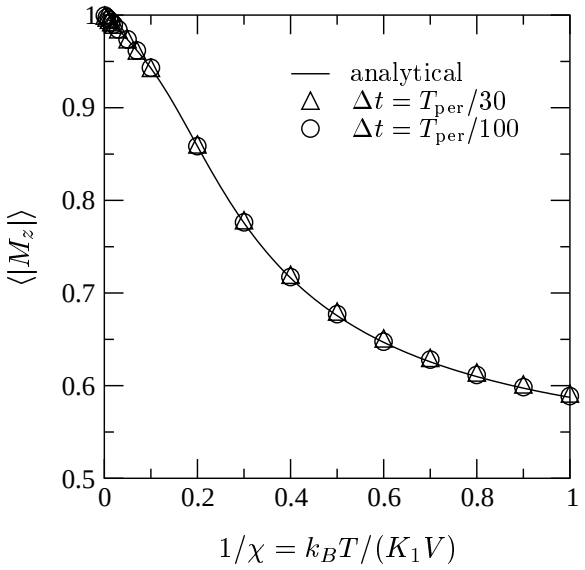

Figure 9.8: Average magnetization for Boltzmann distribution

However, as χ increases (temperature increases or the particle size or the anisotropy are decreased) the magnetization vector does not stay in its energy minimum. The thermal perturbation can be become strong enough to make it cross the energy barrier and jump into another energy minimum. In this case a magnetization reversal or switching event occurs. Figure 9.9 shows, how the number of switching events depends on χ. The probability for the magnetization vector to surmount the energy barrier and escape into the other energy minimum is given by the classical Arrhenius formula of chemical reaction theory, which states, that it is proportional to

$$\exp\left(-\frac{\Delta E}{k_B T}\right) \quad .$$

ΔE denotes the energy barrier, which is in our case given by the magnetocrystalline anisotropy energy. The fit of this law (since we do not know the prefactor) to the data is also given in figure 9.9.

Of course, it depends on the measurement time, how many switching events are detected. No matter how small the temperature is (in a realistic model it will always be finite), a switching event can always occur. At lower temperatures or for larger particles it is just less likely, than for higher temperatures and smaller particles. If we wait for more than 3×10^{13} s ($\approx$ 10 million years), we can measure the decay of magnetization in magnetic stone. The typical relaxation time is proportional to $\exp(1/\chi)$ (cf. section 10.1). Researchers in the field of rock magnetism study such phenomena, because the initial susceptibility is frequently used as a palaeoclimatic indicator in sediments [54, 55]. If we want to store information on magnetic tape, the particles should be large enough and their anisotropy strong enough to have a relaxation time larger than 10^8 s ($\approx$ 1000 years). If the particles are still smaller,

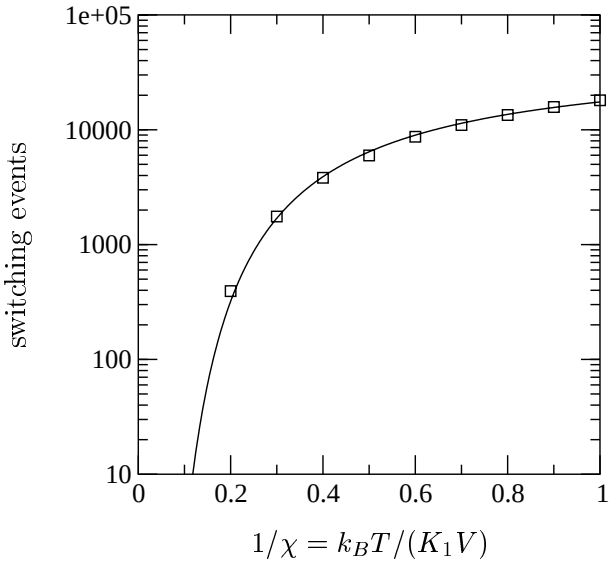

Figure 9.9: Number of switching events as a function of $1/\chi$. The solid line is a fit of the classical Arrhenius formula.

they might be suitable for the measurement of switching dynamics (cf. section 10.4). Finally, if the relaxation time reaches the order of the Larmor precession period, the magnetization flips back and forth many times during the measurement time of experiments. Therefore in zero applied field, the measured average value of the magnetization will be zero. In figure 9.8 $\langle |M_z| \rangle$, the average of the absolute value of M_z, has been plotted, because the average magnetization $\langle M_z \rangle$ would vanish, as soon as switching events occur.

For very small relaxation times, an ensemble of magnetic particles behaves essentially like paramagnetic atoms. Thus, the magnetization can be described by a Langevin function and there is no hysteresis. But we find a very high saturation magnetization, because each particle behaves like a huge atom with 10^3 or even 10^4 spins. A conventional paramagnet requires very high fields to reach saturation, because each atom carries only one spin. Since our magnetic particles carry a very large magnetic moment, the magnetic fields necessary to saturate the ensemble are easy to obtain. Hence, this phenomenon of the loss of ferromagnetism in small particles is known as *superparamagnetism*.

9.3 Time step dependence

The time step dependence of the numerical integration schemes has been investigated by simulating a single rigid magnetic moment. The material parameters were chosen as $M_\mathrm{s} = 1281197\ \frac{\mathrm{A}}{\mathrm{m}}$, $K_1 = 6.9 \times 10^6\ \frac{\mathrm{J}}{\mathrm{m}^3}$, $\alpha = 0.1$, and $V = 1\ \mathrm{nm}^3$. The effective

field, which is just the anisotropy field, is then given by

$$H_{\mathrm{ani}} = \frac{2K_1}{\mu_0 M_{\mathrm{s}}} = 8571 \ \frac{\mathrm{kA}}{\mathrm{m}} \quad .$$

For the time for one full precession of the magnetization vector we obtain

$$T = \frac{1}{f} = \frac{2\pi}{\omega} = \frac{2\pi}{\gamma H_{\mathrm{ani}}} = 3.32 \ \mathrm{ps} \quad ,$$

where $\omega = \gamma H$ is the Larmor frequency For the average magnetization in thermal equilibrium we find with (9.2)

Temperature	$\langle M_z \rangle / M_{\mathrm{s}}$
10 K	0.98979
50 K	0.94268
200 K	0.71976

With the Milshtein scheme we find the correct values for time steps smaller than 0.01 ps, which is about 1/300 of the precession time. The Heun scheme is also suitable for time steps, which are ten times larger, because it has a higher order of convergence. As a rule, the discretization time step should be at most 1/30th of the precession time of the magnetization vector in the effective field. This behaviour is verified at higher temperatures of 50 and 200 K. The results shown in figure 9.11 confirm, that the same rules apply for higher temperatures and therefore larger thermal fluctuations.

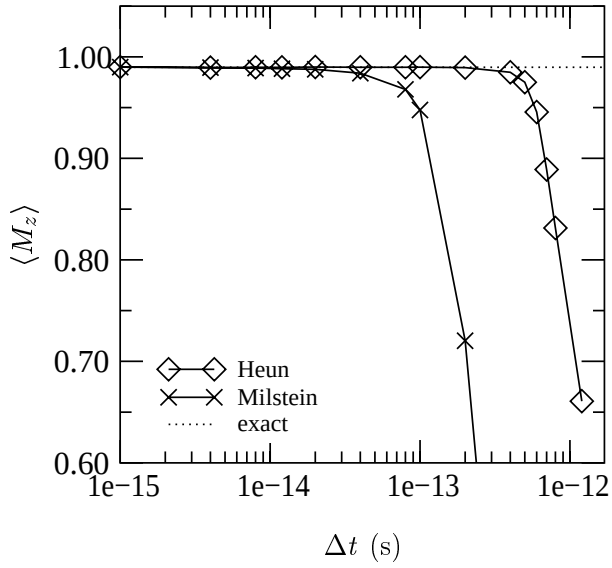

(a) Average magnetization at 10 K

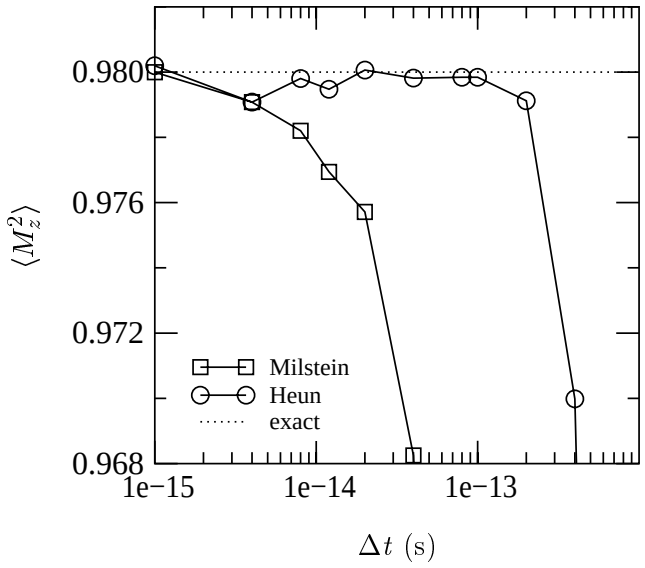

(b) $\langle M_z^2 \rangle$ at 10 K

Figure 9.10: Time step dependence of numerical integration schemes

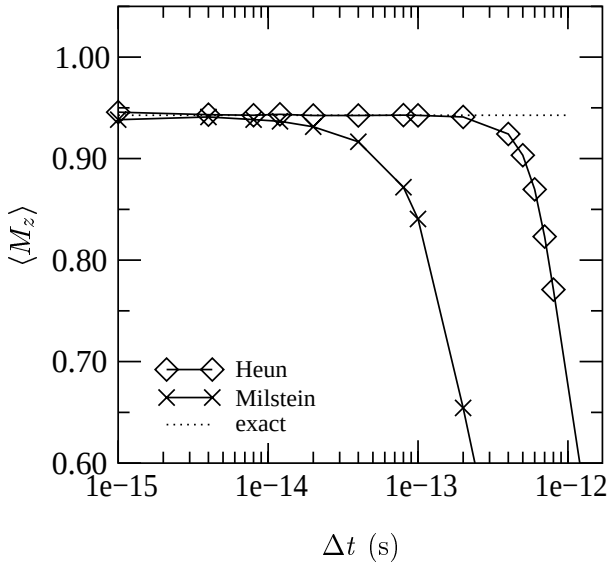

(a) Average magnetization at 50 K

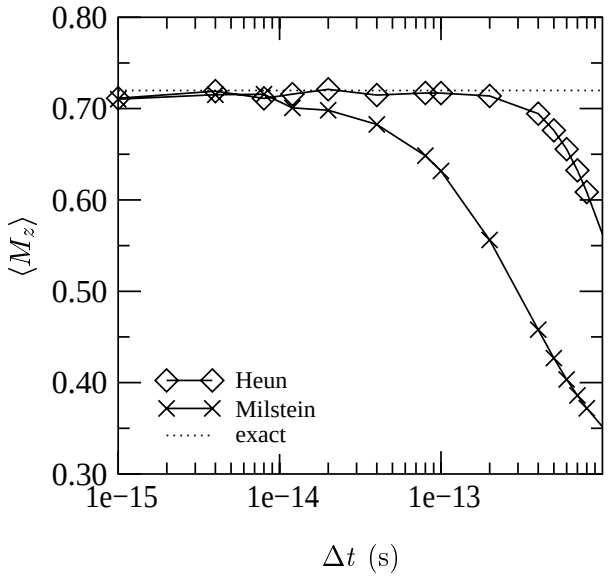

(b) Average magnetization at 200 K

Figure 9.11: Time step dependence at higher temperatures

Chapter 10

Simulation of fine particles

10.1 Cubic particles

Cubes are easy to handle with finite difference packages, because they have no curved boundaries. Thus, cubic particles are good candidates to compare the results of the finite difference program with those of the finite element package. In addition the results are compared with those of Nakatani et al. [56], whose material parameters have been used. They are chosen as $M_s = 0.4 \times 10^6 \ \frac{\mathrm{A}}{\mathrm{m}}$ and $K_1 = 2 \times 10^6 \ \frac{\mathrm{J}}{\mathrm{m}^3}$, $A = 1 \times 10^{-11} \ \frac{\mathrm{J}}{\mathrm{m}}$. In all simulations the number of switching events was counted for at least 100 ns up to 1 μs and the results extrapolated to 1 μs.

Figure 10.1 shows the time dependence of the magnetization for a cubic particle of 32 nm edge length at 300 K. The magnetization fluctuates in the energy minimum around ± 1. From time to time reversal processes occur when the magnetization crosses the energy barrier and switches to the other energy minimum. The probability per unit time, that M_z jumps over the energy barrier E in thermal equilibrium, is proportional to

$$\exp\left(-\frac{E}{k_B T}\right) \quad .$$

We consider a single energy barrier model and take only anisotropy into account. The reciprocal of the switching probability is the relaxation time τ which can thus be written in the form of the Arrhenius-Néel law [57]

$$\frac{1}{\tau} = f_0 \exp\left(-\frac{K_1 V}{k_B T}\right) \quad , \tag{10.1}$$

where f_0 is the characteristic dynamic frequency. The original estimation of Néel was $f_0 \approx 10^9 \ \mathrm{s}^{-1}$, but recently it has become more customary to take $f_0 \approx 10^{10} \ \mathrm{s}^{-1}$ up to $f_0 \approx 10^{12} \ \mathrm{s}^{-1}$. As we will see, the characteristic dynamic frequency depends on the damping constant, which is a material parameter.

The number of reversal processes should, of course, be independent of the time discretization. This has been verified and the results are shown in figure 10.3(a)

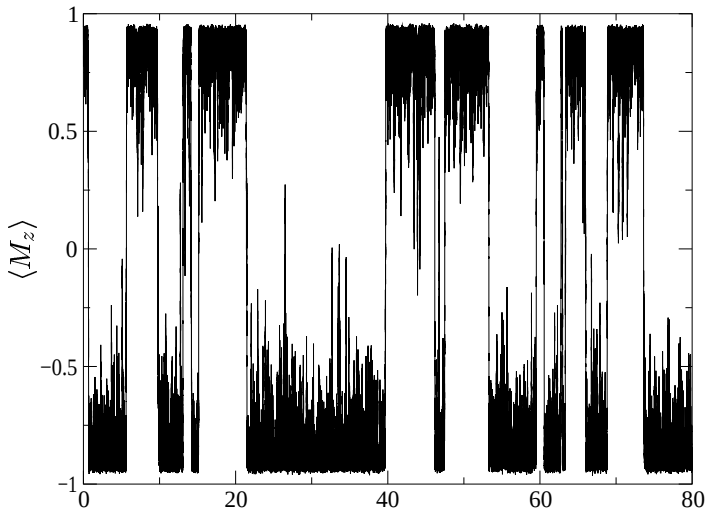

(a) $\alpha = 1$

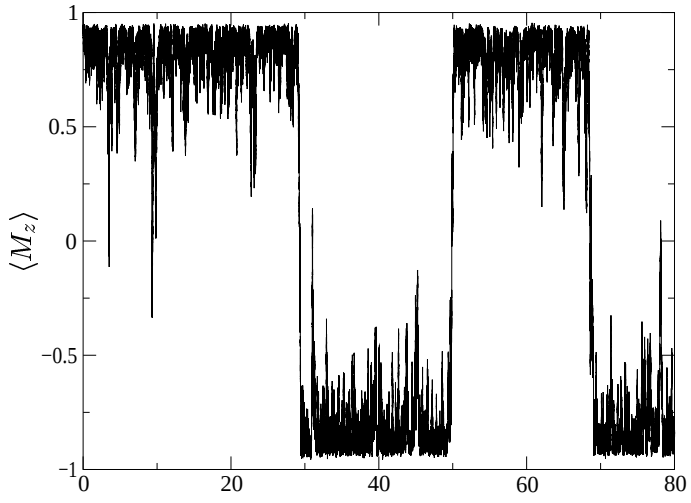

(b) $\alpha = 0.1$

Figure 10.1: Magnetization reversal of a cubic particle

for a $2 \times 2 \times 2$ discretization. As the time step is decreased from 10^{-12} s to 5×10^{-14} s, the number of switching events increases and converges. Then, the space discretization dependence is investigated (fig. 10.3(b)) and we find for three different space discretizations ($2 \times 2 \times 2$, $3 \times 3 \times 3$, $4 \times 4 \times 4$) consistent results (within fluctuations due to the stochastic nature of the underlying processes).

In addition, the results for a finite element model are plotted in figure 10.3(b). The cube has been discretized into 64 nodes and 135 tetrahedral elements and the results are in excellent agreement with those of the finite difference model.

If we fit the data of the smallest time step in the linear region in figure 10.3(a) with the Arrhenius-Néel law, we find a characteristic dynamic frequency of $f_0 = 3.52610 \times 10^{11}$. The exponent is $-4.7 \times 10^{25} \cdot V$ and it is in good agreement with the value

$$-\frac{K_1}{k_B T} = -4.8 \times 10^{25}$$

which we would expect for a single (anisotropy) energy barrier. This approximation is sensible, if the magnetization reverses coherently. The magnetization vectors, which are represented by cones, at different times are plotted in figure 10.2 for a 64 nm^3 particle and we see, that the particle switches coherently.

The characteristic dynamic frequency obtained above is quite high compared to the estimate of Néel. However, it is a question of the definition of a switching event. This fact is illustrated in figure 10.3(c). If the magnetization changes its sign and its absolute value exceeds m_{trh}, then a switching event is counted. For $m_{\mathrm{trh}} = 0.1$ we get a number of switching events which is one order of magnitude larger than that for $m_{\mathrm{trh}} = 0.7$. This is due to the fact, that there are many switching events, in which the magnetization does not complete a full reversal, but it already switches back at an earlier stage. Such events can also be identified in figure 10.1, where we find "spikes" of incomplete switching events. Thus, the characteristic dynamic frequency depends on the definition of a switching event. The exponent of the Arrhenius-Néel law is not influenced, since the slope of the graphs in figure 10.3(c) remains the same.

Physically interesting is the dependence on the damping constant, because this is a material parameter, which can be obtained from ferromagnetic resonance experiments (cf. section 9.1). As the damping constant is increased from $\alpha = 0.01$, the number of switching events increases, too. At a temperature of 0 K the reversal time of a fine particle is proportional to $(1+\alpha^2)/\alpha$ [51]. Therefore, it is reasonable, that the characteristic dynamic frequency is proportional to $\alpha/(1+\alpha^2)$. The solid line in figure 10.4(a) is a fit of the $\alpha/(1+\alpha^2)$ law to the data obtained by computer simulations (circles).

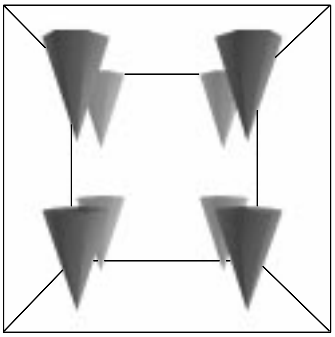

(a) Initial magnetization ($t = 0$ ps)

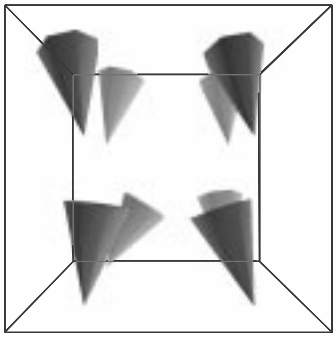

(b) Thermally perturbed magnetization distribution ($t = 0.09$ ps)

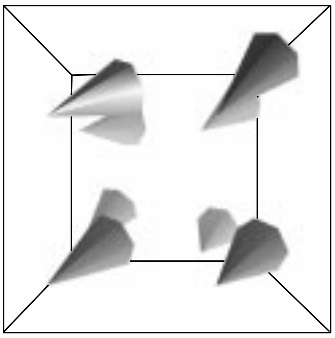

(c) Switching starts ($t = 0.1500$ ps)

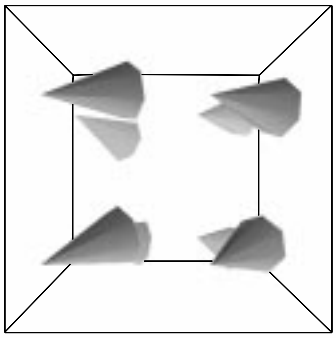

(d) The reversal process progresses ($t = 0.1556$ ps)

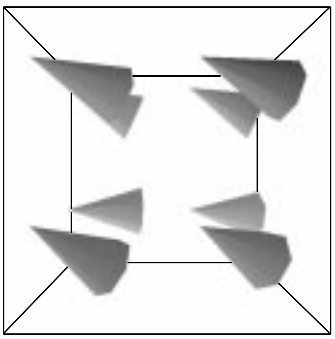

(e) Crossing the energy barrier ($t = 0.160$ ps)

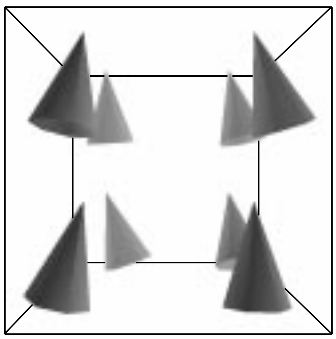

(f) Reversal process completed ($t = 0.176$ ps)

Figure 10.2: Snapshots of a switching event

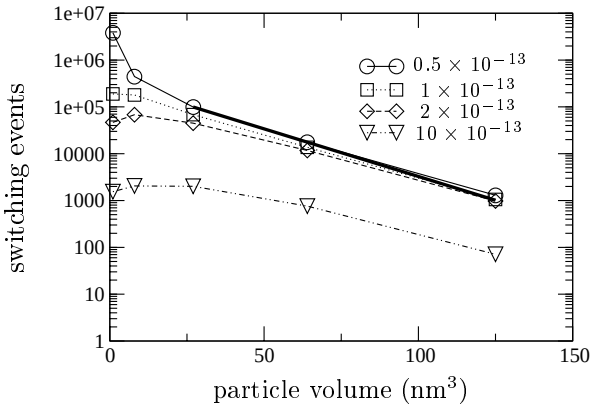

(a) Time step dependence

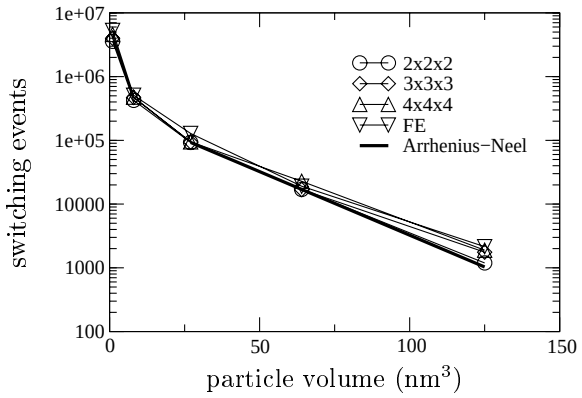

(b) Discretization dependence

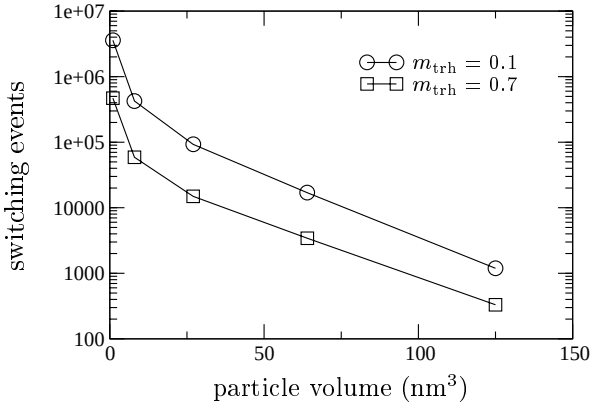

(c) Dependence on definition of switching

Figure 10.3: Dependence of the number of switching events on the simulation parameters

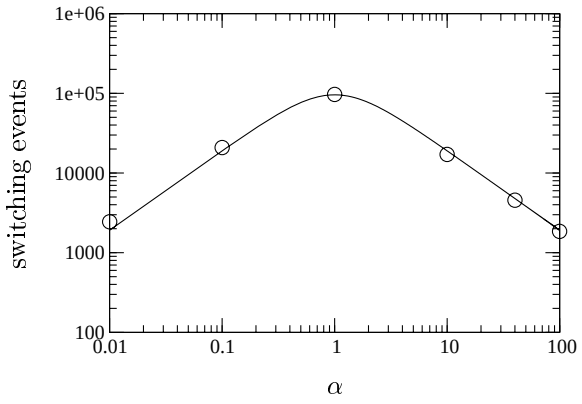

(a) Dependence on damping constant

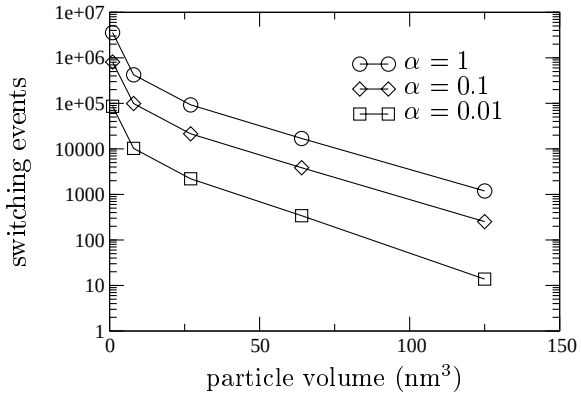

(b) Dependence on damping constant for different particle sizes

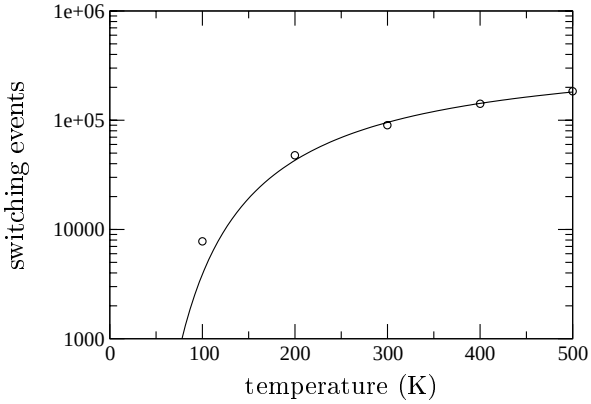

(c) Temperature dependence

Figure 10.4: Dependence of the number of switching events on damping constant and temperature

10.2 Spherical particles

The mechanism of thermally activated magnetization switching in small spherical ferromagnetic particles has been investigated using the finite element model. The material parameters have been chosen as $M_\mathrm{s} = 0.4 \times 10^6 \ \frac{\mathrm{A}}{\mathrm{m}}$, $A = 3.64 \times 10^{-12} \ \frac{\mathrm{J}}{\mathrm{m}}$, $\alpha = 1$, and a radius $R = 11.5$ nm. The finite element mesh consists of 115 nodes and 440 elements. The mean diameter of the finite elements is 3 nm. This discretization is sufficient, if the we assume a rather low magnetocrystalline anisotropy. For $K_1 = 2 \times 10^5 \ \frac{\mathrm{J}}{\mathrm{m}^3}$ we find a typical domain wall width of

$$\delta = \pi \sqrt{\frac{A}{K_1}} \approx 57 \text{ nm} \quad .$$

The initial magnetization is homogeneous and parallel to the easy axis of the particle. Its magnetization distribution is destabilized by an external magnetic field, which is parallel to the easy axis but antiparallel to the initial magnetization. Since this is a metastable state, we can expect the particle to overcome the energy barrier, which is called the *activation energy*, and reverse its magnetization after some time. In contrast to Monte Carlo simulations [58], we obtain not only information about the dynamical behaviour, but also about the switching times. The metastable lifetime (or relaxation time) τ is defined as the time, which passes from the initially saturated state $M_z(\tau) = M_\mathrm{s}$ until $M_z(\tau) = 0$.

In order to measure the metastable lifetime a large number of simulations has been performed for each set of parameters. After 200 measurements a waiting time histogram was obtained (e.g. fig. 10.5(a)). The integral of this histogram (or a cumulative histogram) is proportional to the switching probability $P(t)$, that is the probability, that the particle has switched by a certain time (cf. fig. 10.5(b)). However, it is more common to draw graphs for the (rescaled) probability of not switching (fig. 10.6) $P_\mathrm{not}(t) = 1 - P(t)$.

The magnetization reversal process can happen in different reversal modes. In a particle with low anisotropy the magnetization rotates coherently (figure 10.7(a)), which means, that the magnetization remains almost homogeneous during the reversal process except for small thermal fluctuations. If the anisotropy is increased, it becomes favourable to form a nucleus with reversed magnetization. Thus, a droplet nucleates near the surface (figure 10.8(a)) and expands (figure 10.8(b)) until the magnetization is completely reversed.

The external field has been chosen to be comparable to the anisotropy field

$$H_\mathrm{ani} = \frac{2K_1}{\mu_0 M_\mathrm{s}} \quad .$$

Figure 10.9 shows, how the metastable lifetime decreases, when the external field is increased. $K_1 = 2 \times 10^5 \ \frac{\mathrm{J}}{\mathrm{m}^3}$ and $\mu_0 H_\mathrm{ext} = \mu_0 H_\mathrm{ani} = 1$ T have been used at a temperature of 500 K. The negative sign indicates, that the external field is

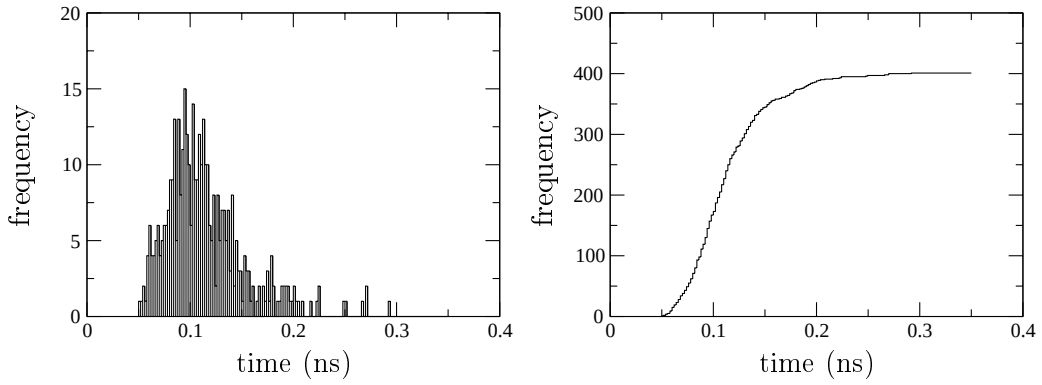

(a) Switching time histogram (b) Cumulative histogram

Figure 10.5: Results of switching time measurements

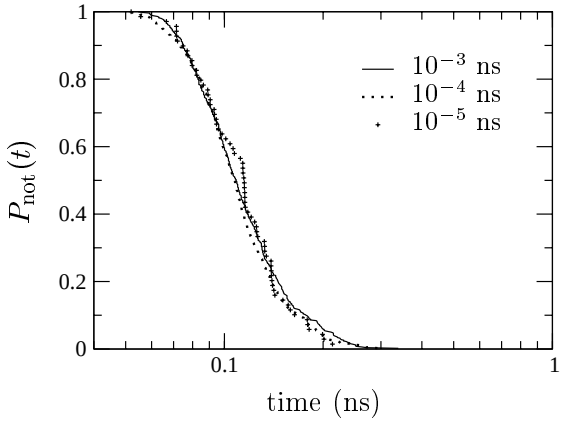

Figure 10.6: Probability of not switching for different time step sizes

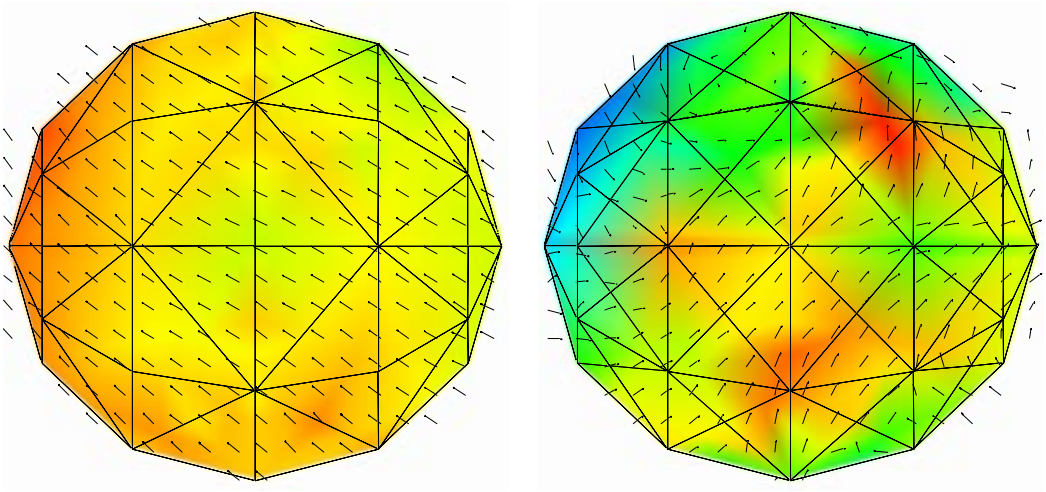

(a) Coherent rotation

(b) Incoherent switching

(c) Colour map of M_z

Figure 10.7: Magnetization reversal mechanisms in small spherical particles

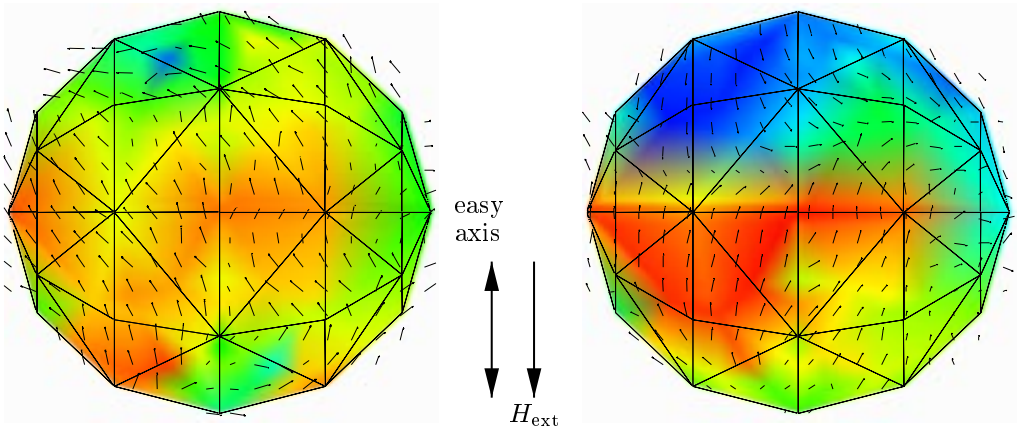

(a) Droplet nucleation (b) Droplet expansion

(c) Colour map of M_z

Figure 10.8: Nucleation of a droplet of reversed magnetization

antiparallel to the initial magnetization. If we fit the data with the empirical law

$$\tau = \tau_0 \exp\left(H_0/H\right)$$

we can identify three different regimes with different slopes. At low fields ($|H| < 0.8H_{\text{ani}}$) we find $H_0 = -3$. Figure 10.10 shows, that in this regime the magnetization switches coherently. For higher fields ($0.8H_{\text{ani}} < |H| < 0.9H_{\text{ani}}$) the fit results in $H_0 = -7$. The reason for the different behaviour is found in the different switching mechanism. The isosurface plot for M_z (fig. 10.11) shows the nucleation of a reverse droplet. As it expands the magnetization is switched. Finally, a third regime is found for even higher fields ($|H| > 0.9H_{\text{ani}}$). In this case the decay of magnetization is driven by several droplets, which nucleate independently at different places (fig. 10.12). The fit parameter is given by $H_0 = -20$.

A similar behaviour has been observed in Monte-Carlo simulations [59], where this behaviour is interpreted in terms of droplet theory.

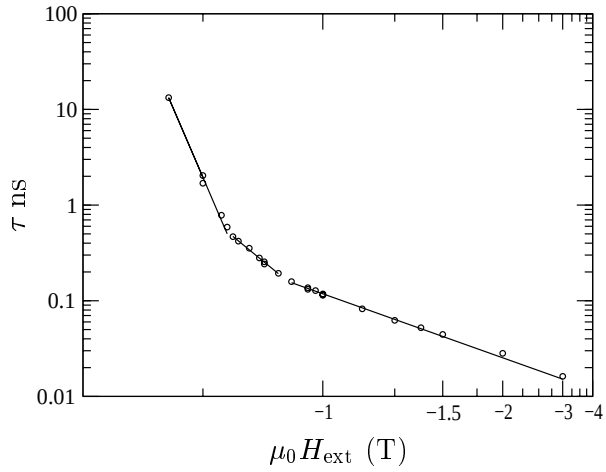

Figure 10.9: Dependence of the metastable lifetime on the external field

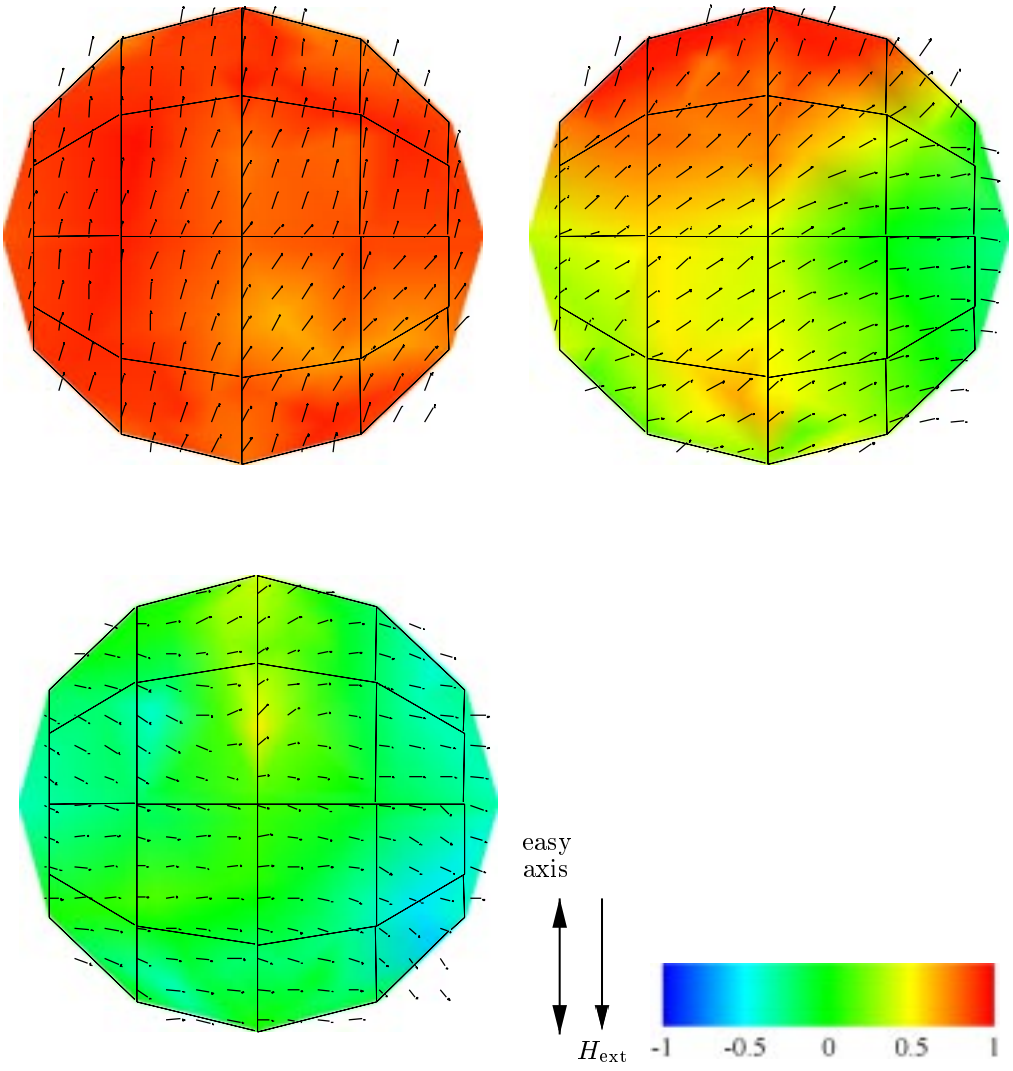

(a) Colour map of M_z

Figure 10.10: Coherent rotation of the magnetization at an external field of -0.75 T

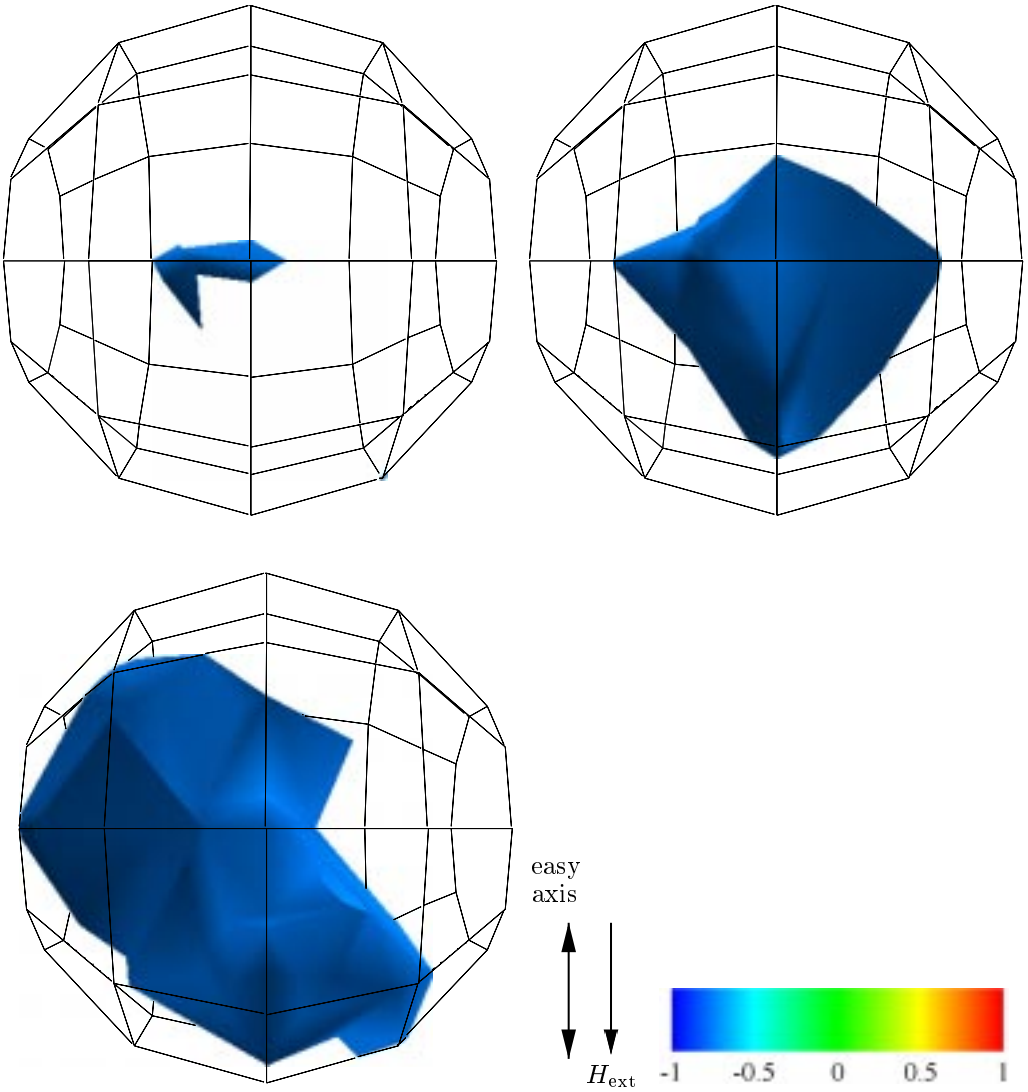

(a) Colour map of M_z

Figure 10.11: Nucleation and expansion of a single droplet at an external field of -0.83 T

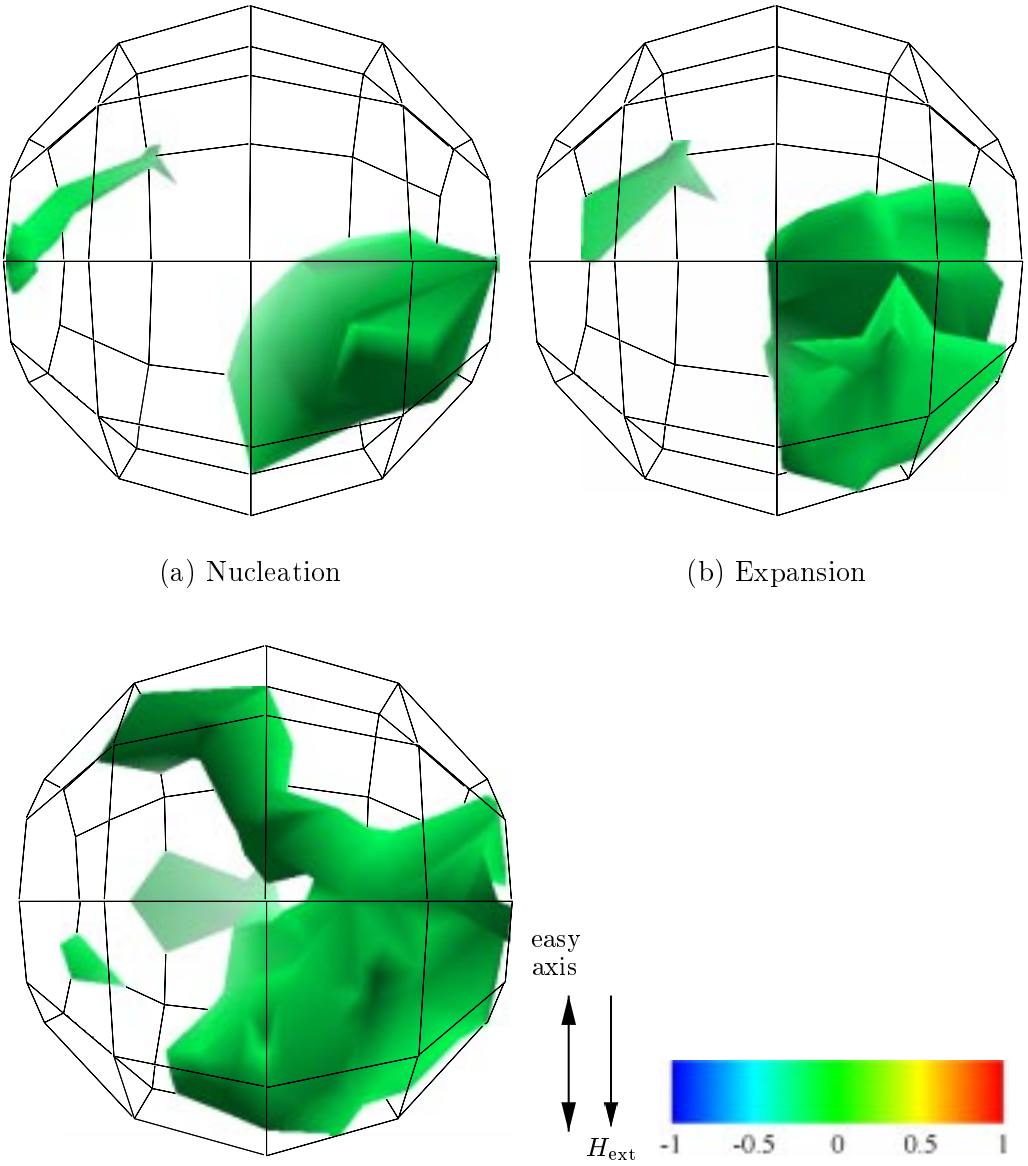

(a) Nucleation

(b) Expansion

(c) Droplets join each other

(d) Colour map of M_z

Figure 10.12: Multi-droplet nucleation at an external field of -1.5 T

Figure 10.13: Horizontal arrangement of two particles with a centre to centre distance of 1.2 times the diameter

10.3 Interacting particles

In order to study the interaction between particles, pairs of two small ferromagnetic spheres have been simulated in different arrangements with respect to their easy axes. The same material parameters as in section 10.2 with a magnetocrystalline anisotropy constant of $K_1 = 2 \times 10^5 \frac{\text{J}}{\text{m}^3}$ have been used and a temperature of 500 K was assumed.

The metastable lifetime has been measured as the time, until the average magnetization over both particles has decreased to zero, because this quantity can also be measured in experiments (cf. section 10.4).

If the two particles are placed in the normal plane to their easy axes (figure 10.13) and far apart (the centre to centre distance is four times their diameter, plot "2f" in figure 10.14), then we find a probability of not switching, which is almost identical to that of a single particle (plot "1" in figure 10.14). Thus, the influence of the other particle is negligible. However, if the centre to centre distance between the two particles is reduced to 1.2 times the diameter (plot "2c" in figure 10.14), the probability of not switching changes dramatically. The slope increases and the relaxation time τ decreases. For a single sphere we find $\tau = 0.114$ ns, for the two spheres far apart $\tau = 0.116$ ns, whereas the two close spheres give $\tau = 0.0987$ ns. We can interpret this as a stray field effect. The stray field of one particle (for a homogeneously magnetized sphere it is the field of a dipole) is antiparallel to the initial magnetization in the other. Thus, it "strengthens" the external field and leads to an earlier magnetization reversal process.

Another interesting configuration is the vertical alignment of the particles parallel to their easy axes. In this configuration the stray field is much stronger and tries to align the magnetization of both particles parallel. Hence, this arrangement leads to a kind of "shape anisotropy", which stabilizes the magnetization. The average metastable lifetime for the vertically aligned spheres (plot "2v" in figure 10.16) $\tau = 0.113$ ns is considerably higher than for the horizontally aligned spheres (plot "2h" in figure 10.16), where we find $\tau = 0.0987$ ns. It is also interesting to note, that the slope for the interacting particles is much larger than that for a single particle

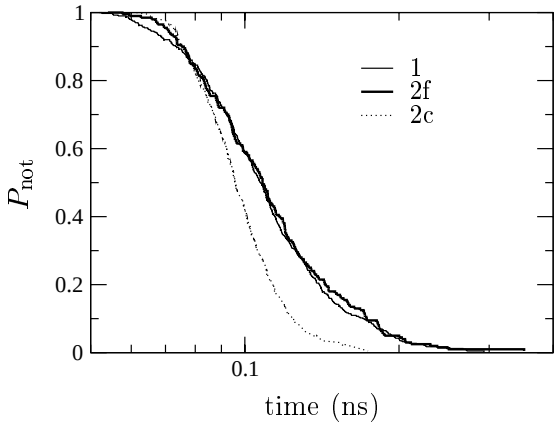

Figure 10.14: Probability of not switching for a single (1) and two interacting particles at a centre to centre distance of 4 (2f) and 1.2 (2c) times the diameter

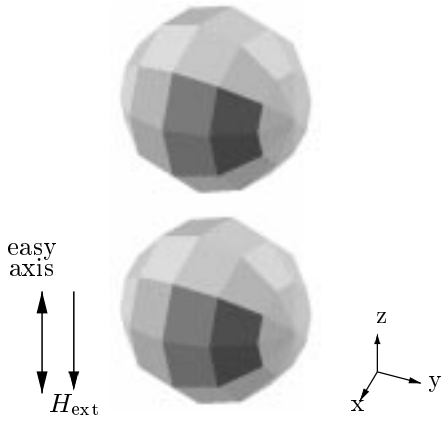

Figure 10.15: Vertical arrangement of two particles with a centre to centre distance of 1.2 times the diameter

(plot "1" in figure 10.16), which was identical to that of two horizontally arranged particles far apart.

A similar behaviour is observed for vertically aligned particles at a centre to centre distance of four times the diameter (figure 10.17). In this case the mean metastable lifetime is again reduced as compare to the vertically aligned spheres at a distance of only 1.2 times the diameter.

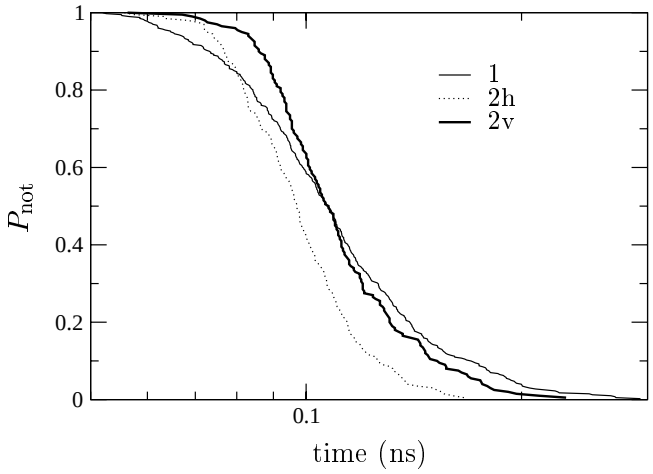

Figure 10.16: Probability of not switching for a single (1) and two horizontally (2h) and vertically (2v) aligned particles with a centre to centre distance of 1.2 times the diameter

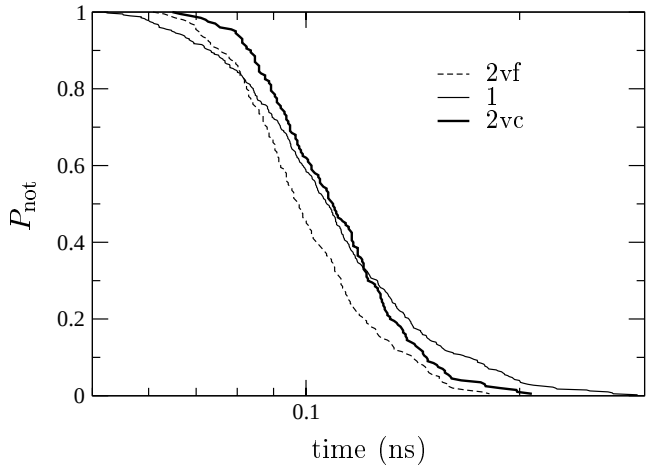

Figure 10.17: Probability of not switching for a single (1) and two vertically aligned interacting particles at a centre to centre distance of 1.2 (2vc) and 4 (2vf) times the diameter

10.4 Experimental results

The measurement of thermally activated magnetization reversal is a very tricky task for several reasons. First, it is very difficult to produce "perfect" monocrystalline single domain particles of cobalt or iron. As the particles have to be only a few nanometres in diameter, the surface to volume ratio is large and surface effects are very important. Thus, the particles should have a sufficiently smooth surface. Furthermore, they must not contain too many lattice defects, which act as nucleation sites for magnetization reversal processes and pinning sites for domain walls.

The second main obstacle is the measurement of the magnetization of these small particles. Only superconducting quantum interference devices (SQUIDs) have a sufficiently high sensitivity to measure the flux changes during the magnetization reversal process of single domain particles.

Only in recent years it has become possible to measure the magnetization of individual single-domain particles. The first study of the dynamics and temperature dependence of magnetization reversal in individual submicronic single-domain Co particles at very low temperatures was done by Wernsdorfer et al. [60].

They used a planar Nb micro-bridge dc-SQUID of 1 μm diameter on which the ferromagnetic particle was placed. The SQUID loop collects the flux produced by the samples magnetization. The close proximity between sample and SQUID results in a very efficient and direct flux coupling, which allows the detection of magnetization reversals corresponding to $10^4\mu_B$. The elliptic ferromagnetic particles were fabricated by electron beam lithography and lift-off techniques out of sputtered thin films. A 10 nm thin Si film protected them against oxidation.

The dynamics of magnetization reversal is studied by two types of experiments: Switching field measurements and switching time measurements.

In the case of switching field measurements, the external field is increased at a given rate and fixed temperature until the sample's magnetization switches. The value of the switching field is stored. This experiment is repeated 100 to 200 times to obtain a switching field histogram. From that, the mean switching field and a width of the switching field distribution can be obtained.

For switching time measurements, the magnetic field is applied antiparallel to the magnetization of the sample and increased to a set value at fixed temperature. After the magnetic field is stabilized, the time until the magnetization switches, is measured. This experiment has to be repeated many times again to obtain a switching time histogram. The integral of this histogram gives the probability of switching.

The results [61] show good agreement with the Arrhenius-Néel law and the validity of the Néel-Brown theory for thermally assisted switching over a single energy barrier. Figure 10.4 gives the probability of not-switching of magnetization as a function of time at different applied fields at 0.5 K for a single crystalline Co particle of 20 nm. Full lines are fits to the data with an exponential.

However, the quality of the samples has great influence on the measurements.

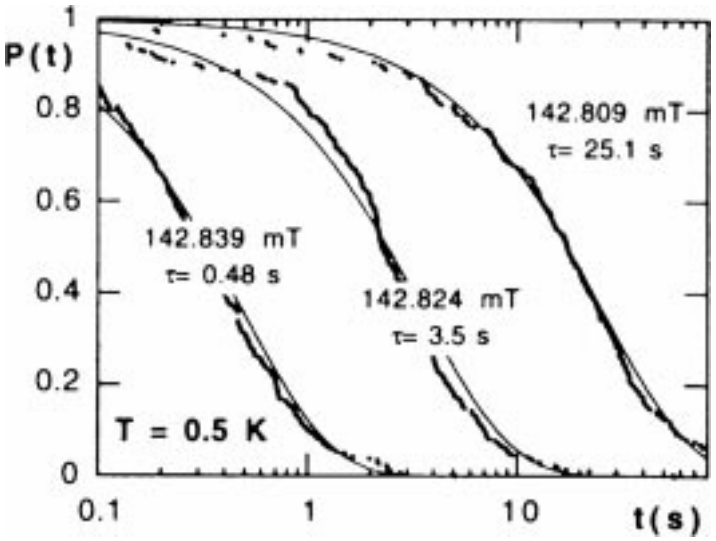

Figure 10.18: Probability of not-switching of magnetization as a function of the time for a 20 nm single crystalline Co particle at 0.5 K. The full lines are fits to the data with an exponential [61]

For particles with antiferromagnetic components (due to, e.g., oxidation) or ferrimagnetic materials disagreement with the Néel-Brown theory has been observed. In these cases, the probability of not switching was flatter than exponential at low temperature (typically $T < 1$ K) and steeper at higher temperatures. Furthermore, the width of the switching field distribution increased for lower temperatures, which might be explained by surface spin disorder.

Another interesting property is described by the Barkhausen volume, which is the smallest switching unit in magnetization reversal. It is also called "activation volume" and can be estimated from the energy barrier at zero field [61] or from the coercive field at different sweeping speeds of the external field [62].

Lederman et al. [63] used a magnetic force microscope to study the angular dependence of the switching field and switching time behaviour of a rectangular single-domain permalloy particle. It was found, that the angular dependence differs significantly from that expected for coherent rotation. In addition, the dependence of the probability for not switching cannot be fit with a simple exponential for applied fields close to the switching field. This indicates, that multiple-energy barriers of similar height are involved in the thermally activated process responsible for the reversal. The rectangular shape of the particle results in vortices at both ends of the particle. This complex magnetization distribution results in complicated switching dynamics, which cannot be described by the Arrhenius-Néel law any more.

Conclusions and outlook

The Langevin dynamics approach proved to be a suitable method to model the effects of thermal activation in magnetic materials.

- Simulations of a single rigid magnetic moment showed, that the Heun scheme is a suitable time integration method, which allows a time step size one order of magnitude larger than that for the Milshtein scheme. Moreover the stochastic Landau-Lifshitz equation of motion in Stratonovich interpretation leads to the correct thermal equilibrium properties.

- The magnetization switching behaviour found for a small cubic particle is identical for the finite difference and finite element model, even though their method of calculating the effective field is substantially different. The finite element method is better suited for the simulation of particles with curved or very complex surfaces and allows the modeling of polycrystalline grain structures.

- For a small cubic ferromagnetic particle magnetization reversal by coherent rotation has been found. As a result, is switching dynamics is well described by the Arrhenius-Néel law for reversal over a single energy barrier.

- Complex magnetization reversal mechanisms have been found for small spherical magnetic particles. The magnetocrystalline anisotropy and the strength of the external determine the switching mechanism and three different regimes have been identified. For fields, which are smaller than the anisotropy field, magnetization by coherent rotation has been observed. If an external field comparable to the anisotropy field is applied single droplet nucleation occurs and for higher fields multi-droplet nucleation is the driving reversal process.

- The interaction of two particles changes the dynamic behaviour, depending on the position and distance of the particles. Two spherical particles aligned along their easy axes can stabilize each other, whereas two horizontally aligned particles exhibit a reduced metastable lifetime.

As the bit size shrinks, the bit density grows and the read/write frequencies increase, the effects of thermal perturbations become more and more important. The

design of magnetic recording media has to guarantee reliability, stability of the stored information and a fast switching mechanism for high frequency writing processes. Micromagnetic simulations based on the programs developed and tested in this thesis will provide important information about the magnetization distribution, the dynamics of the reversal process and the interaction between the elements.

- A detailed study of the shape and arrangement of nano-elements for quantum disks can optimize their thermal stability.
- For high frequency recording applications the switching mechanism can be investigated and the design optimized to minimize the switching time.
- Interaction effects are determined by the pattern, in which the elements are arranged. The distance and position of neighbouring elements has been found to influence the switching time, which has to be considered in the design of quantum discs.
- In thin film recording media the grain structure plays a vital role for the magnetic properties [64]. The finite element package allows the design of arbitrary shapes of the grains and any material composition.
- Predictions of the activation volume will enhance the understanding how microstructural features influence thermally activated magnetization reversal [62].

Thus, the simulations will provide theoretical insight for the development of future recording media.

Appendix

The finite difference program

Dimensionless equations

For the implementation of the finite difference model all physical quantities have been converted to dimensionless values.

The magnetization vectors $\mathbf{m}$ of the computational cells are dimensionless unit vectors

$$\mathbf{m} = \mathbf{M}/M_\mathrm{s} \quad .$$

The magnetic field $\mathbf{H}$ is converted by

$$\mathbf{h} = \frac{\mathbf{H}}{M_\mathrm{s}}$$

and the time is rescaled by

$$t' = tM_\mathrm{s}\gamma$$

where $\gamma = 2.210173 \times 10^5 \frac{\mathrm{m}}{\mathrm{As}}$ is the gyromagnetic ratio.

Thus, the Landau-Lifshitz-Gilbert equation (2.25) can be rewritten as

$$\frac{d\mathbf{m}}{dt'} = -\mathbf{m} \times \mathbf{h} - \alpha \mathbf{m} \times (\mathbf{m} \times \mathbf{h}) \quad .$$

The contributions to the local magnetic field are rescaled by the material constants.

Anisotropy field

$$\mathbf{h}_\mathrm{ani} = k\mathbf{a}(\mathbf{m} \cdot \mathbf{a}) \quad , \qquad k = \frac{2K_1}{\mu_0 M_\mathrm{s}^2}$$

Exchange field

$$\mathbf{h}_\mathrm{exch} = \sum_j^{NN} a\mathbf{m}_j \quad , \qquad a = \frac{2A}{\Delta x^2 M_\mathrm{s}^2}$$

Dipole field

$$\mathbf{h}_{\mathrm{dip}} = -\frac{1}{4\pi} {\sum_j}' \frac{\mathbf{m}_j}{r_j^3} - 3\frac{\mathbf{r}_j(\mathbf{m}_j\mathbf{r}_j)}{r_j^5} \quad , \qquad \mathbf{r}_j = \mathbf{R}_j/\Delta x$$

Thermal field

$$\mathbf{h}_{\mathrm{th}} = \eta\sqrt{2\frac{\alpha}{1+\alpha^2}\frac{k_B T}{\Delta x^3 M_{\mathrm{s}}^2 \Delta t'}}$$

η denotes a standard Gaussian stochastic process with mean zero and variance 1.

Program structure

The finite difference program has been implemented in FORTRAN 77. First, because there are highly optimized compilers and mathematics libraries for the "Alpha processors" in the workstations, which have been used for the calculations. Secondly, compatibility with the finite element package, which has been implemented in FORTRAN 77, saved development time, because it was not necessary to rewrite the time integration algorithm. Only the interface of the subroutine had to be adapted.

Since there is no standard method in FORTRAN 77 to allocate memory at run time, all array sizes have to be defined at compile time. This makes the maintenance of the source code difficult and leads to inconsistencies easily. In order to avoid these pitfalls, the C preprocessor is used to substitute the desired array sizes for symbolic constants just before compilation. This method is also used for file names, file handles, output strings, and, most importantly, simulation parameters. All integer simulation parameters, like the maximum number of time steps, the frequency of log file entries, the choice of the time integration algorithm, etc., are stored in a single array of type integer. In the same way all floating point parameters, like the material parameters, the external field, and the time step size, are stored in a single array of type double precision. However, they are not accessed with the array name and an index, but with symbolic names, which more easily identify their content. A precompiler directive in each source code file makes the precompiler read a special header file, in which the translation of the symbolic names into proper Fortran variables is defined.

In figure 10.19 the head of the function, which reads the simulation parameters from files into the corresponding Fortran data structures, is given. The parameters `iparm` and `dparm` are arrays of integer and double precision parameters. Their entries are defined in the header file, of which a few lines are given in figure 10.20.

Figure 10.21 shows a flow chart of the finite difference program. Its main parts are described in the following.

```
#include "parm.h"
      integer function init_par(
     &                   liparm,iparm,ldparm,dparm,
     &                   eaxis,m,nn)
```

Figure 10.19: Function header with precompiler directive

```
#define nx       1
#define ny       1
#define nz       1

#define magpar   "mag.par"
#define mztdat   "mzt.dat"

#define nstep    iparm(4)
#define dataout  iparm(3)
#define tintalg  iparm(12)

#define aexch    dparm(1)
#define kani     dparm(2)
#define alph     dparm(3)
#define temp     dparm(4)
#define ms       dparm(8)

#define dx       dparm(10)
#define dy       dparm(11)
#define dz       dparm(12)
```

Figure 10.20: Header file with precompiler directives

main program

In the main program all global variables are defined (cf. table 10.1). The simulation is initialized by a call to the function `init_par`. Then, the time step loop is entered. From the current magnetization distribution the effective fields for each computational cell is calculated by a call to the function `calc_bloc`. Next, the time integration function `timestep` is called, to update the magnetization vectors according to the chosen time integration algorithm. Finally, all interesting data like the contributions to the total energy and the total magnetization are calculated, the time average values and histograms updated, and the results written to log files. At regular intervals the magnetization distribution is saved for visualization with the postprocessing programs AVS and Geomview by the subroutine `magdistwrite`. When the maximum number of time steps is reached, the time step loop is exited,

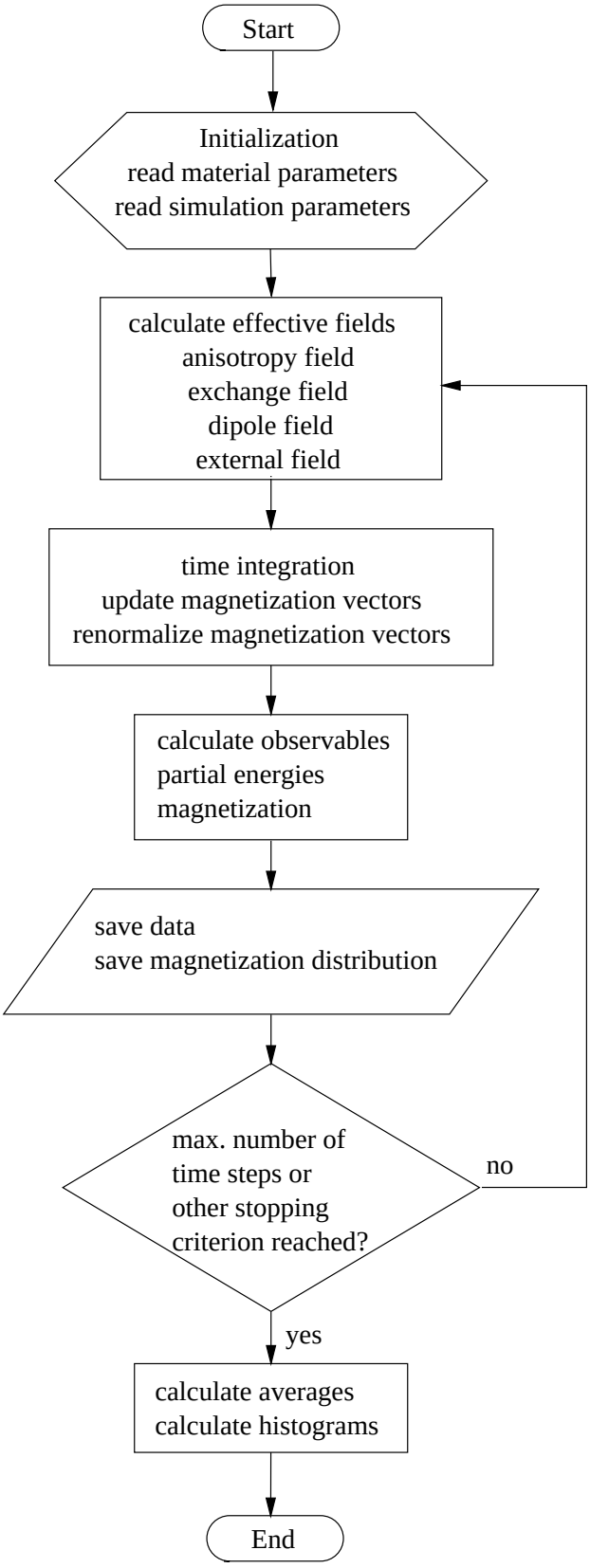

Figure 10.21: Flow chart of the finite difference program

the average values, histograms, number of switching events, etc., are written to log files and the program exits.

`integer`	`liparm`	length of iparm array
`integer`	`ldparm`	length of dparm array
`parameter`	`(liparm=30, ldparm=30)`	
`integer`	`iparm(liparm)`	array of integer parameters
`double precision`	`dparm(ldparm)`	array of double precision parameters
`double precision`	`eaxis(nx,ny,nz,3)`	cartesian comp. of easy axes
`double precision`	`m(nx,ny,nz,3)`	magnetization vectors
`double precision`	`bloc(nx,ny,nz,3)`	cartesian comp. of local field
`double precision`	`bext(nx,ny,nz,3)`	external field
`double precision`	`bani(nx,ny,nz,3)`	anisotropy field
`double precision`	`bexch(nx,ny,nz,3)`	exchange field
`double precision`	`bdip(nx,ny,nz,3)`	dipole field
`integer`	`nn(nx,ny,nz,6)`	table of nearest neighbours

Table 10.1: Global variables of the FD program

`init_par.F`

For the initialization of the simulation all parameters are read from the file `mag.par`. An example is given in figure 10.22. Then, some interesting quantities, like the anisotropy field, the Néel time, or the ratio of the external field to the anisotropy field are written to a log file. Next, all parameters are converted to dimensionless quantities, which are defined at the beginning of the appendix. Finally, the nearest neighbour table is assembled in consideration of simple or periodic boundary conditions and the magnetization vectors are initialized.

`calc_bloc.F`

The deterministic contributions to the effective field are calculated in this function. The dimensionless equations for the magnetocrystalline anisotropy field, the exchange and dipole field are given at the beginning of the appendix. For the calculation of the exchange and dipole field the boundary conditions have to be taken into account. For periodic boundary conditions the minimum image convention is applied.

```
0.08d7   ms           [A/m]     saturation magnetization

1d-11    aexch        [J/m]     exchange constant
4d5      kani         [J/m^3]   anisotropy constant
1        demag                  demagnetizing field 0:off 1:on

1d0      alph         [1]       damping constant

0d0      bext(1,1)    [T]       external field
0d0      bext(1,2)
0d0      bext(1,3)

300d0    temp         [K]       temperature

20d-9    dx           [m]       lattice constant
0d0      dy           [m]       lattice constant:  dy=0d0 ?  dy=dx
0d0      dz           [m]       lattice constant:  dz=0d0 ?  dz=dy
1d-15    step         [s]       time step size step < 0:  step=(precession
                                period)/abs(step)
0d0      tavrg        [s]       when to start averaging
100      datasmp                save data after every nth timestep
1000     magdistsmp             save magnetization distribution after every
                                nth timestep
100000   nstep                  number of time steps
0        initmag                initial magnetization 0:homogeneous 1:random
                                2:start from magdist.dat 3:  M rotates in
                                x-z-plane one full period 4:vortex state 5:M
                                in easy axis 6:M at 45 degrees from z-axis in
                                x-z plane 7:  M rotates in x-y-plane one full
                                period else:almost homogeneous
30       dataout                select data to be saved 1:trajectory
                                2:histogram 4:final magnetization 8:<mz>(t)
                                16:energy 32:fourier analysis
0        verb                   verbosity level 0:no messages 1:check norm of
                                m
0.0d0    sweep        [T/s]     sweeping rate of external field
3        tintalg                time integration algorithm 1:Euler/Ito
                                2:Euler/Strato.  3:Heun 4:Milshtein 5:LaBonte
1        randalg                random number generator 1:Gauss 2:Honerkamp

0d0      eaxis(1)     [1]       easy axis
0d0      eaxis(2)
1d0      eaxis(3)

1        bound                  boundary conditions:  1:simple 2:periodic
```

Figure 10.22: Initialization file `mag.par`

`timestep.F`

For the numerical integration several deterministic and stochastic time integration algorithms have been implemented. The stochastic Euler scheme in Itô and Stratonovich form, the Milshtein scheme and the Heun scheme. The deterministic schemes are obtained by setting the temperature to zero. In addition the fixpoint iteration method has been implemented. After all magnetization vectors have been updated, they are renormalized, to fulfill the micromagnetic constrain, which requires the saturation magnetization to stay constant.

The finite element program

Program structure

`vecmesh`

This program is a preprocessing tool, which prepares all input data for the calculations with the finite element program `vecu` and its descendants. The finite element mesh can be read in several different formats. The "neutral file" format of PATRAN and GEOMPACK finite element definition files are supported. In addition, there is an interface to AGM, the adaptive grid manager, which can be used to adaptively refine finite element meshes.

Then, the input data are checked for consistency. All normals of surface elements, whose orientation is defined by the node numbers of the corners, have to point in outward direction. To take full advantage of the sparsity of the finite element matrices, they must have a band structure. Thus, the nodes of the mesh are renumbered, if necessary.

The main task of `vecmesh` is the computation of the boundary matrix for the hybrid finite element/boundary element method (cf. section 4.2). Finally, the material parameters are read and all data are stored in a suitable data structure for the finite element package VECFEM, on which the finite element programs are based.

`vecuws`

The finite element calculations are performed by a descendant of `vecu`, which has been adapted for the solution of the stochastic Landau-Lifshitz equation (cf. section 5.2). Like the finite difference program it consists of three main parts.

An initialization part, in which the preprocessing data are read and the VECFEM subroutines are prepared for the calculations. Then, there is the time step loop. The implementation of the time integration is described in the following section. After each time step, all interesting quantities are calculated and stored in log files. The magnetization distribution is saved for postprocessing with the visualization program AVS.

Stochastic time integration

For the deterministic time integration two algorithms have been used so far: An implicit backward difference integration scheme and a Runge-Kutta type explicit method. Since the latter is quite similar to the deterministic part of the Heun scheme, it has been used as a template. The data structures and the interface to `vecuws` have been reused. Thus, the necessary updates have been reduced to a minimum and the maintenance of the finite element program is kept simple.

The call in the time step loop of the main program `vecuws` to the Runge-Kutta time integration subroutine `rkc` has been replaced by a call to the stochastic time

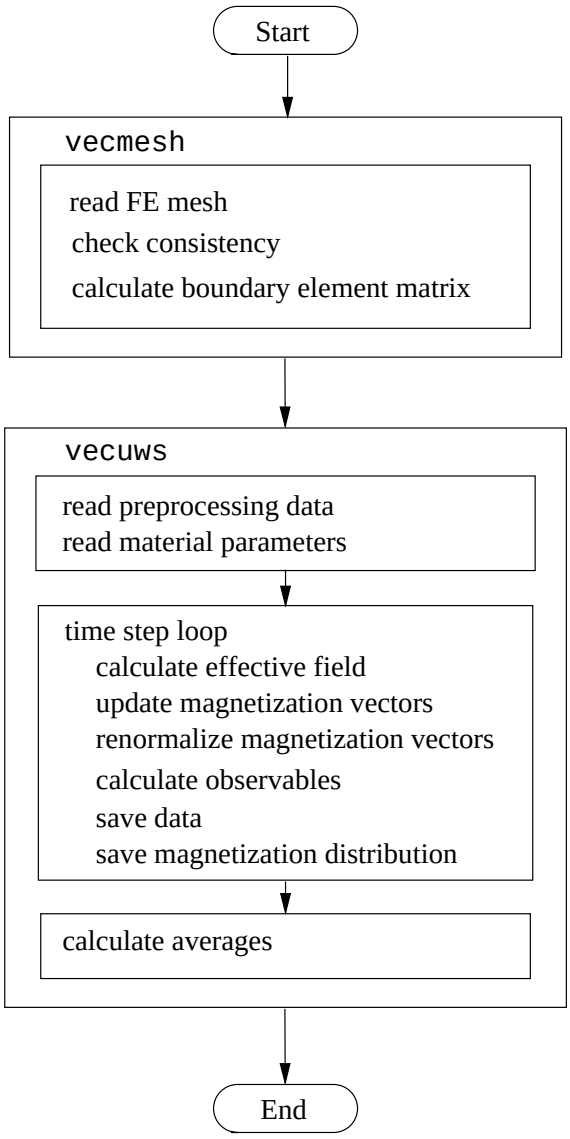

Figure 10.23: Flow chart of the finite element package

```
      subroutine rks(neqn,f,y,t,tstep,dy,idid)

C*********************************************************************
C                                                                     *
C Formal Parameters                                                   *
C                                                                     *
C (in - not modified / out - modified)                                *
C                                                                     *
C name        type      in/out   meaning                            *
C-------------------------------------------------------------      *
C neqn        integer   in       number of equations=
C                                degrees of freedom=
C                                3*number of nodes
C f           subroutine         for calculation of the effective field
C y(neqn)     double    out      magnetization on nodes
C t           double    out      simulated time (reduced units)
C tstep       double    in       discrete time step
C dy(2*neqn)  double    out      temporary array as storage space
C                                for magnetization increments
C*********************************************************************
```

Figure 10.24: Subroutine header of the stochastic time integration

integration subroutine `rks`. Its subroutine header with a description of the expected parameters is given in figure 10.24. In `rks` the stochastic Heun scheme is implemented as given in section 8.3.2.

The second argument, which is passed to `rks` is the subroutine, which calculates the effective field. This subroutine is implemented as `rkx`. The evaluation of the effective field is based on the energy terms given in section 2.1 [15]. The demagnetizing field is calculated with the hybrid finite element/boundary element method and a magnetic scalar potential as described section 4.2.

Then, the increments for the magnetization vectors are evaluated in `calc_mdotx`. In this subroutine, the thermal field is computed and added to the effective field. Of course, for the Heun method it is necessary to calculate two different increments, one for the Euler type predictor and the true increment, which is a function of the current magnetization and the result of the Euler type predictor (cf. section 8.3.2).

The sequence of subroutines, which are called from `vecuws` for the time integration is plotted as a directed graph in figure 10.25.

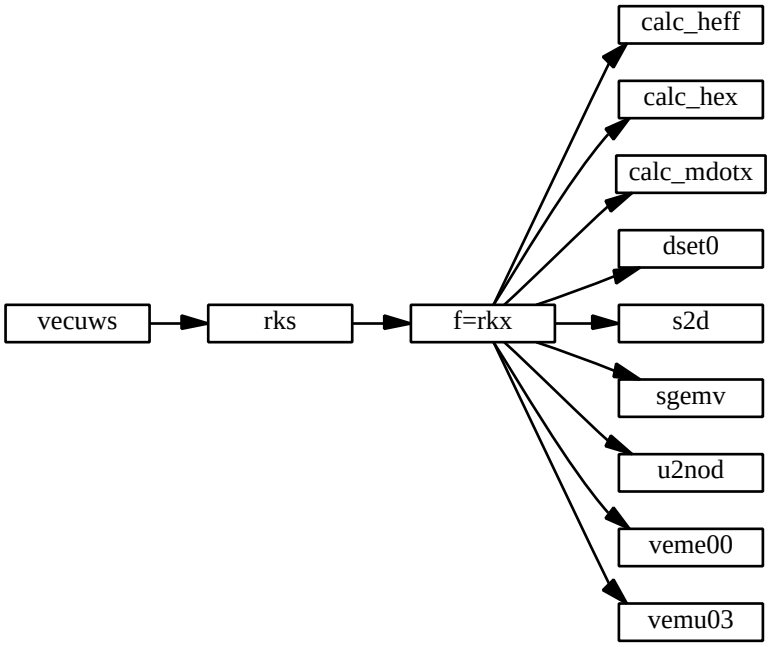

Figure 10.25: Sequence of subroutine calls for time integration

Bibliography

[1] H. Breuer, *dtv-Atlas zur Physik*. Deutscher Taschenbuch Verlag, 1991.

[2] J. Fidler, "Physics of magnetic materials." lecture notes, 1996.

[3] K. B. Klaassen, R. G. Hirko, and J. T. Contreras, "High speed magnetic recording," *IEEE Trans. Magn.*, vol. 34, pp. 1822–1827, July 1998.

[4] T. Schrefl, J. Fidler, D. Süss, and W. Scholz, "Hysteresis and switching dynamics of patterned magnetic elements," *Physica B*, submitted.

[5] D. Süss, T. Schrefl, J. Fidler, and J. N. Chapman, "Micromagnetic simulation of the long range interaction between NiFe nano-elements using the BE-method," *J. Magn. Magn. Mater.*, pp. 617–619, 1999.

[6] T. Schrefl and J. Fidler, "Reversal modes and reversal times in submicron-sized elements for MRM applications," *Proc. E-MRS-Meeting, Strasbourg*, 1999.

[7] T. Schrefl, J. Fidler, C. Kirk, and J. N. Chapman, "Simulation of magnetization reversal in polycrystalline patterned Co-elements," *J. Appl. Phys.*, vol. 85, pp. 6169–6171, 1999.

[8] T. Schrefl, J. Fidler, K. J. Kirk, and J. N. Chapman, "A higher order FEM-BEM method for the calculation of domain processes in magnetic nano-elements," *IEEE Trans. Magn.*, no. 33, pp. 4182–4184, 1997.

[9] G. Bertotti, *Hysteresis in Magnetism – For Physicists, Materials Scientists and Engineers*. Electromagnetism, Academic Press, 1998.

[10] A. H. Morrish, *The physical principles of magnetism*. New York: Wiley, 1975.

[11] D. Spisák and J. Hafner, "Frustrated exchange interactions at the interface of antiferromagnetic films with ferromagnetic substrates," *Phys. Rev. B*, vol. 55, pp. 8304– 8312, 1997.

[12] D. Spisák and J. Hafner, "Theory of bilinear and biquadratic exchange interactions in iron: bulk and surface," *J. Magn. Magn. Mat.*, vol. 168, pp. 257– 268, 1997.

[13] W. F. Brown, *Micromagnetics*. New York: Interscience, 1963.

[14] A. Aharoni, *Introduction to the Theory of Ferromagnetism*. Monographs on Physics, Oxford University Press, 1996.

[15] D. Süss, "Mikromagnetische Simulation der Keimbildung in SE Magneten," Diplomarbeit, TU Vienna, 1999.

[16] C. E. Patton, "The Landau-Lifshitz equation - precessing magnets." Intermag '97 tutorial on high speed switching, 1997.

[17] T. L. Gilbert, "A Lagrangian formulation of gyromagnetic equation of the magnetization field," *Phys. Rev.*, vol. 100, p. 1243, 1955.

[18] L. Landau and E. Lifshitz, "On the theory of magnetic permeability in ferromagnetic bodies.," *Physik. Z. Sowjetunion*, vol. 8, p. 153, 1935.

[19] C. Grossmann and H.-G. Roos, *Numerik partieller Differentialgleichungen*. Stuttgart: Teubner, 2nd ed., 1994.

[20] J. B. Cole, "Generalized nonstandard finite differences and physical appications," *Computers in Physics*, vol. 12, pp. 82–87, jan./feb. 1998.

[21] M. J. Donahue and R. D. McMichael, "Exchange energy representations in computational micromagnetics," *Physica B*, vol. 233, pp. 272–278, 1997.

[22] C. W. Gardiner, *Handbook of stochastic methods: for physics, chemistry and the natural sciences*. Springer, 2nd ed., 1996.

[23] M. E. Schabes and A. Aharoni, "Magnetostatic interaction fields for a three-dimensional array of ferromagnetic cubes," *IEEE Trans. Magn.*, vol. MAG-23, no. 6, pp. 3882–3888, 1987.

[24] J. H. J. van Opheusden and E. M. C. M. Reuvekamp, "Computer simulation of a thin magnetic film with vertical anisotropy," *J. Magn. Magn. Mater.*, vol. 88, pp. 247–259, 1990.

[25] E. D. Boerner and H. N. Bertram, "Dynamics of thermally activated reversal in nonuniformly magnetized single particles," *IEEE Trans. Magn.*, vol. 33, pp. 3052–3054, September 1997.

[26] A. Aharoni, "Magnetostatic energy calculation," *IEEE Trans. Magn.*, vol. 27, no. 4, pp. 3539–3547, 1991.

[27] E. Della Torre, "Magnetization calculation of fine particles," *IEEE Trans. Magn.*, vol. MAG-22, pp. 484–489, September 1986.

[28] D. V. Berkov and N. L. Gorn, "Quasistatic remagnetization processes in two-dimensional systems with random on-site anisotropy and dipolar interaction - numerical simulations," *Phys. Rev. B*, vol. 57, no. 22, pp. 14332–14343, 1998.

[29] K. Fabian, A. Kirchner, W. Williams, F. Heider, T. Leibl, and A. Hubert, "Three-dimensional micromagnetic calculations for magnetite using FFT," *Geophysical Journal International*, vol. 124, no. 1, pp. 89–104, 1996.

[30] D. Lewis and E. Della Torre, "Identification of stiff modes in micromagnetic problems," *IEEE Trans. Magn.*, vol. 33, pp. 1596–1599, March 1997.

[31] G. J. Parker, C. Cerjan, and D. W. Hewett, "Embedded curve boundary method for micromagnetic simulations," *J. Appl. Phys.*, 2000. to be published.

[32] M. R. Gibbons, G. Parker, C. Cerjan, and D. W. Hewett, "Finite difference micromagnetic simulation with self-consistent currents and smooth surfaces." paper O1-5, Second International Symposium on Hysteresis Modeling and Micromagnetics, Perugia, Italy, 1999.

[33] M. Eiermann, O. Ernst, and W. Queck, "Finite element tutorial," 1996. URL: `http://www.mathe.tu-freiberg.de/AMM2/PS/FEintro_2.ps.gz`.

[34] T. Schrefl, *Numerical Simulation of Magnetization Reversal Processes in Hard Magnetic Materials*. Dissertation, TU Vienna, 1993.

[35] M. Jung and U. Langer, "Finite-Elemente-Methode – Eine Einführung für Ingenieurstudenten," 1995. URL: `http://http://www.numa.uni-linz.ac.at/Teaching/Lectures/nupdglg.ps.gz`.

[36] B. Streibl, "Dynamische mikromagnetische Simulation von μMAG Standardproblemen," Diplomarbeit, TU Vienna, 1998.

[37] D. R. Fredkin and T. R. Koehler, "Hybrid method for computing demagnetizing fields," *IEEE Trans. Magn.*, vol. 26, no. 2, pp. 415–417, 1990.

[38] R. Kubo, M. Toda, and N. Hashitsume, *Statistical Phyiscs II: Nonequilibrium statistical mechanics*. New York, Berlin, Heidelberg: Springer, 2nd ed., 1991.

[39] J. L. García-Palacios and F. J. Lázaro, "Langevin-dynamics study of the dynamical properties of small magnetic particles," *Phys. Rev. B*, vol. 58, pp. 14937–14958, December 1998.

[40] P. E. Kloeden and E. Platen, *Numerical Solution of Stochastic Differential Equations*. No. 23 in Application of Mathematics, Berlin, Heidelberg: Springer, 2nd corrected ed., 1995.

[41] J. Honerkamp, *Stochastische Dynamische Systeme: Konzepte, numerische Methoden, Datenanalysen.* Weinheim, Basel, Cambridge, New York: VCH, 1990.

[42] W. Horsthemke and R. Lefever, *Noise-Induced Transitions.* Berlin, Heidelberg, New York, Tokyo: Springer, 1984.

[43] A. E. LaBonte, "Two-dimensional Bloch-type domain walls in ferromagnetic films," *J. Appl. Phys.*, vol. 40, pp. 2450–2458, 1969.

[44] G. N. Milshtein, "Approximate integration of stochastic differential equations," *Theory. Prob. Appl.*, vol. 19, pp. 557–562, 1974.

[45] R. Toral, "Computational field theory and pattern formation," in *Third Granada Lectures in Computational Physics* (P. L. Garrido and J. Marro, eds.), Springer, 1994.

[46] W. H. Press, S. A. Teukolsky, W. T. Vetterling, and B. P. Flannery, *Numerical Recipes in Fortran 77: The Art of Scientific Computing.* Cambridge University Press, 1997.

[47] "NAG - The Numerical Algorithms Group." URL: `http://www.nag.co.uk/`.

[48] "μmag micromagnetic modeling group." URL: `http://www.ctcms.nist.gov/~rdm/mumag.html`.

[49] W. Rave, K. Fabian, and A. Hubert, "Magnetic states of small cubic particles with uniaxial anisotropy," *J. Magn. Magn. Mater.*, vol. 190, pp. 322–348, 1998.

[50] S. Chikazumi, *Physics of Ferromagnetism.* Monographs on Physics, Oxford: Clarendon Press, 1997.

[51] R. Kikuchi, "On the minimum of magnetization reversal time," *J. Appl. Phys.*, vol. 27, pp. 1352–1357, November 1956.

[52] Y. Yu and J. W. Harrell, "Fmr spectra of oriented γ-Fe_2O_3, Co-γ-Fe_2O_3, CrO_2, and MP tapes," *IEEE Trans. Magn.*, vol. 30, no. 4, pp. 4083–4085, 1994.

[53] E. C. Stoner and E. P. Wohlfarth, "A mechanism of magnetic hystersis in heterogeneous alloys," *Phil. Trans. R. Soc.*, vol. 240, pp. 599–642, 1948.

[54] D. J. Dunlop, "Magnetism in rocks," *Journal of Geophysical Research – Solid Earth*, vol. 100, no. B2, pp. 2161–2174, 1995.

[55] F. Heider, A. Zitzelsberger, and K. Fabian, "Magnetic susceptibility and remanent coercive force in grown magnetite crystals from 0.1 μm to 6 mm," *Physics of the Earth & Planetary Interiors*, vol. 93, no. 3-4, pp. 239–256, 1996.

[56] Y. Nakatani, Y. Uesaka, N. Hayashi, and H. Fukushima, "Computer simulation of thermal fluctuation of fine particle magnetization based on Langevin equation," *J. Magn. Magn. Mater.*, vol. 168, pp. 347–351, 1997.

[57] L. Néel, "Theorie du trainage magnetique des ferromagnetiques en grains fins avec applications aux terres cuites," *Ann. Geophys.*, vol. 5, pp. 99–136, 1949.

[58] U. Nowak and D. Hinzke, "Magnetization switching in small ferromagnetic particles: Nucleation and coherent rotation," *J. Appl. Phys.*, vol. 85, no. 8, p. 4337, 1999.

[59] P. A. Rikvold, H. Tomita, S. Miyashita, and S. W. Sides, "Metastable lifetimes in a kinetic ising model: Dependence on field and system size," *Phys. Rev. E*, vol. 49, p. 5080, 1994.

[60] W. Wernsdorfer, K. Hasselbach, A. Benoit, G. Cernicchiaro, D. Mailly, B. Barbara, and L. Thomas, "Measurement of the dynamics of the magnetization reversal in individual single-domain Co particles," *J. Magn. Magn. Mater.*, vol. 151, pp. 38–44, 1995.

[61] W. Wernsdorfer, E. B. Orozco, B. Barbara, K. Hasselbach, A. Benoit, D. Mailly, B. Doudin, J. Meier, J. E. Wegrowe, J.-P. Ansermet, N. Demoncy, H. Pascard, L. Francois, N. Duxin, and M. P. Pileni, "Mesoscopic effects in magnetism: Submicron to nanometer size single particle mesurements," *J. Appl. Phys.*, vol. 81, pp. 5543–5545, April 1997.

[62] H. Kisker and T. Suzuki, "Coercivity mechanism in data storage media," in *Proceedings of Magneto-optical Recording International Symposium '96*, vol. 20 Supplement, pp. 185–188, The Magnetics Society of Japan, 1996.

[63] M. Lederman, G. A. Gibson, and S. Schultz, "Observation of thermal switching of a single ferromagnetic particle," *J. Appl. Phys.*, vol. 73, pp. 6961–6963, May 1993.

[64] S. M. Stinnett, W. D. Doyle, P. J. Flanders, and C. Dawson, "High speed switching measurements in thin film disk media," *IEEE Trans. Magn.*, vol. 34, pp. 1828–1833, July 1998.

List of Figures

List of Tables

Acknowledgment

I would like to express my sincere thanks to my supervisor Prof. J. Fidler for his encouragement, guidance, support and fruitful discussions throughout this work.

I am very grateful to Univ. Doz. Dr. Thomas Schrefl for many stimulating discussions, his advice related to all aspects of this work, and his patience in answering all my questions and concerns. He supported me with many references to important literature, tips for implementing the finite difference model, and his implementation of the finite element model, which I adapted for my needs.

Prof. Fidler initiated this work and gave me the opportunity for a short term visit to the "Computational Magnetism" group of Prof. Roy W. Chantrell at the University of Wales, Bangor. Thus, I wish to express my sincere thanks to Prof. Chantrell for his invitation to Bangor, where I learned a lot from his knowledge on thermal activation in micromagnetics and started the finite difference model.

Special thanks to Dieter Süss for many helpful discussions and support.

Finally I would like to express my sincere thanks to my parents, who made my studies possible, for their continuous support and encouragement.

Curriculum vitæ

Werner Scholz